ANISOTROPY AND MAGNETOSTRICTION OF $GdAl_2$ AND RELATED COMPOUNDS

by

JOHN FERRIS BURD

A Thesis Submitted for the Degree of
Doctor of Philosophy

DEPARTMENT OF PHYSICS
UNIVERSITY OF SOUTHAMPTON

JULY, 1977

To

J. M. M.

and

H. S. B.

CONTENTS

CHAPTER 5 EXPERIMENTAL

UNIVERSITY OF SOUTHAMPTON

ABSTRACT

FACULTY OF SCIENCE

PHYSICS

Doctor of Philosophy

ANISOTROPY AND MAGNETOSTRICTION OF $GdAl_2$ AND RELATED COMPOUNDS

by John Ferris Burd

Single crystals of the binary and pseudobinary compounds RAl_2 and $R_xR'_{1-x}Al_2$, where R and R' are rare-earth metals, have been grown by the Czochralski technique. Measurements of the magnetostrictions and anisotropies of disc-shaped samples of the compounds $GdAl_2$, $Gd_{0.98}Tb_{0.02}$ and $Gd_{0.95}Tb_{0.05}Al_2$ have been made between 4.2K and their Curie temperatures in applied magnetic fields up to 2.5T.

Anisotropy constants were measured by means of a torque magnetometer. The methods by which anisotropy constants can be derived from torque curves were investigated using a well-documented single crystal of cobalt and the conclusions drawn were applied to the measurements on the rare-earth alloys. The derived values of the first two anisotropy constants of $GdAl_2$ were $K_1 = (-2.8 \pm 0.1) \times 10^3$ J m^{-3} and $K_2 = (-1.4 \pm 0.2) \times 10^{-3}$ J m^{-3} at 0 K. Magnetostriction measurements were performed using resistive strain gauges and a precision D.C. Wheatstone bridge circuit. The values of the first two magnetostriction constants of $GdAl_2$ are $h_1 = (6.0 \pm 0.2) \times 10^{-6}$ $h_2 = (-25.1 \pm 0.2) \times 10^{-6}$ at 4.2K.

The dilute alloys were measured in the same way and derived values of their anisotropies and magnetostrictions were used to determine the anisotropy constant and the first two magnetostriction constants of $TbAl_2$. The values are $K_1 = -2 \times 10^7 \pm 10\%$ J m^{-3} ; $h_1 = 1400 \times 10^{-6}$; $h_2 = 920 \times 10^{-6}$. The method used to derive these values and a theoretical model developed to test its validity is also discussed.

ACKNOWLEDGEMENTS

Initially I would like to express my thanks to my supervisor Professor E. W. Lee for his guidance, help and support throughout this work, and to Dr. D. W. Jones, Dr. R. G. Jordan and the staff of the Centre for Materials Science for their assistance during my stay at the University of Birmingham.

I would also like to thank the many friends who have given me encouragement and especially those members of the magnetism group with whom I have had many helpful and interesting discussions.

Also my thanks to Mr. C. D. Strange for his technical assistance and for tracing the diagrams and to Mrs. M. Wainwright for producing the typescript.

Professor Barnes for providing laboratory facilities.

Mr. P. Cleverly for supplying liquid helium, and to many other members of the Physics Department who have helped me in the past.

CHAPTER I

INTRODUCTION

The compounds RAl_2 where R is a rare-earth metal have been studied extensively in polycrystalline form. The recently developed techniques by which single crystals have been produced have provided the opportunity to study the directional properties of these materials. A review of previous work and a general introduction to these compounds is presented in chapter 2.

The measurements with which this work was concerned were those of the magnetic anisotropy and magnetostriction in these compounds which have a single magnetic sub-lattice. The theories of anisotropy and magnetostriction are described in chapters 3 and 4 respectively.

Initially, the project involved the growing of these materials in single crystal form, subsequently experimental measurements of the magnetic anisotropy using a torque magnetometer, and the magnetostriction, using a sensitive strain gauge bridge were performed.

The apparatus used in these three parts of the experimental work is described in the three parts of chapter 5.

The methods by which anisotropy constants can be derived from torque curves were investigated in some detail and, from some measurements on a single crystal of cobalt, conclusions were drawn as to the methods most appropriate for particular field and temperature regimes.

Torque curves were measured for $GdAl_2$ and, because of the small values of the anisotropy constants together with its high Curie temperature, this material was used as a host for diluting the highly anisotropic properties of $TbAl_2$. Further measurements were made of the anisotropy of single crystals grown from $GdAl_2$ containing 2% and 5% $TbAl_2$. All the torque

results are given in chapter 6.

Magnetostriction measurements were also made on the single crystal samples described above and these are reported in chapter 7.

In addition to the measurements on the dilute alloys, a theoretical model was developed to determine the means by which the measurements could be extrapolated to 100% $TbAl_2$. This model, along with some computer calculations, is described in chapter 8.

CHAPTER 2

2. THE INTERMETALLIC COMPOUNDS RAl_2

2.1. Introduction

The compounds of stoichiometric composition RAl_2 , where R is a rare earth, will form for all the lanthanide series (1) and crystallise in the cubic $McCu_2$ - type C15 Laves phase (2). They all have melting points at around 1500°C and examination of the phase diagrams of the R - Al systems (3) reveals a congruent melting point at composition RAl_2 . Most of the series are ferromagnetic (4) with $GdAl_2$ having the highest Curie temperature of approximately 170 K. The bulk magnetic properties of these materials, in polycrystalline form, have been extensively investigated. Early measurements were performed by Williams et al (4) on all the rare earth dialuminides except La, Eu and Y. More recently the possibility of producing single crystals of these compounds has been realised (5,6) and experiments involving neutron diffraction and magnetisation on single crystals have been performed (7-10).

Structural investigations (11) have reported the lattice parameters for all RAl_2 compounds as well as showing that the C15 phase exists, for most combinations of rare earths, in the ternary form $R_x R'_{1-x} Al_2$ (12). However, substitution on the transition metal lattice with Fe, Co or Ni introduces a modification of the cubic C15 structure to hexagonal C14 (13,14) at intermediate compositions.

From single crystal measurements (8) the magnetocrystalline anisotropy has been explained in terms of the crystalline electric field and exchange interactions and a successful agreement between theory and experiment obtained.

Subsequent sections in this chapter will discuss previous work on these compounds with particular reference to properties relevant to this work and concentrating on the two compounds $GdAl_2$ and $TbAl_2$.

2.2. Structure and Lattice Parameters

The cubic Laves C15 structure contains 32 atoms per unit cell which, for RAl_2 , is eight formula units. The rare earth lattice is a simple diamond structure (i.e: F.C.C. and F.C.C. + $^1/_4$, $^1/_4$, $^1/_4$) and the aluminium atoms occupy the vertices of tetrahedra which are linked, forming an interpenetrating lattice. This is shown in fig.(2.1). The lattice parameter determinations, using X-rays, for the RAl_2 and the related RCo_2 compounds were performed by Harris et al (11) who gave values of 7.903 Å for $GdAl_2$ and 7.867 Å for $TbAl_2$.

2.3. Magnetic Measurements

The magnetic behaviour of these compounds has been the subject of considerable investigation. Early work by Williams et al (4) showed that the compounds were ferromagnetic, as were some solid-solution ternaries with substitution on the rare earth lattice. These results were consistent with the earlier investigations of Jaccarino et al (15) who used NMR to determine the magnitude and sign of the conduction electron polarisation.

More extensive determinations of the Curie temperatures and magnetisations of the RAl_2 series were made by Buschow et al (16), who also made measurements on alloys substituted on the rare earth lattice with Y, La and Th thus diluting the magnetic properties with the non-magnetic ions.

FIG. 2.1 The C15 Cubic Laves Phase Crystal Structure

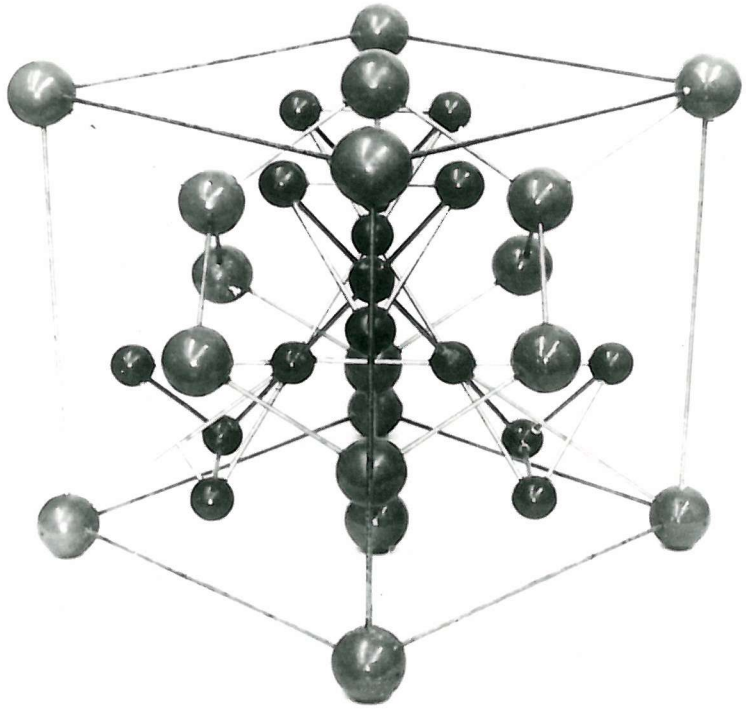

Rare Earth : Large Spheres

Transition Metal : Small Spheres

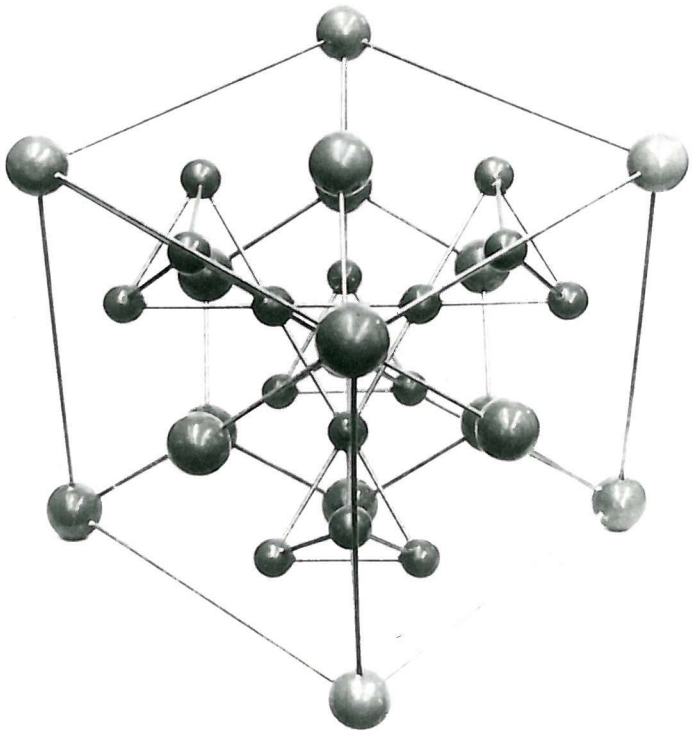

The temperature dependence of the spontaneous magnetisation of $GdAl_2$ is given by several authors (4,16,17,18) and is illustrated in fig.(2.2). Absolute determinations of the saturation moments at low temperature have given 9.0 μ_B/ Tb^{3+} (7,8) and 7.0 μ_B/Gd^{3+} (13.16) for $TbAl_2$ and $GdAl_2$ respectively.

The magnetic anisotropy of these compounds was first investigated using NMR at the ^{27}Al sites in several rare earth dialuminides (19). This gave the easy directions of magnetisation for the first time ($<111>$ in both $GdAl_2$ and $TbAl_2$) and also examined the isotropic RKKY (20) exchange parameters identifying a small anisotropic contribution to the exchange (approximately 10%).

With the availability of large single crystals of the RAl_2 compounds (5,6) further studies were made of the magnetic anisotropy and crystal field effects in these materials (7,10). Neutron diffraction measurements both elastic (21) and inelastic (22,23) were also performed, mainly using $TbAl_2$, to determine magnetic moments, and magnon dispersion relations which may be accounted for in terms of long range oscillatory exchange. Millhouse et al (21) give a value for the saturation moment of $TbAl_2$ of (9.17 $\pm$ 0.04 μ_B/Tb^{3+}) which has been used in this work. Unfortunately gadolinium has a large neutron absorbtion cross-section and neutron diffraction experiments using the $GdAl_2$ compound have not been possible.

2.4. Other Measurements

Resistivity measurements on these compounds have also been reported (24) which were made in an attempt to clarify the interaction mechanism between the localised rare earth spins and the conduction electrons.

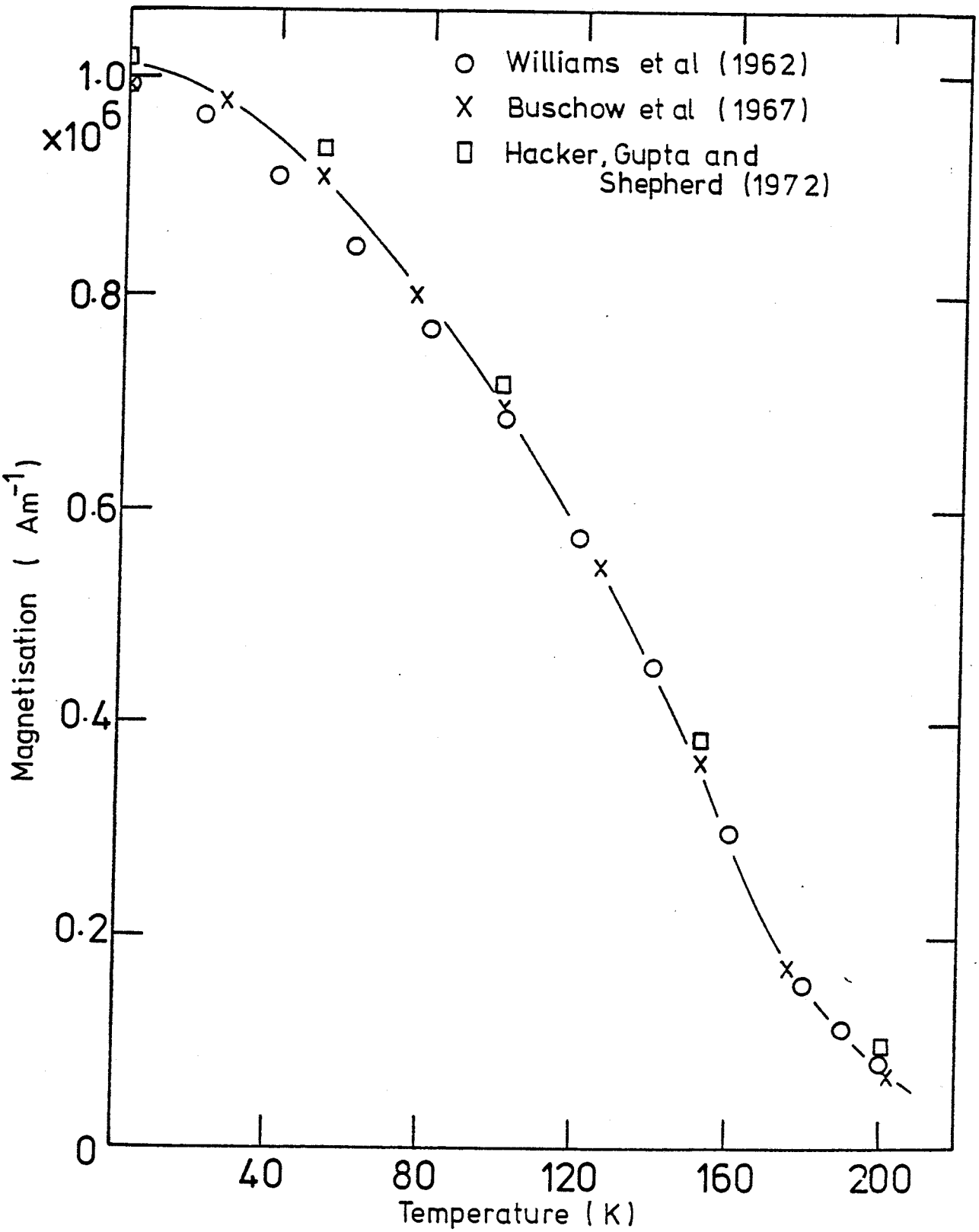

Fig. 2·2 Temperature Dependence of the Magnetisation of $GdAl_2$

More importantly for this work single crystal elastic constants have been determined for both $GdAl_2$ (25) and $TbAl_2$ (26). The values of the three independent constants for these cubic materials, determined by ultrasonic techniques are given in Table (2.1).

TABLE 2.1 - THE ELASTIC CONSTANTS OF SOME R.$A\ell_2$ COMPOUNDS (x 10" N m^{-2})

	4.2K			300K		
	C_{11}	C_{12}	C_{44}	C_{11}	C_{12}	C_{44}
La $A\ell_2$	1.48	0.32	0.44	1.44	0.32	0.43
Y $A\ell_2$	1.76	0.34	0.58	1.71	0.34	0.56
Gd $A\ell_2$	1.69	0.35	0.65	1.61	0.37	0.59
Tb $A\ell_2$	1.52	0.35	0.67	1.44	0.33	0.68

3. MAGNETIC ANISOTROPY

3.1. Introduction

The direction of magnetisation of a single crystal of magnetic material is often observed to prefer to lie in a particular crystallographic direction (the easy direction). This is interpreted as a term in the free-energy expansion for the crystal which depends on the direction of the spontaneous magnetisation. This component will be a minimum when the magnetisation is parallel to an easy direction. This anisotropy will generally reflect the symmetry of the crystal lattice and is known as magnetocrystalline anisotropy.

Further contributions to the total magnetic anisotropy may arise due to the shape, state of stress and previous thermal or magnetic history of the sample. These are known as extrinsic or induced anisotropies. In this chapter only the intrinsic anisotropic properties of the crystals will be considered.

3.2. Phenomenology

When a crystal is saturated the direction of magnetisation may be specified by the direction cosines α_1 , α_2 , α_3 . The anisotropy energy is then expanded as a power series in the α's - it can be shown (see for example Darby and Isaac, ref.1.) that for a cubic crystal, to sixth order in the direction cosines, the anisotropy energy E_K is :-

$$E_K = K_1 (\alpha_1^2\alpha_2^2 + \alpha_2^2\alpha_3^2 + \alpha_3^2\alpha_1^2) + K_2 (\alpha_1^2\alpha_2^2\alpha_3^2) \quad ..(3.1)$$

Where K_1 and K_2 are the first two anisotropy constants and are characteristic of the material.

In the case of a hexagonal crystal, it is customary to write the anisotropy energy as a function of the polar angle (θ,φ), where the angle θ is the angle between the magnetisation (M_S) and the c-direction and φ the angle between M_S and an a-direction in the basal plane. E_K is then given by:-

$$E_K = K_1' \sin^2\theta + K_2' \sin^4\theta + K_3' \sin^6\theta + K_4' \sin^6\theta \cos 6\varphi \qquad \ldots(3.2)$$

The easy directions of the crystals, in both cases, are obtained by minimisation of E_K with respect to the angular position of M_S and therefore depend on the signs and relative magnitudes of the K's. Conditions for easy axes are given in refs. 2 and 3 and table 3.1 shows the conditions, ignoring K_3 and K_4 (after reference 4).

Another method of expressing equations (3.1) and (3.2) is to expand E_K in terms of an orthonormal set of functions, usually related to the spherical harmonics Y_ℓ^m, (e.g. Zener ref. 6 or Turov and Mitsek ref. 5), such that:-

$$E_K = \sum_{\ell=0}^{\infty} \sum_{m=-\ell}^{+\ell} k_\ell^m \, Y_\ell^m \, (\theta , \phi) \qquad \ldots(3.3)$$

A discussion of the advantages of this type of expansion, especially when higher order terms need to be taken into account, in terms of the anisotropy coefficients k_ℓ^m is given by Birss and Keeler (7). However, in the case where only the first two constants are to be determined there is little advantage in using the above method especially when Fourier analysis is used to separate the components of the torque curve and the sine expansion is most convenient.

TABLE 3.1 - CONDITIONS FOR PARTICULAR EASY DIRECTIONS IN CUBIC CRYSTALS

K_1	+	+	+	-	-	-
K_2	$+\infty$ to $-9K_1/4$	$-9K_1/4$ to $-9K_1$	$-9K_1$ to $-\infty$	$-\infty$ to $9\|K_1\|/4$	$9\|K_1\|/4$ to $9\|K_1\|$	$9\|K_1\|$ to $+\infty$
EASY	[100]	[100]	[111]	[111]	[110]	[110]
MEDIUM	[110]	[111]	[100]	[110]	[111]	[100]
HARD	[111]	[110]	[110]	[100]	[100]	[111]

3.3. Microscopic Origins

The spin-spin exchange coupling is inherently isotropic, since its form contains no terms which relate to the orientation of the spins with respect to the lattice. However, the electronic orbits are strongly coupled to the lattice and the spins, through spin-orbit coupling, are able to register the influence of the crystalline environment. Thus the relative strengths of the exchange, the spin-orbit coupling, and the crystalline electric field determine the nature of the anisotropy (8). The single-ion model of anisotropy (9) assumes that the total anisotropy may be determined from the quantum states of a single ion only.

In the rare earth metals, because the 4f-electrons responsible for the magnetic properties are localised and shielded from electrostatic interactions, and as the f shell implies large angular momentum, the spin-orbit coupling is strong and J becomes a good quantum number. Therefore an applied magnetic field will rotate the J vector and change the energy of the crystal through the crystalline electric field. The energy equations determined from crystal field calculations and the phenomenological equations (3.1) and (3.2) may be compared to determine single-ion anisotropy constants.

Therefore, with the exception of Gd, the single-ion anisotropies are large and can be shown to dominate all other mechanisms. Because Gd is an S-state ion the crystal field interaction is zero, the orbital part of J, L = 0; and a different mechanism must be used to explain anisotropic properties.

Such a mechanism might be thought to be the magnetic dipole-dipole interaction, but, for cubic symmetry, this will give no anisotropy to first order. This 'pair-model' considers the coupling of

pairs of spin s_i and s_j by a dipolar interaction which leads to an energy term, E_D, of the form:-

$$E_D = \sum_{i<j} E_{ij} \left[S_i . S_j - 3 (S_i . r_{ij})(S_j . r_{ij}) r_{ij}^{-2} \right] \quad ...(3.4)$$

Where E_{ij} are the dipolar coupling constants. However this form gives far too small values for the anisotropy and empirical constants of greater magnitude, along with pseudo-quadrupolar terms of the form:-

$$E_Q = \sum_{i<j} Q_{ij} (S_i . r_{ij})^2 . (S_j . r_{ij})^2 \quad ...(3.5)$$

have been suggested (10). Further arguments (11,12) using a generalised interaction between a pair of spins, have predicted further pseudo-dipolar interactions which can be thought of as representing an anisotropic exchange coupling (see for example ref.1).

3.4. Temperature Dependence of Anisotropy

The assumption that, in the bulk material, all the spins are aligned along an easy direction is only true at absolute zero. At a finite temperature, T, the spins will fluctuate about the easy direction due to thermal motion. This will result in the reduction of the spontaneous magnetisation and also the anisotropy energy. Because of symmetry considerations it is sufficient to use the phenomenological relations (3.1) or (3.2) for the anisotropy energy but introducing temperature dependent K's; for the cubic case:-

$$E_K(T) = K_1(T) (\alpha_1^2\alpha_2^2 + \alpha_2^2\alpha_3^2 + \alpha_3^2\alpha_1^2) + K_2(T) (\alpha_1^2\alpha_2^2\alpha_3^2) + ...(3.6)$$

The initial derivation of the form of the temperature dependence was made by Akulov (13) in 1936, who showed using a simple classical argument that, in the cubic case:-

$$\frac{K_1(T)}{K_1(0)} \simeq m(T)^{10} \qquad \ldots (3.7)$$

where m(T) is the reduced magnetisation ($M_S(T) / M_S(0)$). The proof assumes an array of independent classical spins which at a finite temperature have a distribution of directions about the easy axis, but have individual energies defined by $E_K(0)$ where the α's are replaced by the individual spin direction cosines. Thus the anisotropy at temperature T is then the statistical average over all the spin directions.

In contrast to this single-ion classical approach Van Vleck (10) employed a quantum theory and the pseudo-dipolar and pseudo-quadrupolar interactions described above to derive power laws for the variation of anisotropy with temperature. However the initial analysis led to a second power law for the dipolar part and a 6th power law for the quadrupolar part which reduced to a 5th power law at higher temperatures, which is in substantial disagreement with Akulov's result.

The 10th power law was generalised by Zener (6) who showed that if the expansion in terms of spherical harmonics (section 3.2) was used, where the coefficients $k_\ell(T)$ are used to replace the k_ℓ (of eq. 3.3) then:

$$\frac{k_\ell(T)}{k_\ell(0)} = m(T)^{\ell(\ell+1)/2} \qquad \ldots (3.8)$$

This result was derived using a random spin distribution within a small volume element of the crystal.

The resolution of the difference between these two theories was achieved by Keffer (14) in 1955. He demonstrated that the molecular field approach of Van Vleck ignored the spin correlation; he used a cluster theory and derived the 10th power law for the pseudo-quadrupolar terms at lower temperatures which changed to the 6th power of the reduced magnetisation as the temperature rose destroying the spin correlations. He also gave a general proof of the $(\ell + 1)\,\ell/2$ power law for single-ion and pseudo-quadrupolar terms. The same power law for the pseudo-dipolar terms, using spin wave theory, was derived by Keffer and Oguchi (15) in 1960. At the same time Van Vleck (16) had used symmetry arguments to give a general proof of the $(\ell + 1)\,\ell/2$ power law. Callen and Callen (17) also demonstrated a more explicit proof of this law showing that it is a consequence of the symmetry of the spin system, may be generalised to other crystal symmetries and is virtually model independent in the single-ion case.

The theory predicts that for cubic symmetry:

$$\frac{k_2(T)}{k_2(0)} = m(T)^{10} \quad ; \quad \frac{k_4(T)}{k_4(0)} = m(T)^{21} \qquad \ldots(3.9)$$

and for hexagonal symmetry:-

$$\frac{k_2^o(T)}{k_2^o(0)} = m(T)^3 \; ; \; \frac{k_4^o(T)}{k_4^o(0)} = m(T)^{10} \; ; \; \frac{k_6^o(T)}{k_6^o(0)} = \frac{k_6^6(T)}{k_6^6(0)} = m(T)^{21} \qquad \ldots(3.10)$$

In a torque experiment the anisotropy constants (K_i) are measured but the coefficients k_i may be determined from linear combinations given

by Birss (18). In the cubic case this leads to the temperature relations

$$K_1(T) = \left[K_1(0) + \frac{1}{11} K_2(0) \right] m(T)^{10} \; ; \; K_2(T) = K_2(0)\, m(T)^{21} \quad \ldots(3.11)$$
$$- \frac{1}{11} K_2(0) m(T)^{21}$$

Experimentally, disagreements have been observed between the measurements and theory for Ni and Co (19). However, the 3d transition metals do not have localised spins. Carr (20) has fitted the results for cobalt to a thermal expansion dependent anisotropy and has used a fitting parameter for nickel. The rare earths which have localised spins give experimental results in good agreement with the theory (e.g. Tb, Dy (21,22)) but, for Gd which is an s-state ion, two-ion effects are significant and the temperature dependence is not correctly predicted (23 - 26).

3.5. Other contributions to anisotropy

As mentioned in the introduction to this chapter there are a number of other contributions to the anisotropy of a crystal. The first to be considered is the shape anisotropy simply due to the difference in magnetostatic energies of the sample in different directions. The experimental samples used in this work were of the form of discs, which may be approximated to an oblate spheroid. However as both semi-major axes in the plane of measurement were almost equal the shape anisotropy constant K_s can be considered to be negligible, from:-

$$K_s = \frac{1}{2} \mu_o (N_a - N_b) M_s^2 \quad \ldots(3.12)$$

Where the N's are the demagnetising factor in the respective directions.

The second contribution to the anisotropy is the magneto-elastic contribution. The anisotropy constants as defined in the previous section are defined at constant (zero) strain, whereas the measurements are made at constant stress. Thus there is a contribution to the measured anisotropy constants due to magneto-elastic effects. This contribution has been calculated (27) and can be written in terms of the magnetostriction constants and the elastic constants of the crystal. In the special case of cubic symmetry the differences in K_1, K_2; ΔK_1, ΔK_2 may be written:

$$\Delta K_1 = h_1^2(C_{11} - C_{12}) - 2h_2^2 C_{44} - 3h_o h_3(C_{11} + 2C_{12}) + \cdots\cdots (3.13a)$$

$$\Delta K_2 = -3h_1 h_4(C_{11} - C_{12}) - 12h_2 h_5 C_{44} + \cdots\cdots \quad \cdots (3.13b)$$

These values may be calculated if the h_i and the elastic constants C_{11}, C_{12} and C_{14} are known and in most cases are found to be small. An explicit relation for hexagonal crystals is given by Mason (28).

4. MAGNETOSTRICTION

4.1. Introduction

When a magnetic crystal is magnetised it undergoes a lattice deformation. This effect is called magnetostriction and may be measured by a fractional change in length $\Delta\ell/\ell$ which is usually of the order 10^{-5}. This strain is a function of magnetic field and reaches a limiting value known as the saturation magnetostriction. The magnetisation process proceeds by domain wall motion and domain rotation, the bulk magnetostriction being the vectorial sum of the spontaneous magnetostrictions within the domains. When all the domain magnetisations are aligned the magnetostriction reaches it saturation value. The formal origin of the spontaneous magnetostriction is a strain dependence of the magnetic energy of the crystal such that appropriate deformations will occur to decrease the magnetic energy, which will be counteracted by the normal elastic energy due to the strains. Hence equilibrium strains may be determined by considering the balance between the magnetoelastic forces and the elastic forces. A further contribution to the total magnetostriction is a volume magnetostriction which is an isotropic effect and will add to the longitudinal magnetostriction at saturation. This may also be called forced magnetostriction and is due to an increase in spin order at high fields. This is a small effect ($\frac{\Delta\ell}{\ell}$ approximately 10^{-7} per Tesla) and may be either positive or negative. Another contribution is the form effect which is due to the change of shape of the crystal with the deformation changing the magnetostatic energy density of the bulk.

4.2. Magnetostriction in Cubic Crystals

If a magnetostrictive strain tensor e_{ij} is employed to describe the deformation when a stress σ_{ij} is applied, the pairs of components are linearly related by a generalised Hookes law:

$$\sigma_{ij} = C_{ijkl} \; e_{kl} \qquad \ldots(4.1)$$

Where the C_{ijkl} are the elastic stiffness constants. The elastic energy density E_{el}, associated with these strain components is:

$$E_{el} = \frac{1}{2} \; C_{ijkl} \; e_{ij} \; e_{kl} \qquad \ldots(4.2)$$

If a Maclaurin expansion is used to expand the magnetic energy density E_{mag} as a function of the strains then the relation:-

$$E_{mag} = E^{o} + E^{o}_{ij} \; e_{ij} + E^{o}_{ijkl} \; e_{ij} \; e_{kl} + \ldots. \qquad \ldots(4.3)$$

is obtained. In this expansion the first term, E^{o}, is identified with the magnetic energy for zero strain (i.e. the magnetocrystalline anisotropy). The second term $E^{o}_{ij} \; e_{ij}$ gives the interaction between the magnetocrystalline anisotropy and the strain and is called the magnetoelastic energy density. The final term $E^{o}_{ijkl} \; e_{ij} \; e_{kl}$ has the same form as equation (4.2) and is interpreted as the magnetostrictive contributions to the elastic stiffness constants C_{ijkl}, however this effect will be normally very small and in any case has already been taken into account if the C_{ijkl} have been determined

below the Curie temperature. It must be noted however, that the E^{o}, E^{o}_{ij} and E^{o}_{ijkl} are defined in equation (4.3) at zero magnetostrictive strain, whereas measurements (e.g. of E^{o}, the magnetocrystalline anisotropy energy) are performed at constant stress.

This difference is discussed in section 3.5 and by Carr (ref.1), but for this work is was found to be a negligible correction and will be neglected.

The equilibrium strain e'_{ij}, is found from the preceeding equations by minimising the sum of E_{el} and E_{mag} with respect to the strains:-

$$e'_{ij} = - \frac{E^{o}_{kl}}{C_{ijkl}} \qquad \ldots(4.4)$$

If the magnetostriction in a particular direction defined by the direction cosines β_i, β_j is denoted by λ then:-

$$\lambda = - \frac{E^{o}_{kl}}{C_{ijkl}} \beta_i \beta_j \qquad \ldots(4.5)$$

This may then be reduced by considering the symmetry of the cubic crystal where there are only three independent C_{ijkl}, $C_{11} = C_{iiii}$ $C_{12} = C_{iijj}$ and $C_{44} = C_{ijij}$ $(i, j = 1,2,3;\ i \neq j)$ and all the others are zero (12).

Using symmetry arguments phenomenological expressions linking the E^{o}_{kl} to the direction cosines of the magnetisation vector $(\alpha_1, \alpha_2, \alpha_3)$ via magnetoelastic coupling constants, have been obtained (3) such that the solution of (4.5) to second powers in α is given by:-

$$\lambda = h_o + h_1 S(\alpha_1^2 \beta_1^2) + 2h_2 S(\alpha_1 \alpha_2 \beta_1 \beta_2) \qquad \ldots(4.6)$$

where S indicates a cyclic permutation of the suffices of α, β and the h's are given in terms of the elastic stiffness constants and the magnetoelastic coupling constants. The explicit form for these together with the five constant derivation of equation 4.6 is given by Birss and Isaac in reference (4). A subtraction of the magnetostriction from the ideal demagnetised state, λ_o, leads to the more usual form of the magnetostriction (5) which to second order (as above) gives:-

$$\lambda - \lambda_o = h_1 \left[S(\alpha_1^2 \beta_1^2) - \tfrac{1}{3} \right] + 2h_2 \left[S(\alpha_1 \alpha_2 \beta_1 \beta_2) \right] \qquad \ldots(4.7)$$

where h_1 and h_2 are the first two magnetostriction constants ($h_1 = 3/2\ \lambda_{100}$; $h_2 = 3/2\ \lambda_{111}$). The corresponding magnetoelastic coupling constants corresponding to this two constant expression are:-

$$b_1 = - h_1 (C_{11} - C_{12}) \qquad \ldots(4.8a)$$

$$b_2 = - 2h_2 C_{44} \qquad \ldots(4.8b)$$

Similar arguments starting with equation (4.5) may be used to determine the relations for other classes of crystal, and many of these (6,7) include up to nine constants. In this work, magnetostriction measurements were performed on cubic crystals where the two constant expression is believed to be sufficient so further extensions of this argument (see for example reference 1) have been omitted here.

4·3 Microscopic Origins of Magnetostriction

The origin of magnetostriction is inherently linked with the magnetic anisotropy since it arises from a strain dependence of the anisotropy energy. Hence the mechanisms which are responsible for the anisotropy will, in turn, through any strain dependence produce magnetostriction. But with magnetostriction, unlike anisotropy (sec. 3·3) the calculation of the magnetostrictive properties of a real material is more complex since first derivatives, to first order in strain, of the energy densities are involved. Furthermore a knowledge of the ordinary elastic constants is necessary. Detailed calculations, however, have been attempted for certain rare earth materials (for example Gd refs. 8, 9) and also for Ni (10) and the Co^{+} ion in spinels (Slonczewski, ref. 11).

In a similar way to the magnetocrystalline anisotropy, the origins of the magnetostriction are considered to be both single-ion and two-ion and as mentioned above their derivatives with respect to the strain must be included. Following the notation of ref. (4) the Hamiltonian, in terms of spin operators, is written:-

$$\mathcal{H} = S_i J^{o}_{ij} S_j + e_a S_i \left(\partial J_{ij} / \partial e_a \right) \cdot S_j + S_i \cdot D^{o} S_i + e_a S_i \cdot \left(\partial D / \partial e_a \right) \cdot S_i + \frac{1}{2} C_a e_a^{2} \qquad \ldots (4.9)$$

where C_a is the appropriate elastic constant for the strain, e_a. A suitable combination of $(\partial J_{ij} / \partial e_a)$ and $(\partial D / \partial e_a)$ will correspond to the magnetoelastic coupling constants b_1, b_2 (4·8) above.

The terms of equation (4.9), in order, are the two-ion exchange and its strain dependence, the single-ion anisotropy and its strain dependence and finally the elastic energy term. The forms of $\partial J_{ij}/\partial e_a$ and $\partial D/\partial e_a$ have been tabulated in the literature (12,13) and the origins of the two-ion interactions discussed further by Kanamori (14) and Wolf(15).

4.3.1. Dipole-Dipole Interactions

This was first investigated by Becker in 1930 (16) in this case the strain dependence of the dipolar energy of the lattice was determined. The dipolar interaction is:

$$E_d = \sum_{ij} \left[\frac{\mu_i \mu_j}{r_{ij}^3} - \frac{3(\mu i \cdot r_{ij})(\mu j \cdot r_{ij})}{r_{ij}^5} \right] \qquad \ldots (4.10)$$

where the μ_i, μ_j are the moments on the i and j lattice points and r_{ij} the vector joining the ionic moments. When the lattice is allowed to deform homogeneously the dipole energy changes and Becker shows that the effect of all homogeneous distortions can be expressed in terms of a single lattice sum:

$$S = \frac{3}{2} \sum \left(\left|\frac{1}{r_{ij}}\right|^3 - 5 \left|\frac{x^4}{r_{ij}}\right|^7 \right) \qquad \ldots (4.11)$$

This original method was further extended by Powell in 1931 (17) and a further clarification of the problem was given by McKeehan in 1933 (18). It was then possible to calculate magnetoelastic coupling constants

from this mechanism which has been attempted more recently (19) using a summing method due to Kornfeld (20). However the fit to experimental results is so far poor (ref.4, p.305) and the dipole-dipole mechanism appears only to account for a fraction of the observed effects.

4.3.2. Single-ion model

In this case the exchange is considered to be isotropic and the magnetostriction is considered to arise from the perturbation to the single-ion by the strain derivative of the crystal field potential. The separate effects then taken to appropriate order will introduce a linear strain dependent perturbation to the single-ion Hamiltonian.

Investigations have been made by Tsuya (19) for various compounds and in Cu ferrite where $S = 1/2$ and crystal field effects vanish, observed a coupling which appeared to be dominated by dipole-dipole effects. Other work using the single-ion approach by Slonczewski (11) Clarke 1966 (21) is described in reference (4).

4.4. The Temperature Dependence of Magnetostriction

The approach to the temperature dependence of the magnetostriction is identical to that employed for the anisotropy (section 3.4). The spontaneous magnetisation, M_S, is reduced by its thermal spread around its preferred direction. In this case it is the E^o and E^o_{ij} of equation (4.3) which are assumed to have their 0 K magnitudes but the spread of directions. Since the E^o_{ij} are only products of the magnetoelastic coupling constants with α_i, the direction cosines, the temperature dependence of the magnetoelastic coupling constants, and through them the magnetostriction constants, may be obtained.

In a similar way to the derivation of the anisotropy constants, the E_{ij} are expanded in terms of spherical harmonics, $Y_{\ell m}(\theta,\phi)$:-

$$E^{o}_{ij} = \sum_{\ell=o}^{\infty} \sum_{m=-\ell}^{+\ell} k^{ij}_{\ell m} Y_{\ell m}(\theta, \phi) \qquad \ldots (4.11)$$

Where the $k^{ij}_{\ell m}$ are the magnetoelastic coupling coefficients (c.f. anisotropy coefficients, equation 3.3) and are related to the magnetoelastic coupling constants. The temperature dependence can then be derived in a similar fashion to the anisotropy coefficients. (for details of the calculation see references 3 and 4) so that:-

$$\frac{k^{ij}_{\ell m}(T)}{k^{ij}_{\ell m}(0)} = m(T)^{\ell(\ell+1)/2} \qquad \ldots (4.12)$$

where m(T) is the reduced magnetisation ($M_S(T) / M_S(0)$). The temperature dependence of the magnetoelastic coupling constants may then be determined from the set of $k^{ij}_{\ell m}$. In the cubic case, for the simple two constant expression (4.7) the two coupling constants b_1 and b_2 (4.8) are given by:-

$$b_1(T) = b_1(0) \left[m(T) \right]^3 \qquad \ldots (4.13a)$$

$$b_2(T) = b_2(0) \left[m(T) \right]^3 \qquad \ldots (4.13b)$$

This relation may also be determined generally for all other, higher order, magnetoelastic coupling constants using the single-ion approach

(Callen and Callen ref.22). This argument has also been extended to cover other crystal symmetries and to include possible two-ion effects (23).

4.5 Volume Magnetostriction

In the expansion for the magnetostriction is is usual to include a term h_o which represents the isotropic volume change due to the change of magnetisation of the sample. Thus the expression for the spontaneous magnetostriction for cubic crystals is:-

$$\lambda = h_o + h_1 (\alpha_1^2\beta_1^2 + \alpha_2^2\beta_2^2 + \alpha_3^2\beta_3^2 - \tfrac{1}{3}) + 2h_2 (\alpha_1\alpha_2\beta_1\beta_2 + \alpha_2\alpha_3\beta_2\beta_3 + \alpha_3\alpha_1\beta_3\beta_1) + \cdots \quad \ldots(4.14)$$

Although rotation of the magnetisation introduces no volume change to first order, (i.e. to α_i^2), the term h_o has a temperature dependence and the appearance of magnetic order at the Curie temperature results in a spontaneous volume strain which will give rise to the anomalous thermal expansion. The isotropic volume change $\Delta V/V$ will be equal to the sum of the three orthogonal cubic strains. Hence, for this case:

$$\frac{\Delta V}{V} = e_{xx} + e_{yy} + e_{zz} \simeq 3h_o(T) \quad \ldots(4.15)$$

4.6 Forced Magnetostriction

In the above section we have considered the change in magnetostriction due to the change in magnetisation with temperature. A change in the constant may also be produced by increasing field above saturation, which increases the alignment of the thermally agitated

spins, sometimes known as the paraprocess.

Since in high fields the magnetisation is parallel to the field, the forced magnetostriction has the same symmetry as the spontaneous magnetostriction and may thus be written, for a cubic crystal, in the same way as equation (4.7)

$$\frac{\partial\lambda}{\partial H} = h_o' + h_1' + (\alpha_1^2\beta_1^2 + \alpha_2^2\beta_2^2 + \alpha_3^2\beta_3^2 - \tfrac{1}{3}) + 2h_2' (\alpha_1\alpha_2\beta_1\beta_2 + \alpha_2\alpha_3\beta_2\beta_3 + \alpha_3\alpha_1\beta_3\beta_1) + \ldots \quad \ldots(4.16)$$

Where the h_i' are the forced magnetostriction constants and are $\partial h_i / \partial H$. The h_o' is usually dominant and hence the forced magnetostriction is often referred to as a "volume" effect (cf. equation 4.15). However, measurements have been performed to determine h_1' and h_2' for several metals and alloys of Ni and Fe (10, 24, 25). The temperature dependence of the forced magnetostriction is expected to follow the temperature dependence of the magnetisation which has been observed to be true for Gd (26).

4.7 The Form Effect

The shape of a sample may also influence the volume magnetostriction because the magnetostatic energy density E^o in equation (4.3) will have a volume dependence due to the volume independence of the demagnetising factor. Analysis shows that a feature of this effect is that it increases as M^2 and reaches a saturation value at M_S (ref 27) of:

$$\left[\frac{\Delta V}{V}\right]_s = \frac{3NM_S^2}{2(C_{11} + 2C_{12})\mu_o} \quad \ldots(4.17)$$

The form effect will also give rise to linear magnetostrictions due to the shape derivatives of the demagnetising factors. This effect has been treated in detail by Gersdorf (28) for both a uniform strain approximation and also taking a non-uniform strain, demonstrated by Brown (29), into account. He has observed that the non-uniform strain effect is not small for a spherical sample, by comparison of some experimental work (30) with the theory.

CHAPTER 5

5. EXPERIMENTAL

This chapter is divided into three main sections. The first describes the procedures used in preparing the single-crystal samples used in this work. The major part of the preparation of these samples was performed at the Centre for Materials Science, University of Birmingham. The second section is a description of the torque magnetometer used for measurements of the magnetocrystalline anisotropy of these samples and the final section describes the apparatus used for the magnetostriction measurements. The work described in the last two section was undertaken at Southampton University.

5.1. Single Crystal Preparation

5.1.1. Introduction

In this section is described the methods employed in the preparation and growth of single crystals of the compounds of the type RAl_2, and their subsequent alignment cutting and characterization. These compounds have congruent melting points at approximately 1500°C and a Czochralski method was employed similar to that described by Purwins et al (1,2) using equipment available at the Centre for Materials Science, University of Birmingham. Most of the characterisation work which included metallographic analysis and X-ray microprobe and powder photography was also undertaken at the Centre.

5.1.2. Metallurgical Aspects

The rare earth dialuminides although having the same C15 cubic Laves structure (3) as the RFe_2, RNi_2 and RCo_2 compounds with rare earths are different in that they are congruent melting (4). i.e. the compound exists at all temperatures upto its melting point, which is a maximum in the phase diagram (see fig. 5.1.1). This peak in the liquidus line means that any variation of the composition RAl_2 in the liquid state brings about a lowering of the melting point. Hence the first crystallisation is of the precise composition RAl_2. Thus a crystal growth technique involving slow solidification can be particularly successful especially where the production of any second phase is to be avoided.

The Czochralski method (5) used in this case utilised a Bridgman 265 (6) apparatus (produced by Metals Research Ltd.) which had been modified for crystal pulling. The apparatus consists of a silica tube which could be evacuated or filled with an inert gas surrounded by a jacket. Radio frequency heating was employed using a 35 kW R.F. generator.

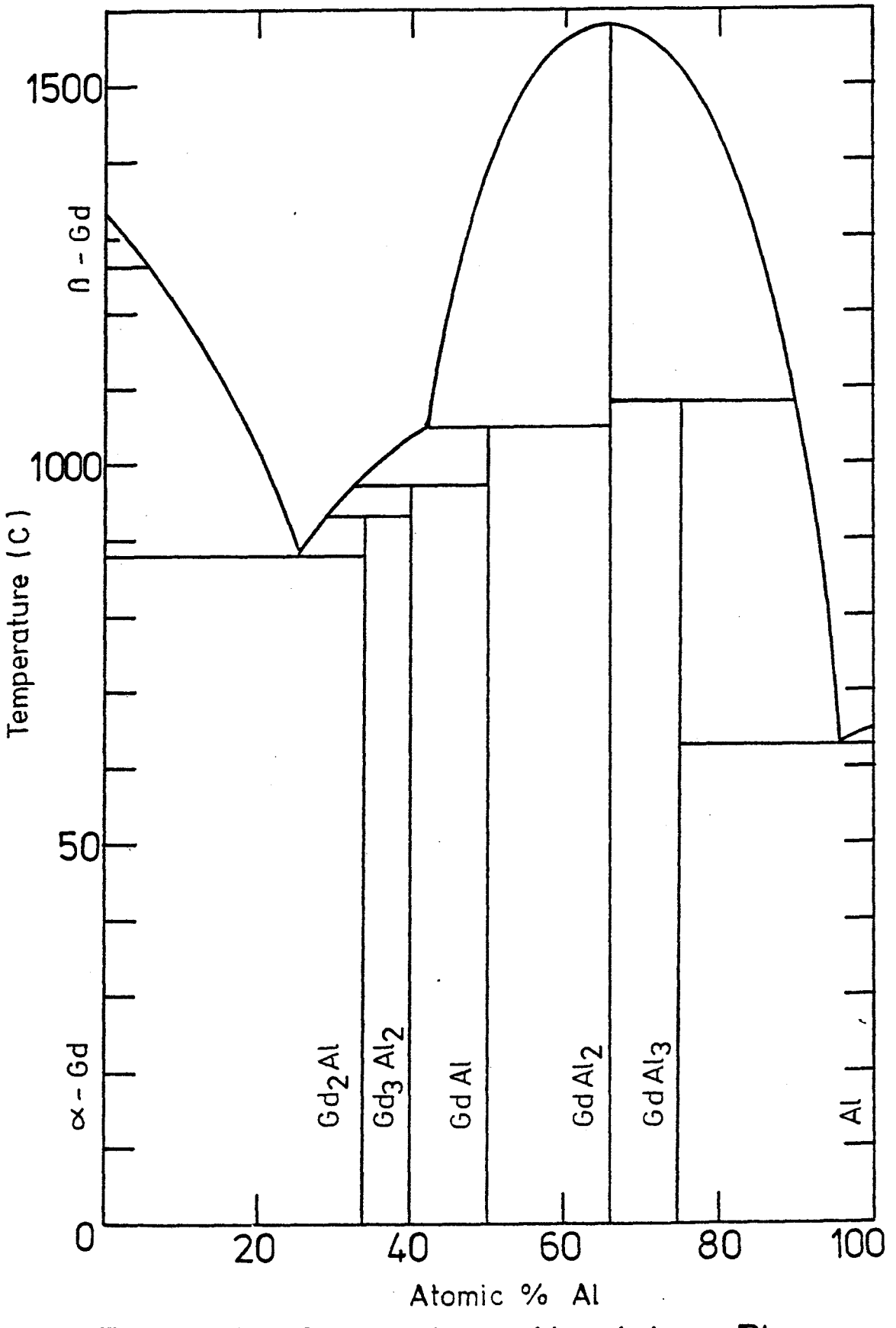

Fig. 5·1·1 Gadolinium Aluminium Phase Diagram

The temperatures employed mean that the molten material, which consists of the rare earth and Al previously melted in stoichiometric composition in an arc furnace, must be within an inert atmosphere. The partial vapour pressure of the Al and in some cases, that of the rare earth precludes the use of an evacuated tube. An over pressure of one atmosphere of ultra high purity argon gas (via a purifier) was used to provide an inert atmosphere and some reduction in the rate of loss of the melt.

A second major problem is containment. The rare earth metals themselves are extremely reactive, even at room temperature, and at the elevated temperatures associated with the molten compound, these effects are even more pronounced. Most refractory oxides are reduced in the presence of rare earth metals and boron nitride is also seriously affected. The only remaining materials are the refractory metals, and tungsten, in spite of machining problems, is the most suitable having very limited solubility in the rare earths, (ref. 7). However the tungsten crucibles used proved to have a very limited lifetime and had to be annealed at 1000°C for several hours before use. However the tungsten turns out to be an extremely good susceptor for the radio frequency eddy current heating field and hence its efficiency is good.

5.1.3. Compound Preparation

This section is written with specific reference to the compound $GdAl_2$; however the process involved in producing the other samples was essentially the same.

The compound was initially prepared from 4N aluminium (Johnson Matthey Ltd) and nominally 3N Gd (Rare Earth Products Ltd), by melting together weighed amounts of the stoichiometric composition

in an argon arc furnace under approximately 1/2 atmosphere of argon on a water cooled copper hearth. After initial melting of the two constituents the reaction was seen to proceed exothermically. The melted button was then inverted and remelted to ensure homogeneity.

Test weights of material were melted by this method and then re-weighed, the loss of material in this stage of the process was found to be negligible.

5.1.4. Crystal Growth Apparatus

The crystal pulling apparatus used was an already existing Bridgman 265 (Metals Research Ltd) with a Czochralski pulling attachment. The system has an inner furnace tube of silica glass and an outer one of pyrex , the intervening space being filled with water flowing at 3 litres/minute. The apparatus also has a vacuum system and facilities for filling the furnace tube with inert gas.

The spun tungsten crucible rests on a silica glass or tantalum support on the water cooled base of the furnace tube. The pulling system consists of a threaded outer rod with a rotatable stainless steel inner, the speed of rotation and pull being controlled by means of two continuously variable speed, operator controlled, electric motors.

Power input to the system is by means of a seven turn induction heating coil formed from 3/8" copper tube which is water cooled, wound around the outside of the outer furnace tube. Radio frequency power input is provided by a 35 kW Stanelco Radio Frequency generator. The R.F. field set up within the coil produces eddy current heating in the tungsten crucible and temperatures up to 2000°C could

be obtained with this system. A small single turn copper coil attached to a rectifier and chart recorder situated near the power coil was used to give a record of power levels throughout the process. The temperature of the crucible contents was monitored using an optical pyrometer. A diagram of the apparatus is given in figure 5.1.2.

5.1.5. Crystal Pulling Procedure

After annealing the tungsten crucible and heating it to a high temperature (approximately 1000°C) to remove the oxide coating, the prepared compound (sec.5.1.3) was loaded into the crucible in the furnace tube and the system evacuated to approximately 10^{-6} torr. The crucible and contents were then outgassed at an intermediate temperature determined by the volatility of the components.

After cooling the furnace was flushed with the high purity argon used as the inert atmosphere during the pulling process. This was supplied from a British Oxygen Company type RGP Ar/He purifier running on industrially pure Ar. The ultimate impurities in the argon after secondary purification are quoted to be less than 2 volumes per million total impurities (8).

The system was then sealed and the argon pressure reduced to approximately 2/3 atmosphere. The R.F.heating was started slowly to avoid thermal shock to the crucible. After the molten-state was achieved the 'seed' rod (also of tungsten and attached to the end of the pulling rod) was lowered into the melt and then withdrawn. The small amount of material acts as a polycrystalline seed and the subsequent pulling procedure is designed to promote the growth of one particular grain. The temperature of the furance was maintained such

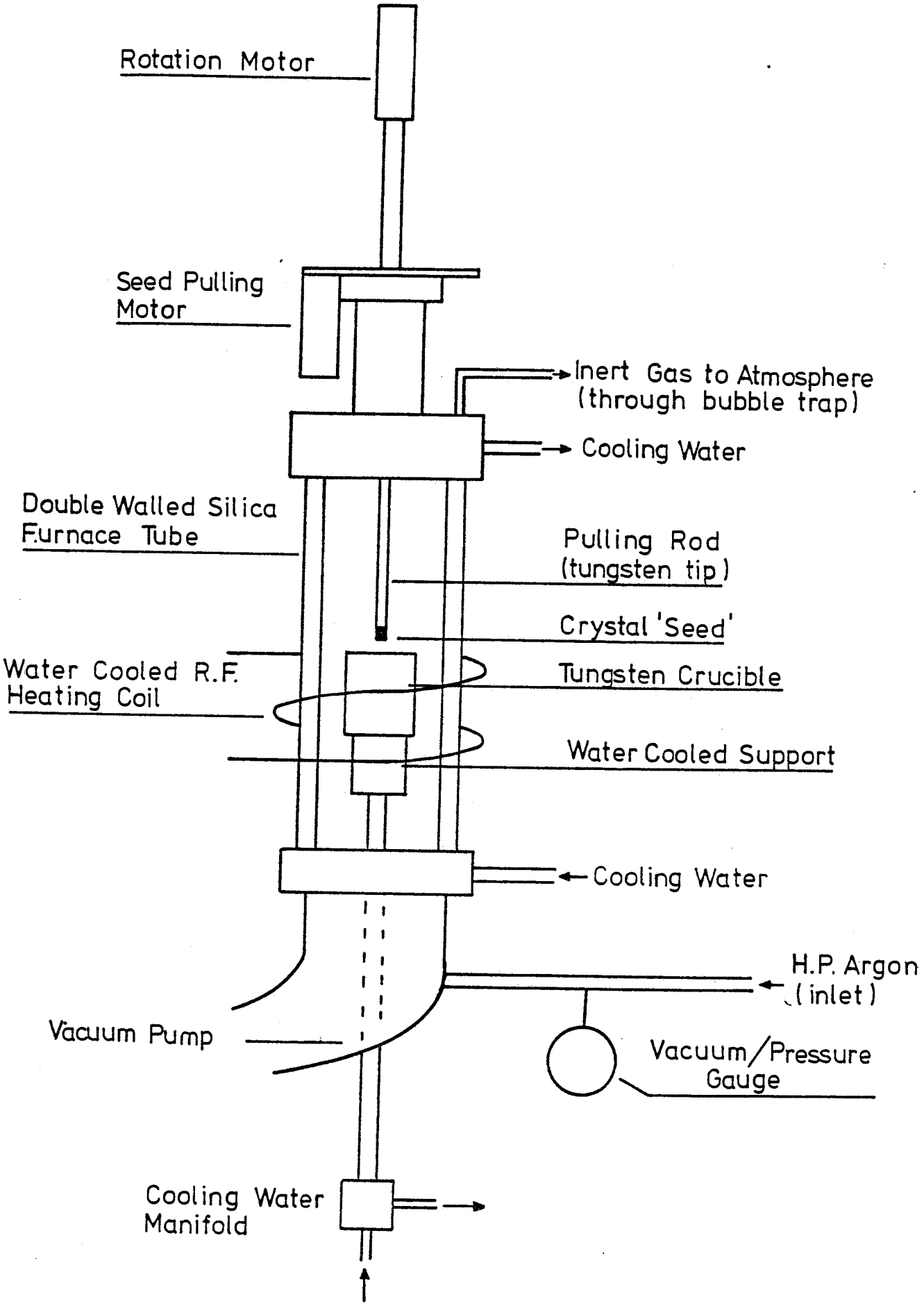

Fig. 5.1.2 The Crystal Growth Apparatus

that the polycrystalline seed grows into a long 'neck' so that one grain only was finally selected. The forming boule was then thickened by reducing the furnace temperature slightly and growth continued. Although attempts have been made to control boule thickness automatically (ref. 8a) constant adjustment using visual observations was found to be satisfactory in this case. Once a sufficiently large sample had been obtained the boule was pulled clear from the melt and the furnace slowly cooled to prevent thermal shock to both crucible and sample material.

The boule size appears not to be critically dependent on the rates of pull or rotation. The boule is rotated to provide a thermal gradient which is cylindrically symmetric with its axis in the pulling direction. By far the most sensitive control is furnace temperature which directly affects the thermal gradient, which must be such that the lowest temperature in the molten system (i.e the solid-liquid interface) is at the base of the seed.

5.1.6. Sample characterization

Characterization falls into two categories, crystallographic and compositional. Firstly we wish to know if the material is single-crystal and if so what its structure / orientation is, and secondly, we wish to know whether it contains a significant amount of impurities and whether it is actually of the correct stoichiometry.

(a) The initial procedure after the boule had been removed from the furnace involved back reflection Laue X-ray photographs taken across the surface of the sample. Where the material was single-crystal identical patterns were obtained from points along the boule length separated by several centimetres. When this test was successful a more intensive

investigation of the whole surface was undertaken to determine the extent and quality of the crystal. For the first $GdAl_2$ crystal the growth direction was found to be nearly a [100] direction. The two ends of the boule were then usually removed by spark machining, the top being polycrystalline (see necking procedure 5.1.5) and the lower end where the sample had been pulled away was often rough; and, if the melt had been almost exhausted, of uncertain composition. The exposed faces were then also X-ray photographed to check that the crystal extended across the diameter of the boule.

The Laue patterns were used also to determine the orientation of the crystal and during final cutting further exposures were taken (see section 5.1.7).

(b) In the compositional characterization another X-ray method was used, that of Debye-Scherrer powder photography which is particularly useful for determining the presence of second phase and also gives an accurate value for the lattice parameter. In this work the parts of the sample to be analysed were ground to a fine powder, placed in a glass capillary and attached to the camera. The resultant films, after exposures of several hours, showed a series of lines, all except one faint line being identified with the Laves phase structure and corresponding to the lattice parameters shown in table (5.1.1). The faint line was identified with the glass capillary material in a separate experiment using an empty capillary. The lattice parameters determined from the d-spacings obtained from the lines were subjected to a Nelson-Reilly extrapolation least squares fitted by computer program to arrive at accurate values.

Further characterization procedures undertaken involved optical and S.E.M. microscopy of surfaces lapped with 2μ diamond paste and etched with dilute HCl which showed no evidence of second phase or grain boundaries in the case of single-crystals. X-ray microprobe and chemical analyses were also undertaken. The results of the chemical analysis for the $GdAl_2$ sample were 73.70 wt% Gd and 25.36 wt% Al and included 0.16 wt% Tungsten; this gives a Al to Gd ratio of 2.005 : 1 which is within measuring accuracy of the ideal ratio. The microprobe examination confirmed some crucible contamination of the sample, which appeared as localised dendritic growths of some unidentified ternary with tungsten at the extreme lower end of the boule (Fig. 5.1.3).

5.1.7. Crystal Orientation and Sample cutting

The pieces of crystal from which samples were to be cut were firstly mounted on a three circle goniometer on the Laue X-ray apparatus. A stereographic pojection method was used to identify a particular crystallographic direction (10) and the goniometer adjusted to bring the required axis into line with the beam direction. Further photographs were taken and any adjustments continued until alignment was obtained (estimated $\pm$ 1/2°). The goniometer was then transferred directly to a spark erosion cutting machine (Cambridge Instruments Servomet). Methods of cutting cylindrical and spherical samples are illustrated in figure 5.1.4 .

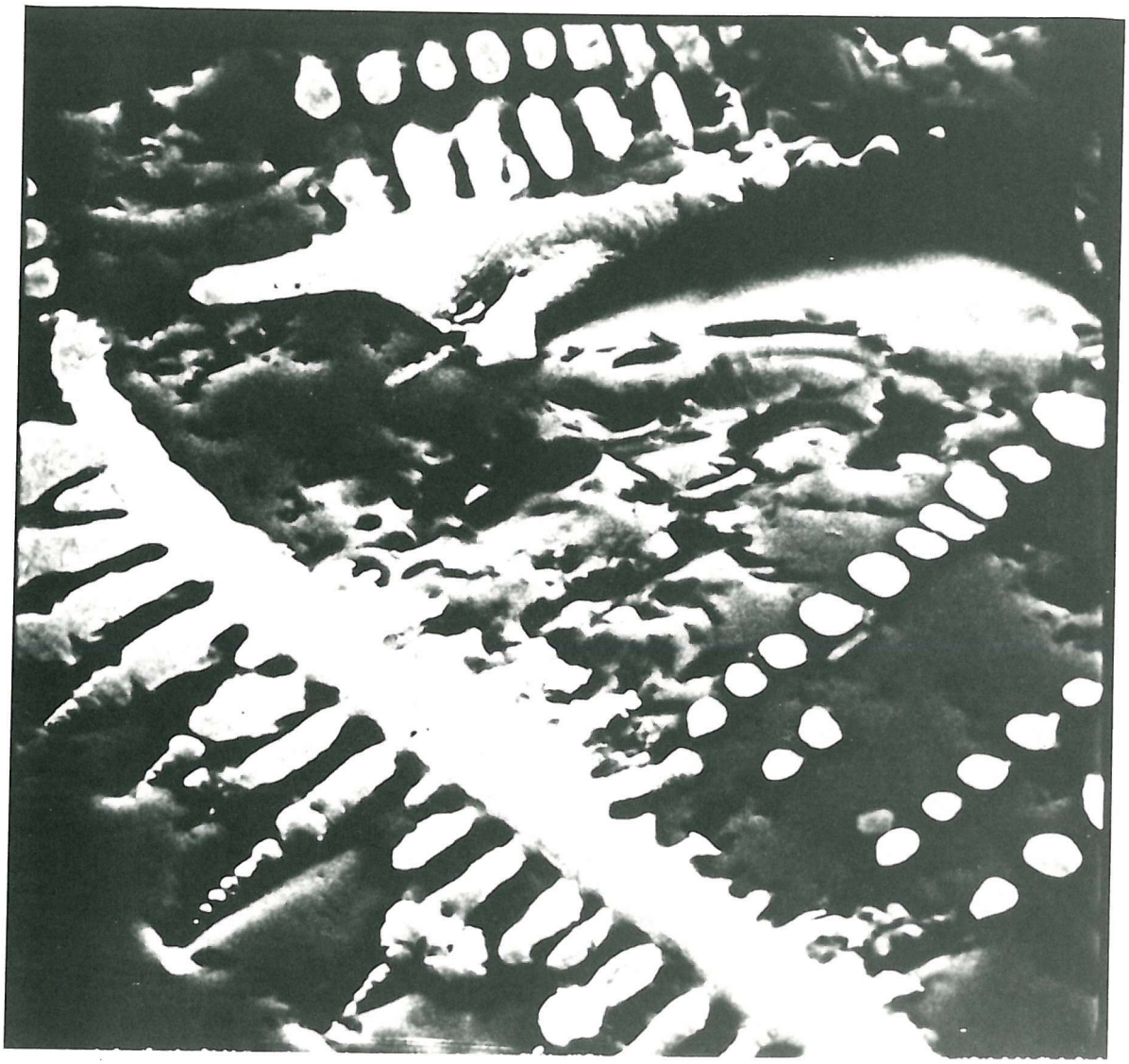

FIG. 5.1.3 Dendritic Second Phase (light areas) of an Unidentified Ternary with tungsten in $GdAl_2$ (x2250)

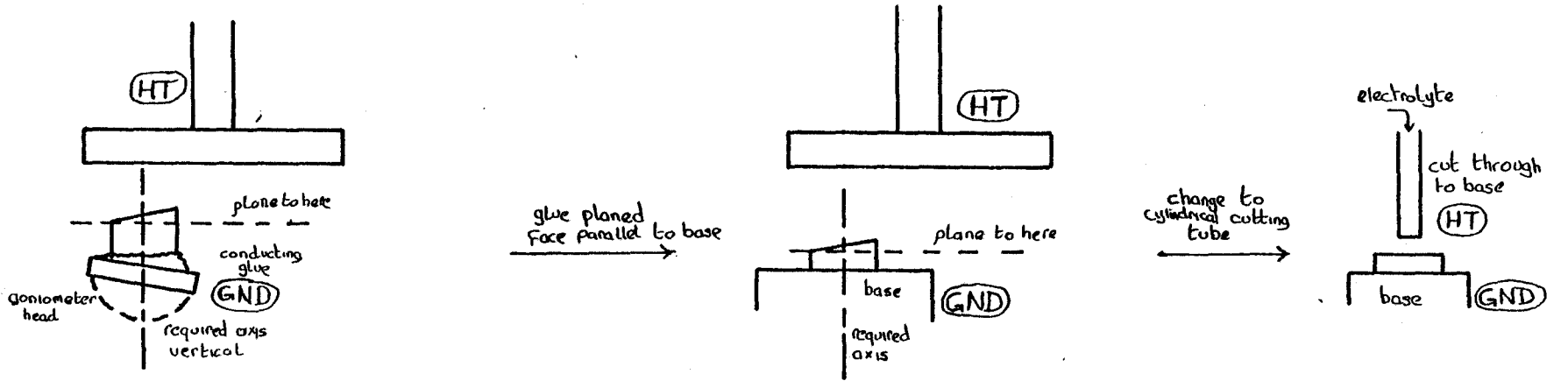

Discs and Cylinders

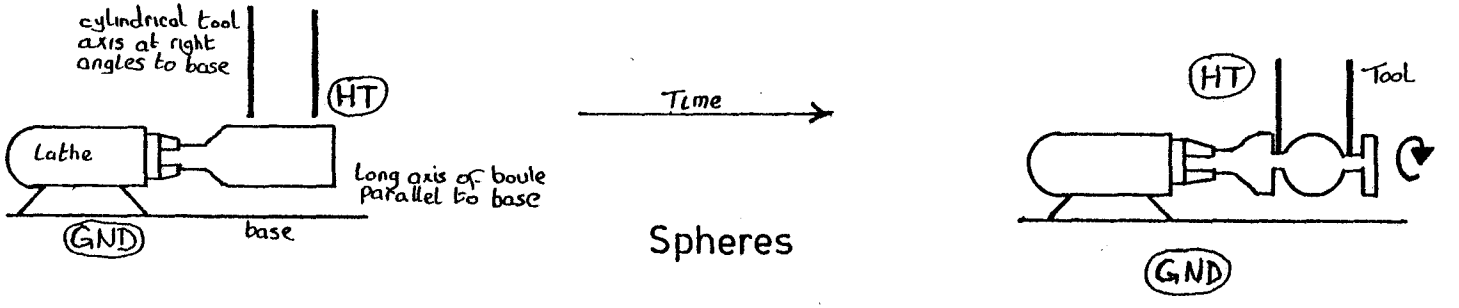

Spheres

Fig. 5.1.4 Sample Cutting Techniques

5.1.8. Summary

The Czochralski Method has been used in this work to successfully produce some binary and pseudobinary RAl_2 compounds and a number of techniques have been used to produce the final samples. The samples produced so far, relevant to this work, are summarised in Table (5.1.2) along with measurements arising from the metallographic studies. This apparatus has also been employed at the Centre for Materials Science, Birmingham University, for producing other rare earth intermetallic compounds by the Czochralski Method (ref.11).

TABLE 5.1.1

Sample	Lattice Parameter (Å)		Theoretical Density	Pyknometric Density
	(This Work)	(Reference 9)	(10^3 kgm^{-3})	(10^3 kgm^{-3})
Gd $A\ell_2$	7.902 ± 0.001	7.901	5.686	5.65 ± 0.07
Tb $A\ell_2$	7.861 ± 0.002	7.864	5.818	
Ho $A\ell_2$	7.817 ± 0.001	7.818	6.086	

TABLE 5.1.2

Sample Material	Orientation and Shape	Dimensions
$Gd\ A\ell_2$	100 Disc	5.54 mm dia x 1.10 mm thick
$Gd\ A\ell_2$	110 Disc	5.50 mm dia x 0.97 mm thick
$Gd\ A\ell_2$	Sphere	2.90 mm dia
$Tb\ A\ell_2$	Sphere	3.10 mm dia
$Tb_{0.02}\ Gd_{0.98}\ A\ell_2$	110 Disc	4.90 mm dia x 1.59 mm thick
$Tb_{0.05}\ Gd_{0.95}\ A\ell_2$	110 Disc	3.80 mm dia x 1.33 mm thick

5.2. Measurement of Anisotropy Constants

5.2.1. Introduction

The measurement of anisotropy constants by means of a torque magnetometer has become an established technique and has several advantages over other methods such as magnetisation curves, ferromagnetic resonance and singular point detection. The magnetisation curve method (12) necessitates accurate alignment of the single-crystal materials and inaccuracies are unavoidable in the assumption that the magnetisation is fully reversible. Furthermore, it may be difficult to separate individual contributions to a particular anisotropy. Ferromagnetic resonance techniques determine an anisotropy field H_a. The resonant condition occurs at a total field which is the sum of the external field and H_a. Singular point detection (13) relies on the appearance in a particular derivative of the M (magnetisation) vs. B curve of a discontinuity which is attributed to $B = B_A$, the anisotropy field. The major disadvantage of this method is that, for successively higher values of n, $\frac{d^nM}{dB^n}$ becomes extremely difficult to detect. The method can successfully be used on polycrystalline samples because only one particular orientation of crystallite will produce the singular point.

The principle of a torque magnetometer is that if a single-crystal is suspended in a magnetic field the magnetisation will prefer to take up a particular orientation with respect to the crystal axes. If the crystal is not free to rotate then the crystal will experience a torque, which is dependent on the anisotropy energy $E_K(\theta)$. The angle θ is the direction of the magnetisation vector with respect to the easy axis in the plane of rotation, and the torque, L, experienced by the crystal is given by:-

$$L = - \frac{d E_K}{d \theta} \qquad \ldots(5.1)$$

Thus, for a particular anisotropy energy expression a measurement of the variation of torque with applied field direction after suitable manipulation will yield the anisotropy constants K. It will be shown in a subsequent chapter that the analysis of torque curves is far from straightforward, and in some cases the extraction of anisotropy constants from torque curves may be inappropriate. However, in the cases where it can be determined that the necessary conditions have been satisfied, torque magnetometry proves to be a powerful method by which all the anisotropy constants of a particular sample may be reliably determined.

5.2.2. The torque magnetometer

Anisotropy measurements were made using the torque magnotometer designed and built at Southampton by Huq (14). This apparatus is similar to that described by Aldenkamp (15) which has a major advantage over the more traditional torsion fibre magnetometers (refs. 16-20) in that the transducer has great lateral rigidity coupled with a high sensitivity to applied torque. Differences exist in the recording system in that whereas Aldenkamp used a differential transformer and automatic recording, in this work the detector is an optical lever and measurements are made at intervals of field rotation. The torque magnetometer can be used over the range of temperatures from 4.2K to 360K and the D.C. electromagnet used is capable of fields up to 2.04 T. An overall diagram of the apparatus is given in Fig. 5.2.1.

5.2.3. The torque transducer and its calibration

The transducers consist of two circular Dural discs approximately 6 cms and 4.5 cms in diameter. The glass rod used to support the sample holder is attached to the lower (small) disc. The two discs are joined by three similar springs made of hard phosphor

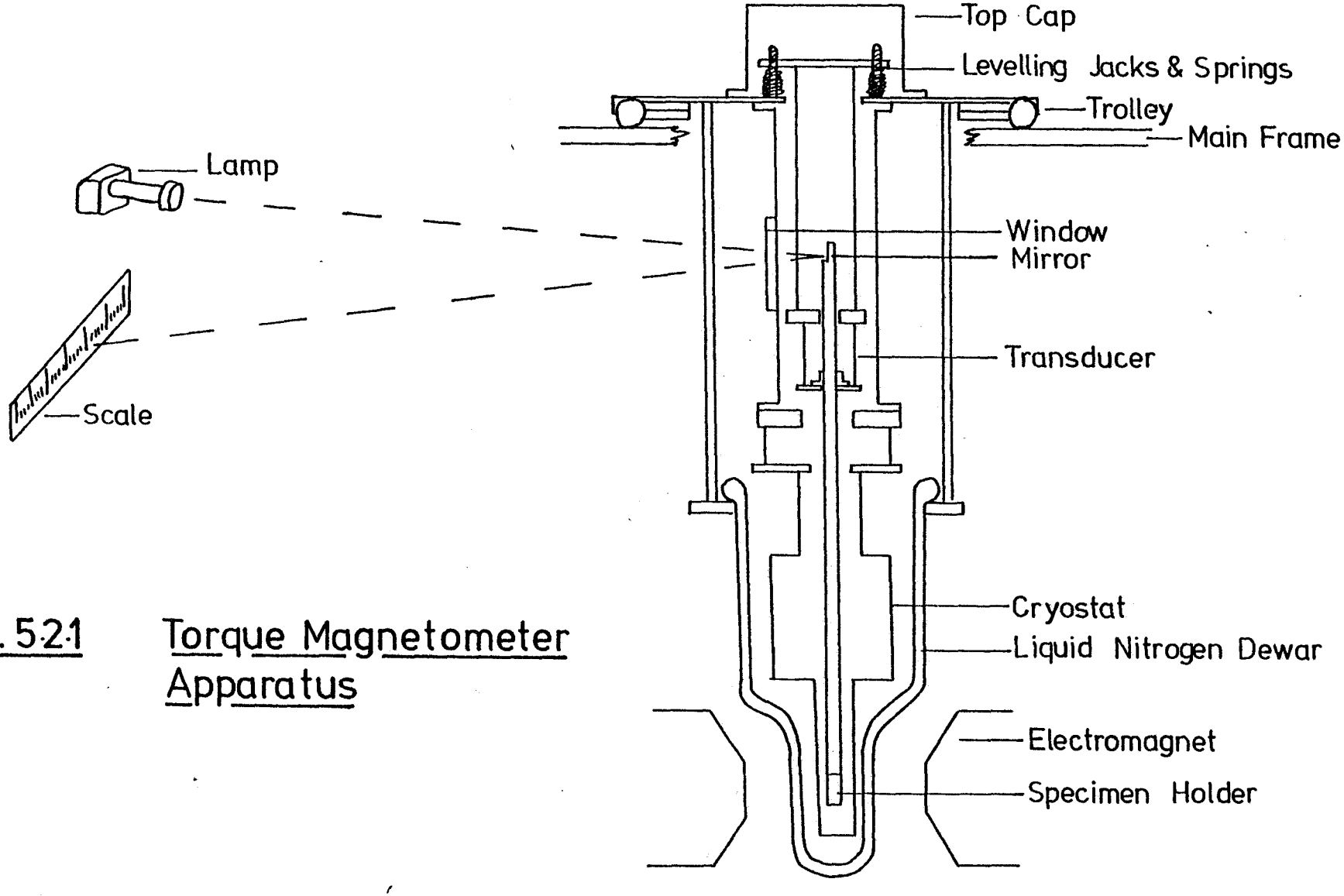

Fig. 5.2.1 Torque Magnetometer Apparatus

bronze mounted at 120° to each other. These springs are etched from sheet material to avoid the edge distortion involved in cutting.

One transducer used was that described and calibrated by Huq (ref. 14). For the measurements on $GdAl_2$ a second, more sensitive transducer was assembled using the same technique. An attempt was made to arrive at some theoretical model which could aid the determination of the spring dimensions and this is discussed in appendix A.

The upper disc is mounted rigidly to the frame of the apparatus via a trolley which has levelling screws and a sliding plate so that the specimen rod may be vertical and central with respect to the pole pieces of the magnet. The disc has a clearance hole in its centre so that the rod which supports the mirror for the optical lever may protrude into the transparent section of the apparatus. The transducer assembly is shown in fig. 5.2.2.

The procedure used for calibration is similar to that described in reference (14). A search coil of approximately 100 turns was wound from 40 s.w.g. wire on a square former which was about 1 cm^2. The coil was used in place of the sample on the end of the sample rod. The deflection was maximised by rotating the magnet keeping the search coil current constant.

For a current i flowing in a coil in a field B (Tesla) the torque L (N m) is given by:-

$$L = B\,(An)\,i \cos\theta \qquad \ldots(5.2)$$

where θ is the angle between the field direction and the plane of the

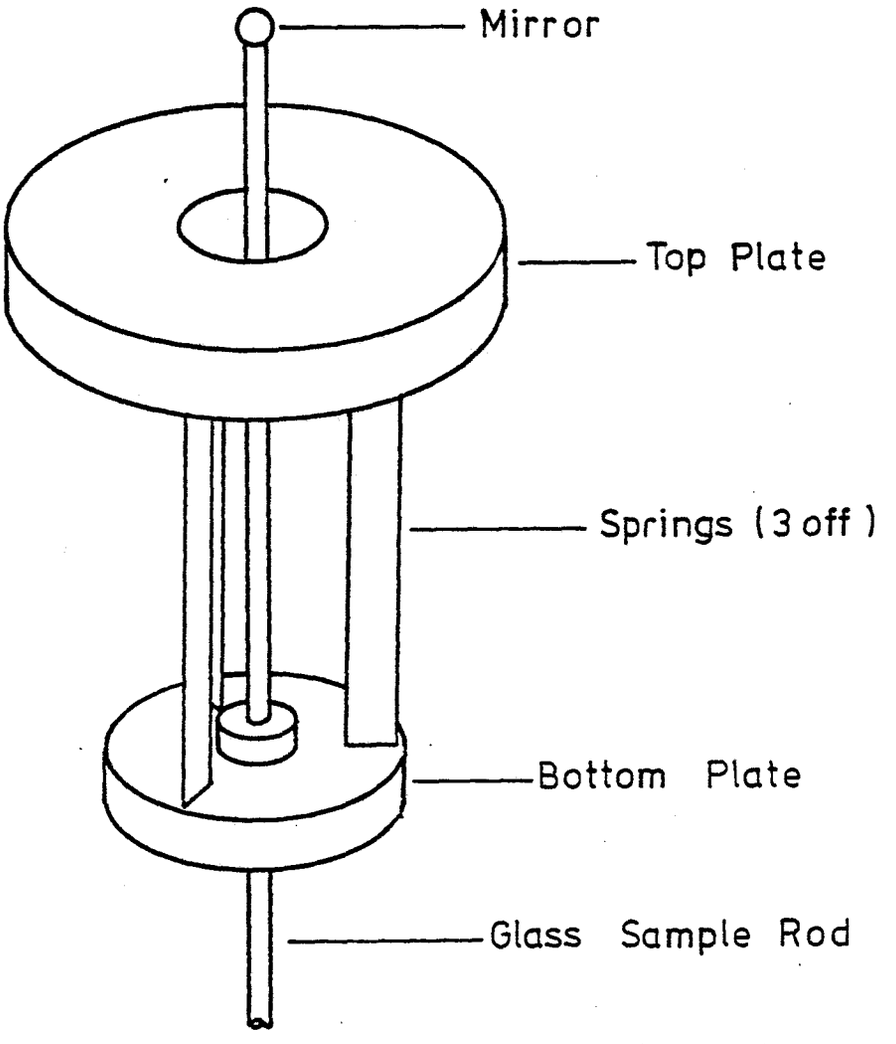

Fig.5·2·2 The Torque Transducer Assembly

coil and An the number of turns multiplied by the coil area.

The turns-area product of the coil was independently determined by rotating it at 50 Hz in a N.M.R. calibrated magnetic field Bo. The e.m.f. produced in the coil was taken off by means of carbon brushes and slip rings and integrated using a Tektronix type O unit, the peak-peak voltage could then be determined from:

$$V = \frac{\partial}{\partial t} \text{Bo (An) } \cos \omega t \qquad \ldots(5.3)$$

for the integrated signal:

$$V \text{ out} = \frac{1}{RC} \int V \, dt \qquad \ldots(5.4)$$

where RC is the time constant of the integrator which, for reliable integration must be $<< \omega$, in this case $RC = 10^{-2}$. This gave a value for the turns-area product of $(1.30 \pm 0.02) \times 10^{-2} \text{ m}^{-2}$.

This calibration in turn gave the sensitivities of the two transducers after deflection vs coil current at constant field had been determined for each transducer. Deflections were measured for both positive and negative torques and both transducers were found to have a high degree of linearity up to large deflections. The sensitivities were, for transducer one, used for cobalt and the dilute alloys $(1.08 \pm 0.02) \times 10^{-4}$ Nm (mm deflection)$^{-1}$ and for transducer two, used for $GdAl_2$ measurements $(8.40 \pm 0.05) \times 10^{-6}$ Nm (mm deflection)$^{-1}$.

5.2.4. The sample holder

The sample holder was similar to that described in reference (14) consisting of a hollow copper cylinder which was attached to the lower end of the sample rod. The disc-shaped single-crystal samples were cemented to a cork spacer which was cemented to the sample holder. Durofix was used having been found to provide satisfactory bonding down to the lowest temperatures used. The holder had wound around it a bifilar-wound heating coil of constantan having a resistance of approximately 50Ω. The temperature of the sample was measured by means of a copper-constantan thermocouple cemented to the sample itself using an ice-point reference. The sample temperature is estimated to be accurate to $\pm$ 0.5K.

5.2.5. The temperature sensors and controller

The temperature sensors were initially a non-inductively wound coil of 48 s.w.g. enamelled copper wire and subsequently an Allen-Bradley carbon 1/8W resistor both attached to the sample holder. The use of two sensors gave reliable performance over the whole temperature range. The copper coil was used from room temperature down to liquid nitrogen (77K) and the Allen-Bradley resistor below 77K. Their individual temperature characteristics are shown in figure 5.2.3.

The sensors could be independently connected to the input of a simple proportional temperature controller. The controller was used successfully above 77K but some difficulty was experienced in stabilisation at lower temperatures, especially between 4.2K and 50K. Some improvement is expected if a more sophisticated controller were

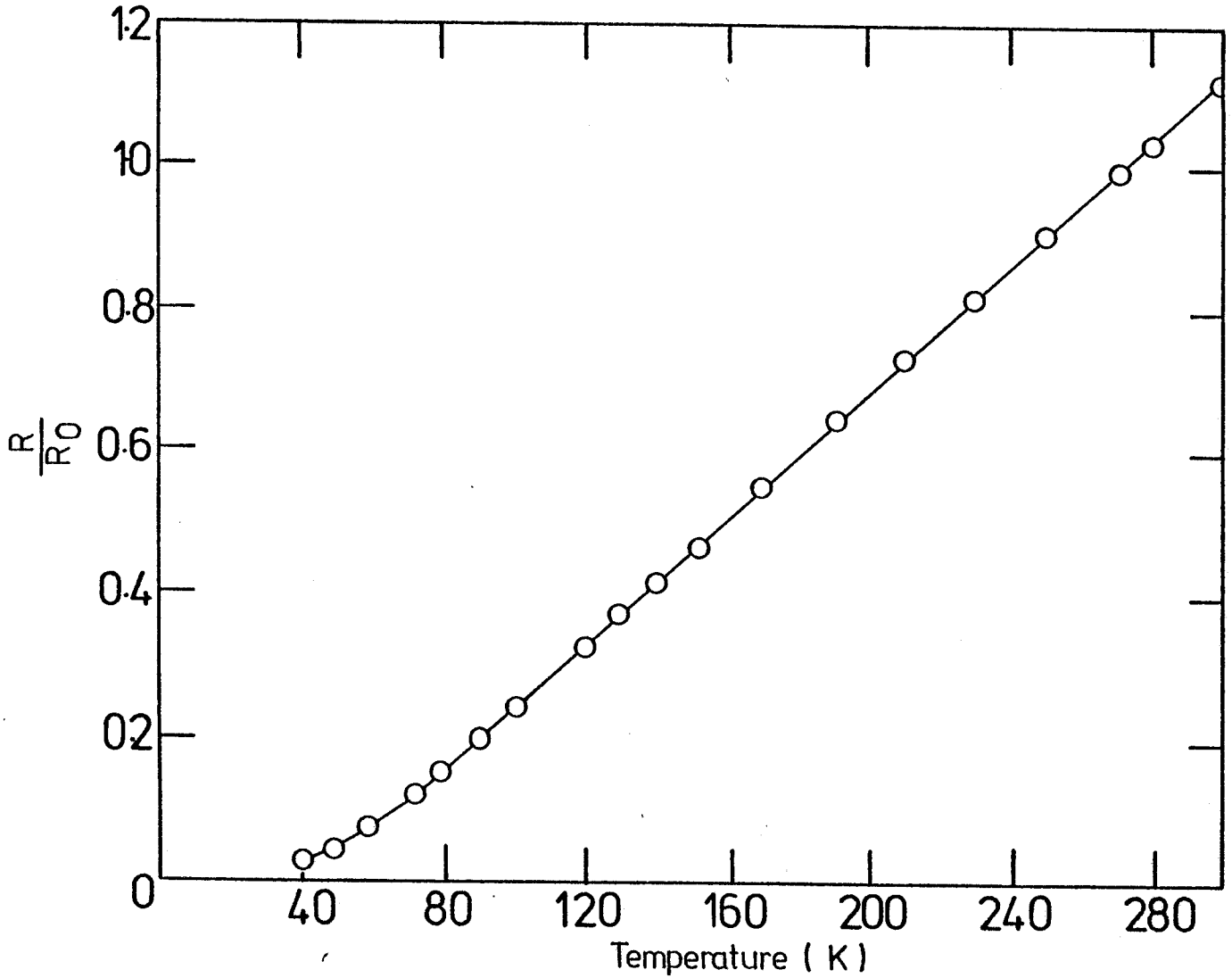

Fig. 5·2·3a Temperature Resistance Curve for a Copper Resistance Thermometer

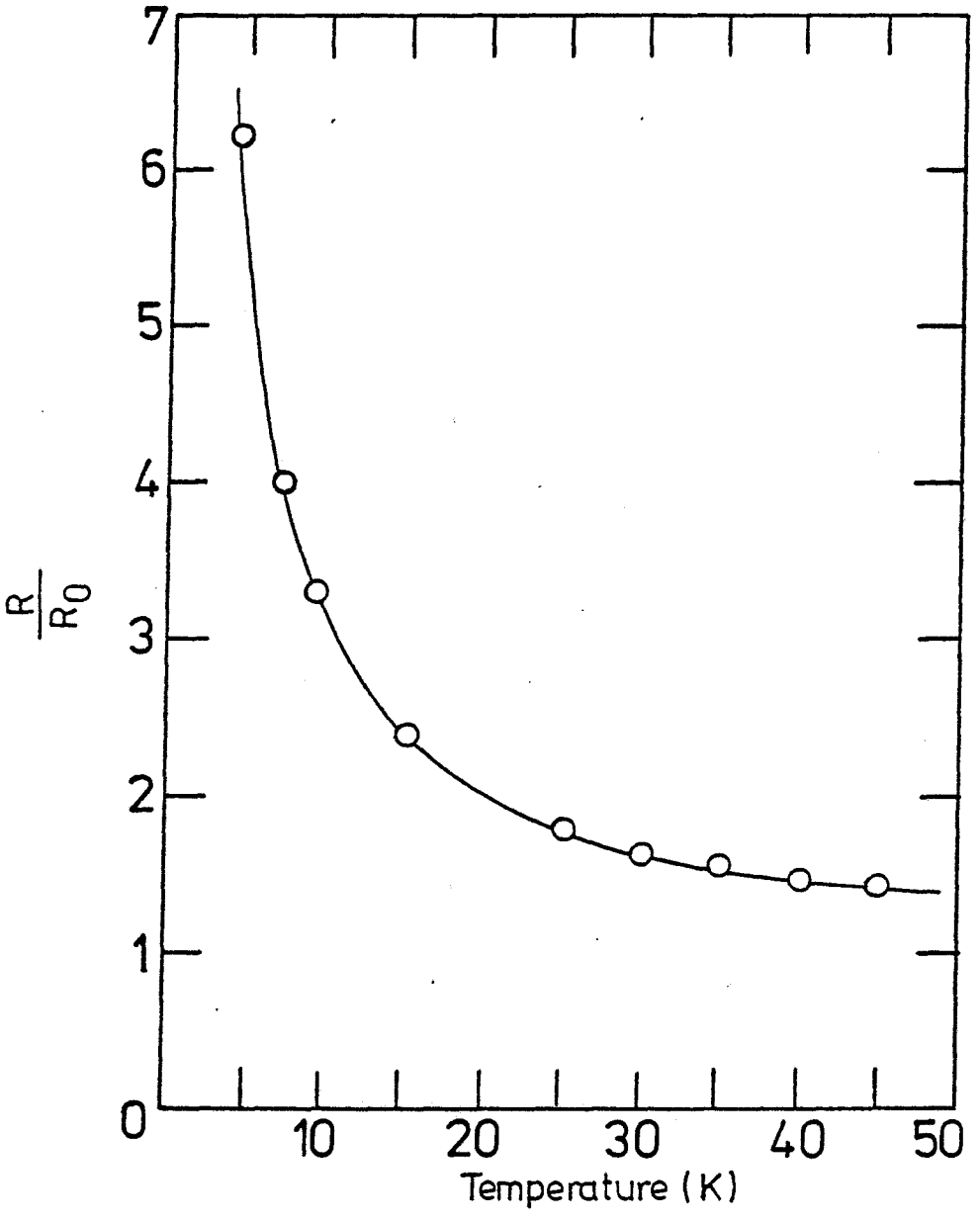

Fig. 5·2·3b Temperature Characteristics of an Allen Bradley Resistor

to be used. The mode of operation, shown in block form in figure 5.2.4. is that the external sensor is in one arm of a bridge network which is compared to the set resistor in the opposite arm. The out-of-balance voltage determines whether an operational amplifier has +ve or -ve feedback; if -ve the output switches off, and if +ve the oscillation is rectified and amplified to produce heater current proportional to the out-of-balance signal.

5.2.6. The vacuum system

The vacuum system was of conventional design with facilities for evacuating each section of the apparatus and cryostat independently. It is also possible to admit inert exchange gas (helium) to the system. A block diagram of the system is shown in figure 5.2.5.

5.2.7. The helium cryostat

The helium cryostat was of the conventional three-wall type with a long tailpiece, external diameter 26 mm to enable it to be placed between the magnet poles. It was constructed in the Physics department workshop and design details are given in reference 14. An outer glass dewar was mounted around the cryostat to contain liquid nitrogen when liquid helium was to be used. Without the dewar temperatures down to 55K (by pumping) could be obtained with liquid nitrogen in the helium can.

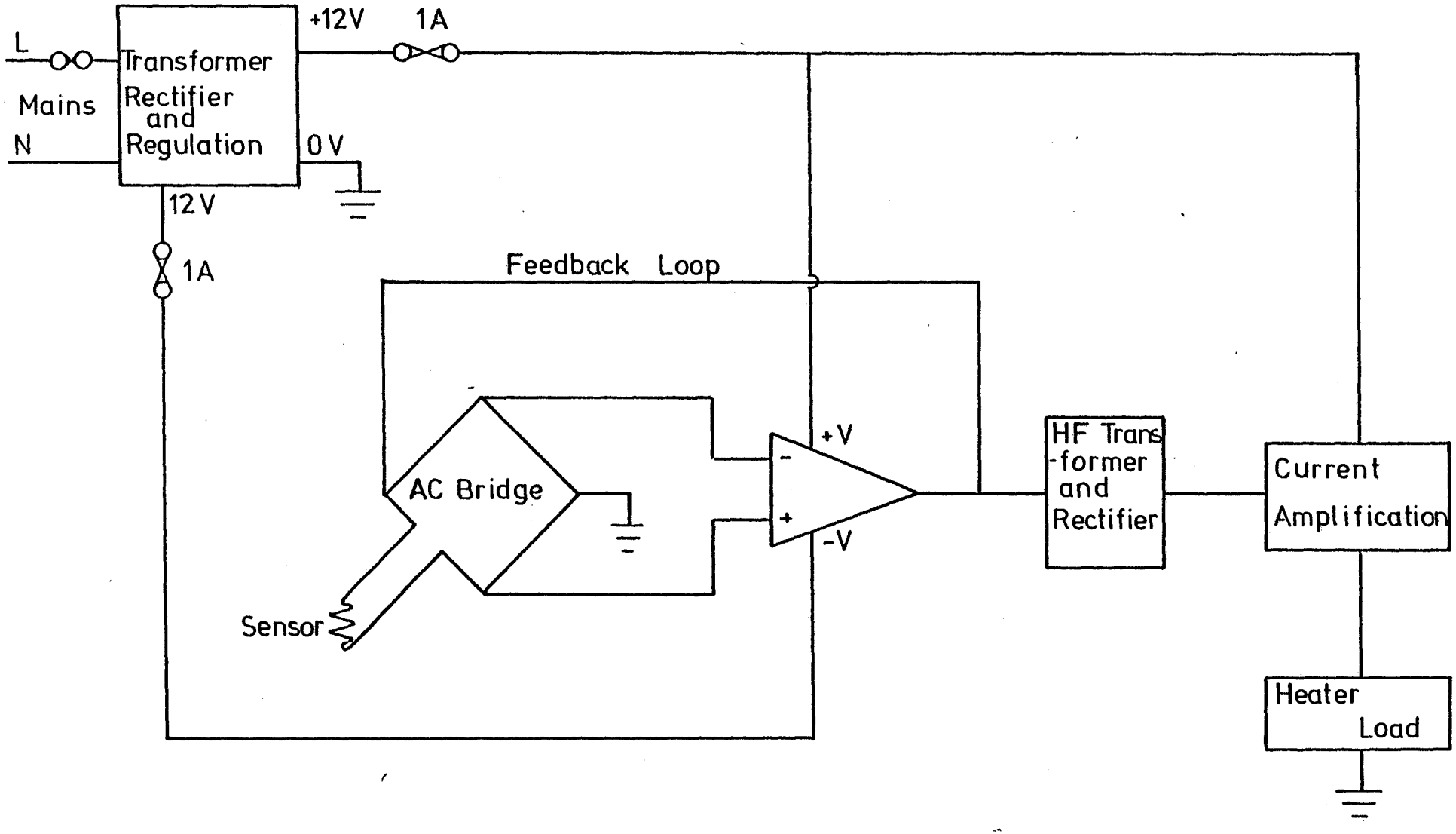

Fig. 5.2.4 Block Diagram of the Temperature Controller

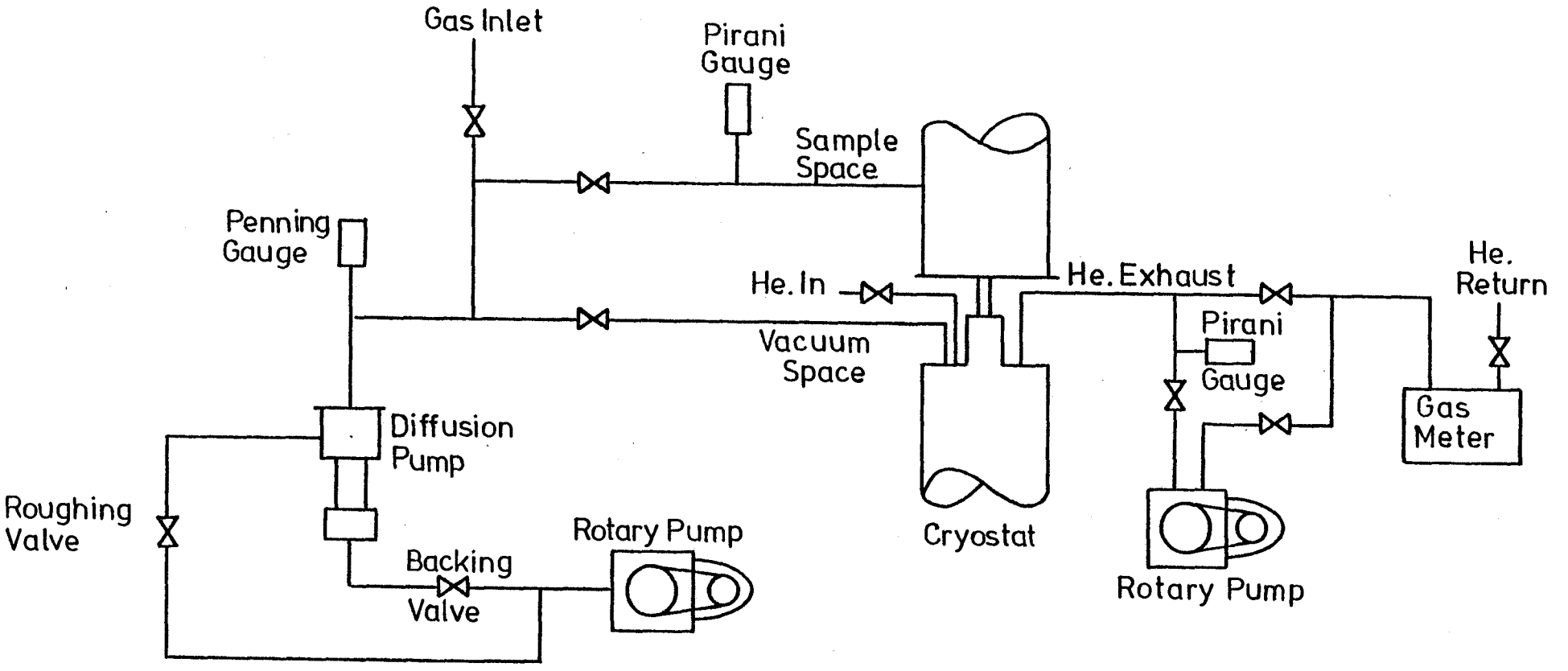

Fig. 5.2.5 Torque Magnetometer Vacuum System

5.2.8. The Electromagnet

The magnet used in this part of the work was an 8" Newport type D. The maximum field available (40 Amp. per coil) was 2.04T with a pole gap of 38mm. The magnet was on a rotatable base with scale markings in degrees and a vernier to allow angular position to be determined to an accuracy of 0.1 degrees.

The magnet was calibrated using a Newport Magnetometer type J, calibrated against NMR standard, also for the work using a cobalt single-crystal a low field calibration was performed using a Hirst FM70 Hall Probe fluxmeter.

The calibration curves are shown in figure 5.2.6.

5.3. The Magnetostriction Measurements

5.3.1. The Magnetostriction Apparatus

Considerable investigation of the behaviour of resistive strain gauges has been undertaken in these laboratories in recent years. The outcome has been that standardisation and some degree of understanding of their low temperature and magnetic behaviour has been achieved. With this knowledge a number of experiments have been made using resistive gauges supplied by Micro Measurements (type SK-09-031DE-350). (refs. 21-24).

In this work strain gauges have been used to measure the magnetostriction at temperatures down to liquid helium of single-crystals of $GdAl_2$ and its related ternaries produced by substituting small percentages of Tb. The apparatus employs a D.C. Wheatstone bridge circuit of high sensitivity, two arms of which are resistive

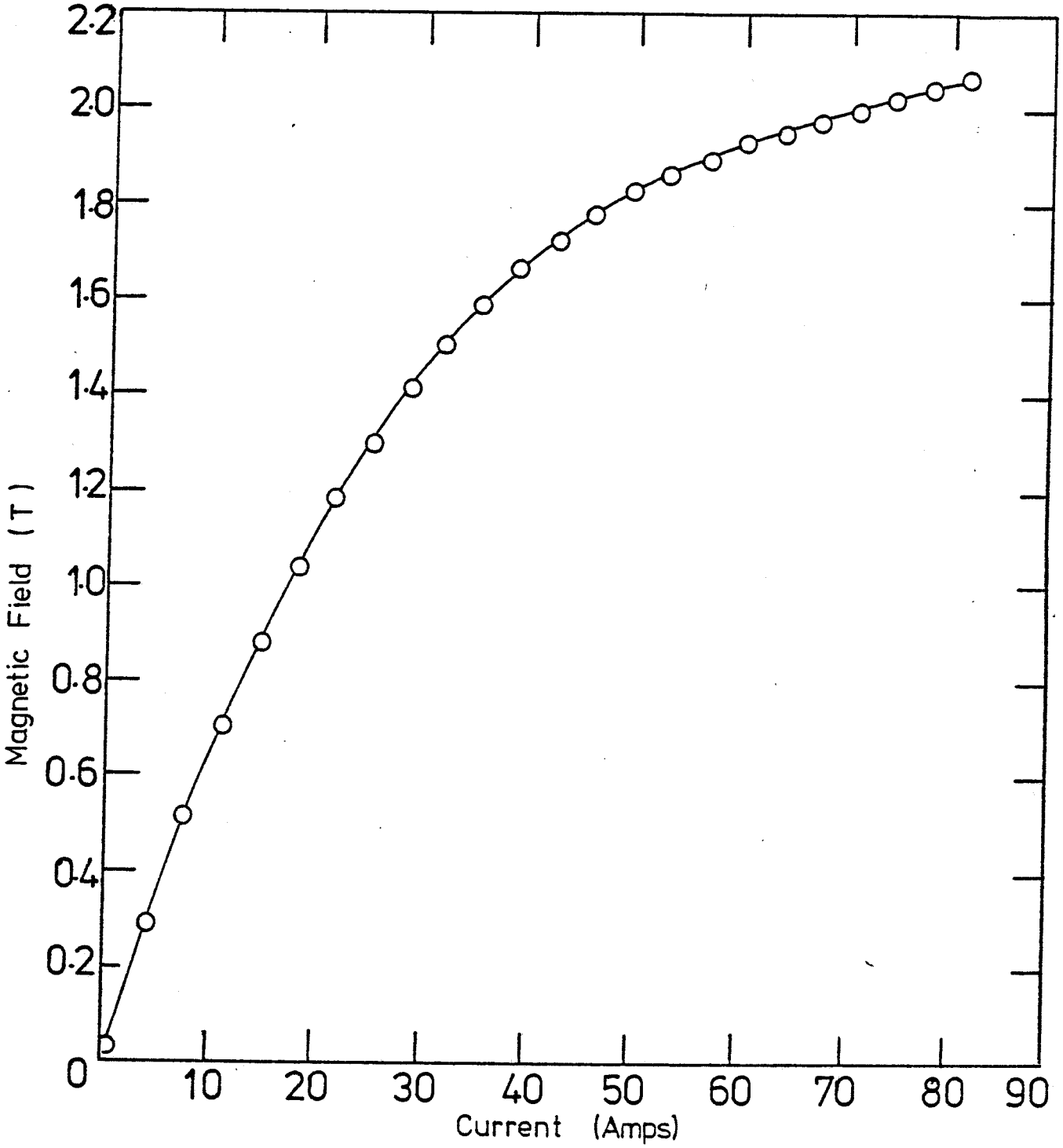

Fig. 5·2·6 Calibration Curve for Magnet

strain gauges in the experimental space - one of which is mounted in a particular crystallographic direction on the sample and the other compensating gauge on a dummy material which exhibits no magnetostriction. The advantages of this method are elucidated in reference 21.

The apparatus used is similar to that used by Asgar (21) and subsequently by Pourarian (22) and has been extensively described in both these references. The salient details are as follows:

5.3.2. The strain gauge bridge

The bridge circuit was a high sensitivity D.C. Wheatstone bridge which used the out-of-balance voltage in the strain indication stage by the use of a D.C. amplifier (Keithley n Voltmeter), the output of which was indicated on a chart recorder (Rikadenki, B-202). Analysis of the bridge circuit shown in Fig. 5.3.1 gives:

$$\frac{\Delta R}{R} = \frac{4}{E} V_{out} \qquad \ldots(5.5)$$

where $\frac{\Delta R}{R}$ is fractional change in resistance/unit-resistance and E and V_{out} are the supply and detected voltages respectively. Equation 5.5. assumes that no current flows through the detector stage. As the impedance of the detector is of the order of 1 MΩ this is a good approximation. A second approximation that $\frac{\Delta R}{R}$ is small is also true; in this work never exceeding 10^{-4}. The bridge was balanced by changing the variable resistors shown in the circuit diagram. These and the standard resistances were allowed to reach a steady temperature within a

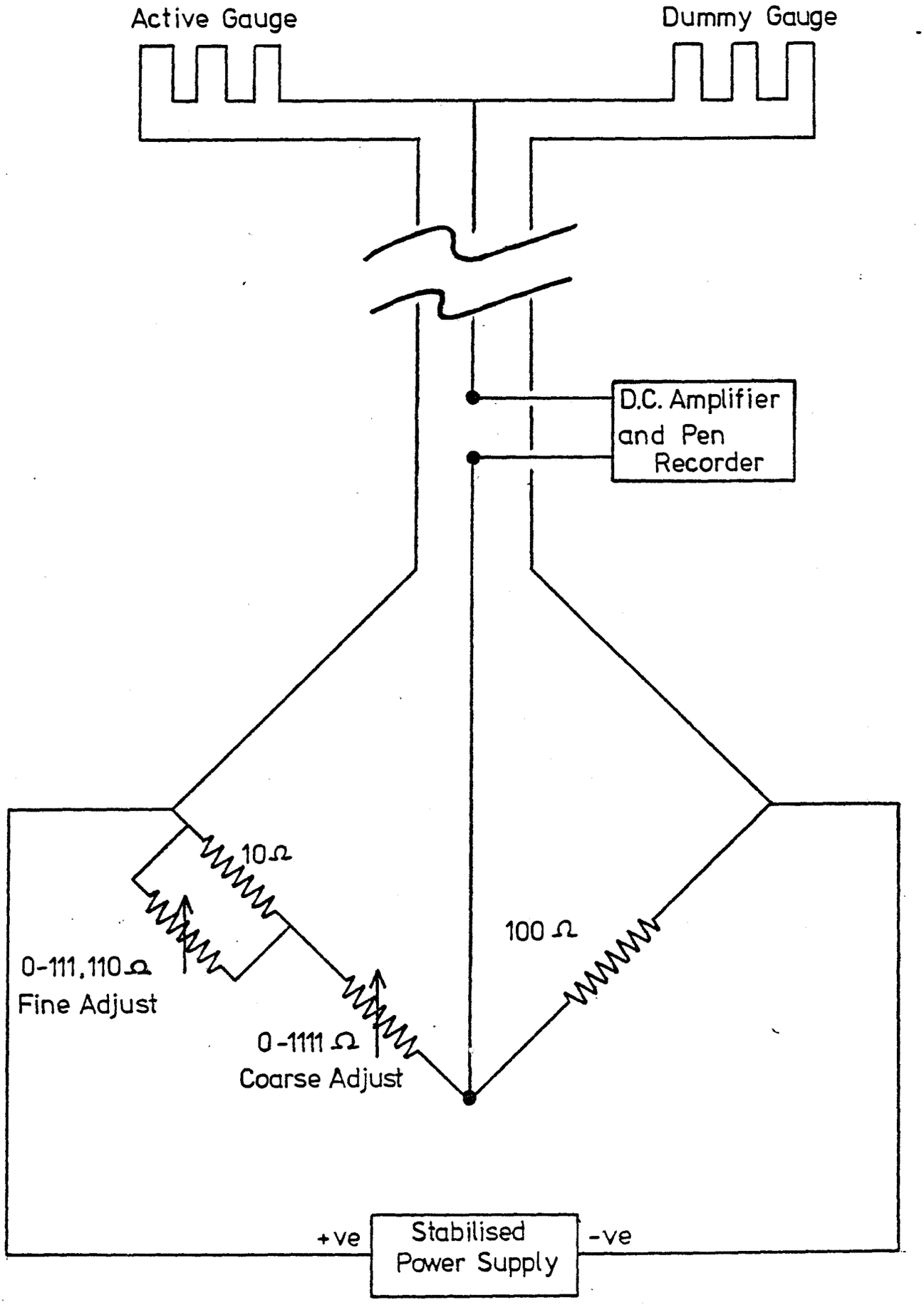

Fig. 5·3·1 The Strain Gauge Bridge

thermally insulated box. All soldered joints were made using low thermal e.m.f. solder to minimise thermally generated e.m.f's in the bridge. As measurements were made of differential strain between two field orientations or two temperatures the variable resistances were used merely as a zeroing device. However a long time, usually several hours was allowed after switching on the supply to the bridge for thermal stabilisation. The energising voltage was two volts and the gauge factor approximately 2. The sensitivity attainable during most of this work was of the order 10^{-8} in strain equivalent.

5.3.3. Strain gauge application

Once a particular crystallographic direction had been determined using X-ray back reflection photography it was necessary to bond the gauge onto the sample using the standard technique (25). The gauges were aligned with the prepared sample using the apparatus described in reference (22). A thin coat of the M-Bond 600 adhesive was then applied and the gauge and sample clamped together and cured for several hours at approximately 85°C. Provided the surface preparation had been done carefully the bonds made were found to be reliable and give reproducible results even after temperature cycling.

5.3.4. The sample holder, temperature measurement and control

The sample holder was of the design described in references (21,22). It is more massive than that described in section 5.2.4., small fluctuations in temperature must be minimised because the magnetostriction to be measured is so small. The temperature controller and

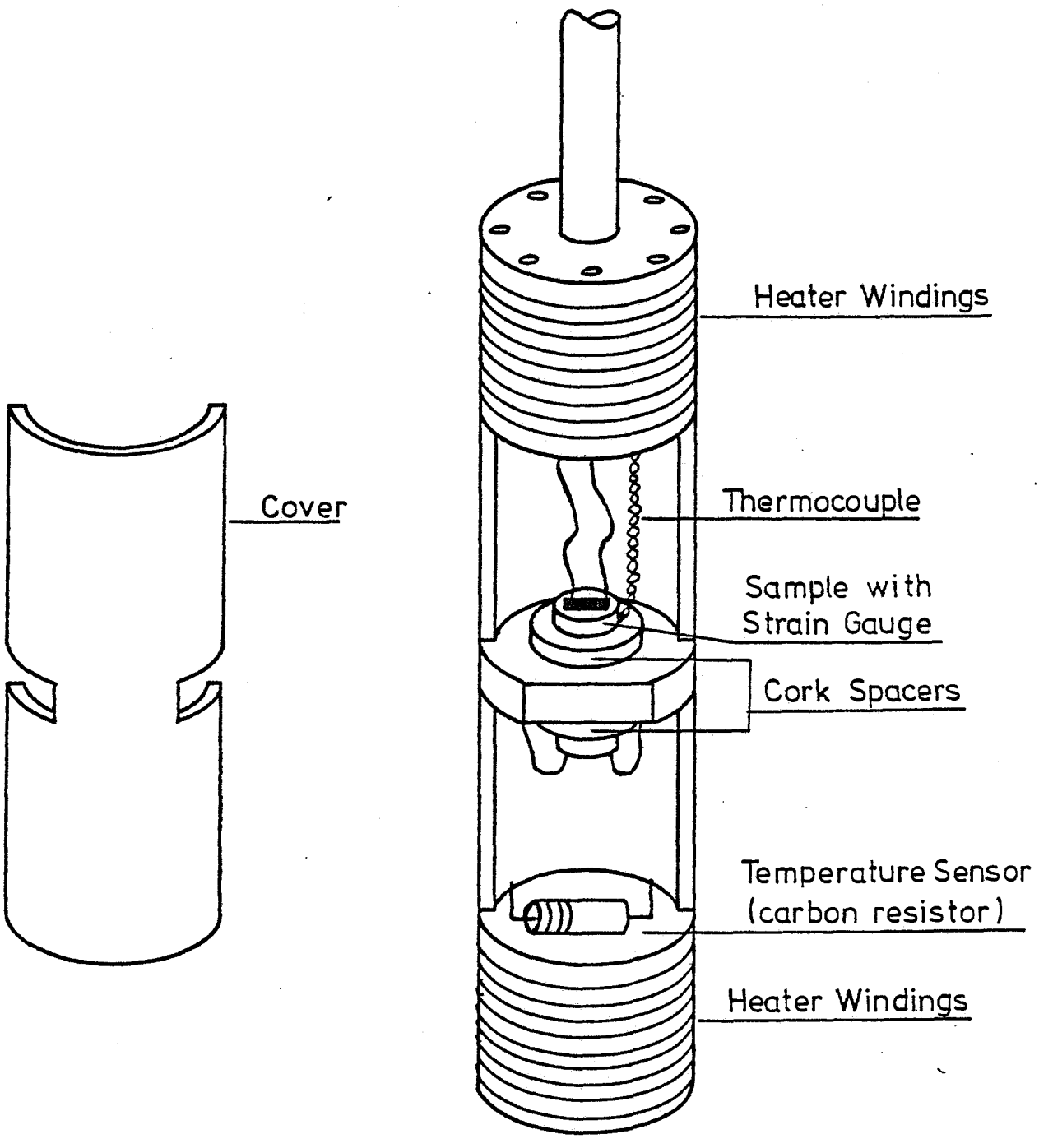

Fig. 5·3·2 The Sample Holder used for the Magnetostriction Measurements

sensors used however, were similar to those used for the torque measurements leading to similar unsatisfactory temperature control at lower temperatures. The larger mass and the proximity of dummy and compensating gauge, separated only by the cork spacers and completely enclosed (fig. 5.3.2) meant that changes due to temperature fluctuations were small. The cork spacers are used in both this apparatus and the magnetometer to give a flexible mounting. They allow the sample to expand but prevent rotation of the sample due to any torque which may be present. The mosaic structure of the cork is believed to give the best compromise for this application. The temperature was measured using a copper-constantan thermocouple mounted on the sample using an ice-point reference, as with the torque magnetometer and giving similar accuracy.

5.3.5. The cryostat and vacuum system

The cryostat and vacuum system used were the same as described in reference (22). The cryostat was similar to that used with the torque magnetometer, the facilities and mode of operation being identical. A diagram of the vacuum system is given in figure 5.3.3. and of the cryostat in figure 5.3 4.

5.3.6. The electromagnet

The electromagnet used for the magnetostriction measurements was an 11" Newport Type F powered from a rectified 3-phase supply capable of supplying up to 98 Amps. The maximum field available was 2.5 Tesla with a pole gap of 32 mm ($1\frac{1}{2}$") . The magnet has been calibrated using a Newport Magnetometer Type J as for the Type D electromagnet (section 5.2.8) and a calibration curve is shown in figure 5.3.5.

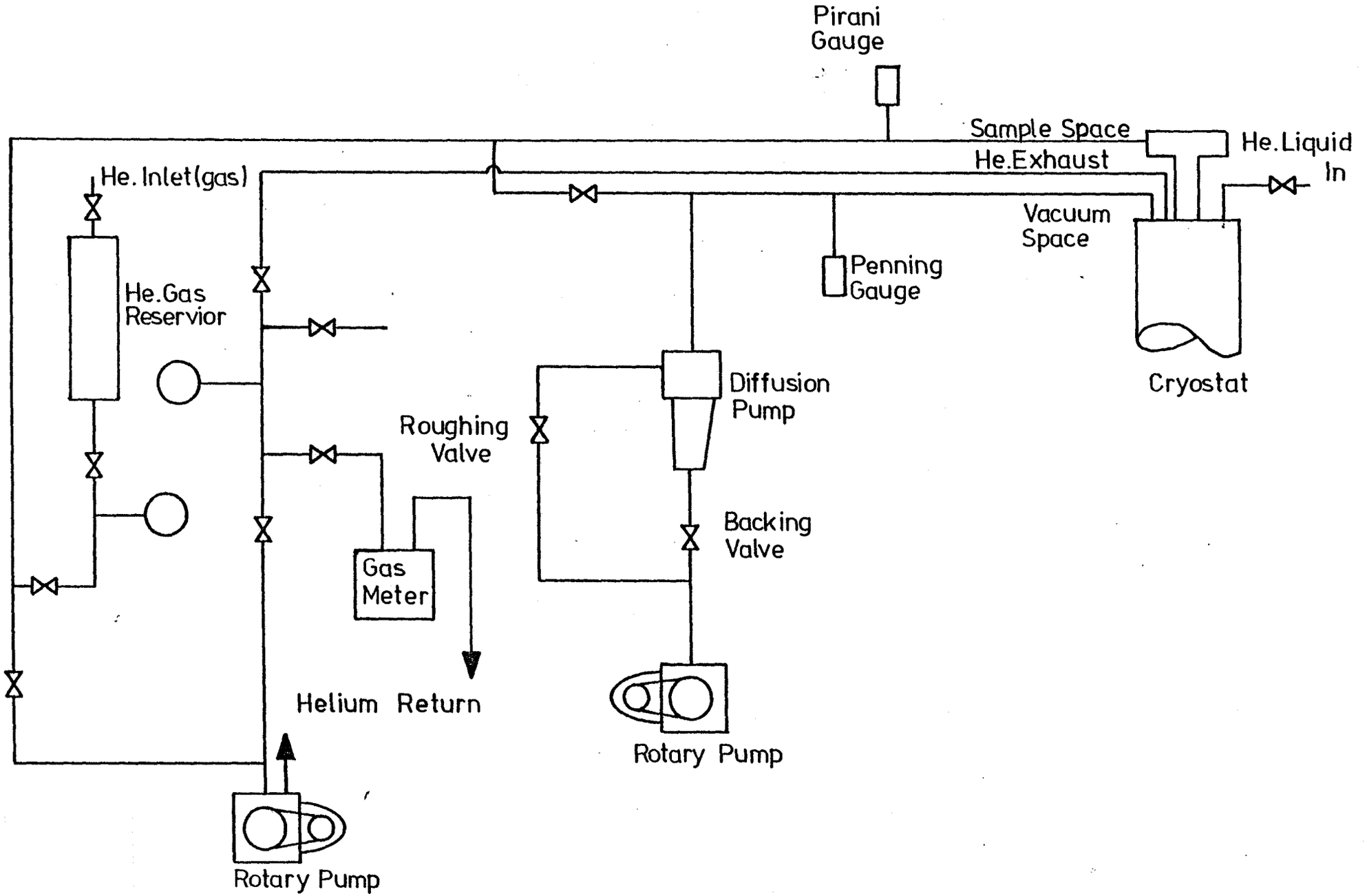

Fig. 5.3.3 Magnetostriction Apparatus Vacuum System

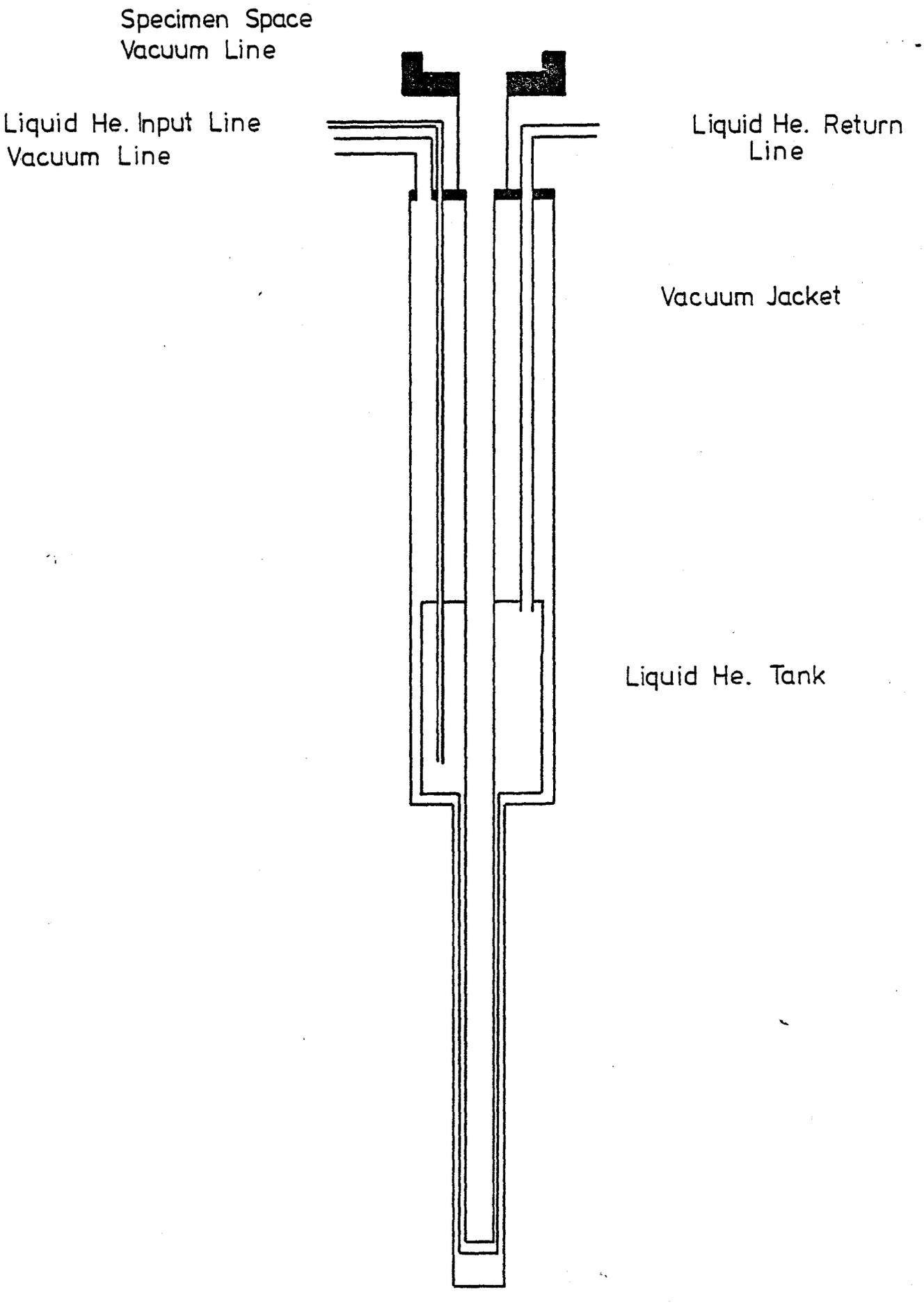

Fig. 5·3·4 The Cryostat for Magnetostriction Apparatus

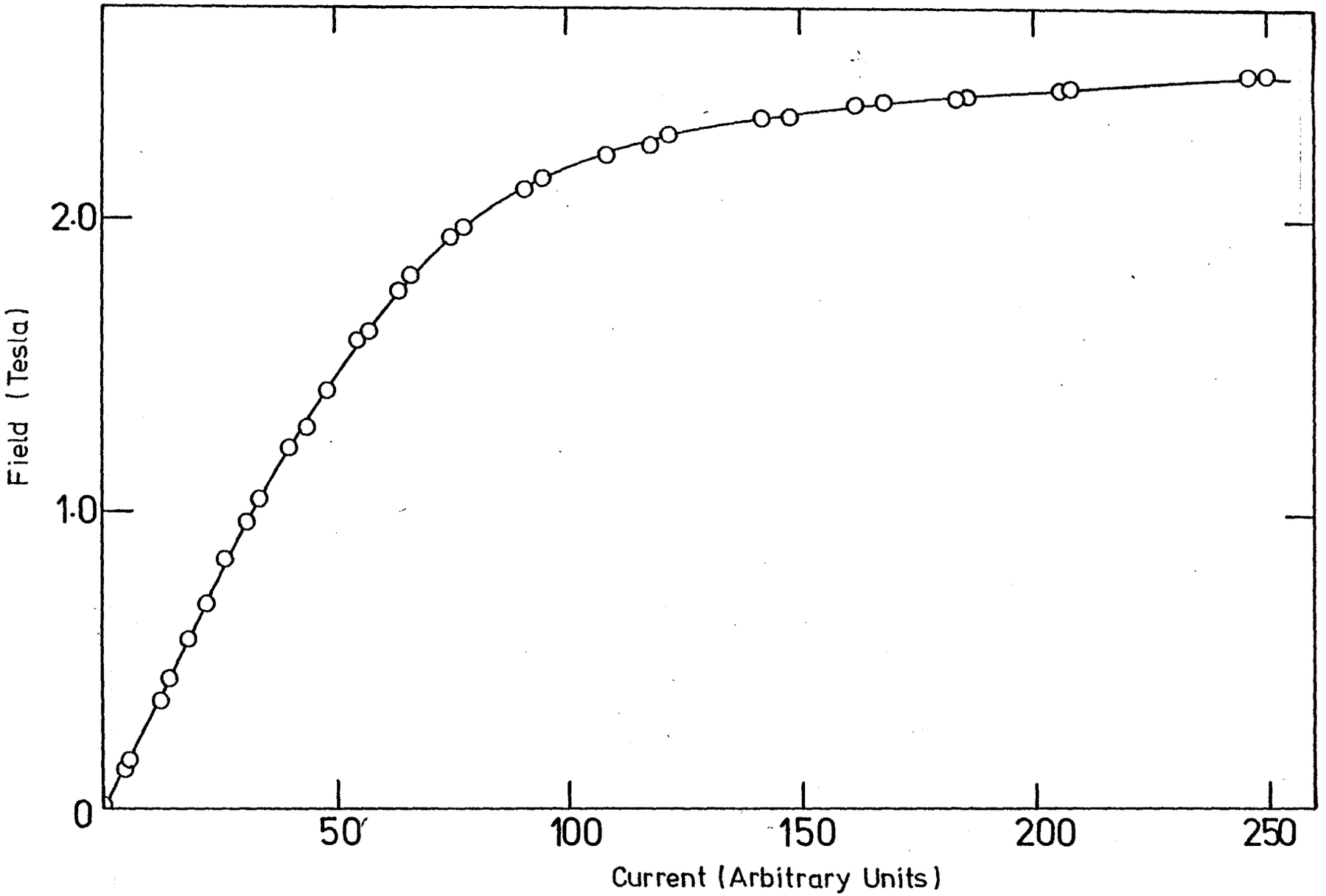

Fig. 5·3·5 Calibration Curve for Magnet

CHAPTER 6

6. MEASUREMENT OF TORQUE CURVES OF COBALT, $GdAl_2$ AND THE DILUTE ALLOYS $Gd_{0.98}Tb_{0.02}Al_2$ and $Gd_{0.95}Tb_{0.05}Al_2$

6.1. The analysis of torque curves

The results of the torque experiments consisted of a series of values of torque at equally spaced angles of the field magnet, for each field and temperature. These results were plotted immediately to give an indication of the behaviour of the system. However to obtain numerical results these curves had to be corrected for a number of effects. As the magnetometer was not a null-deflection device the curves were corrected for the finite rotation of the sample, which is easily calculated from the geometry of the measuring system.

The torque $L(\varphi)$ was then obtained as a function of the angle φ that the applied field makes with the crystallographic axes.

If we consider the simplest energy relation

$$E_K = K_1 \sin^2 \theta \qquad \ldots(6.1)$$

which relates the anisotropy energy to only a single constant and the angle θ between the magnetisation and the crystallographic axis, yielding the torque expression:

$$L(\theta) = - \frac{dE_K}{d\theta} = -K_1 \sin 2\theta \qquad \ldots(6.2)$$

$L(\theta)$ and $L(\varphi)$ are not necessarily equivalent but are related by the expression

$$\theta = \varphi - \alpha \qquad \ldots(6.3)$$

where α is the angle that exists between the applied field and the

magnetisation. This non-collinearity produces a torque on the crystal which is in equilibrium with the anisotropy torque such that

$$L(\theta) = M.B. \sin\alpha \qquad \ldots(6.4)$$

The detailed solution of these equations introduces a field dependence to the apparent anisotropy constants which is dependent on the ratio of applied field to the anisotropy field and also to the approximations used in their analytical solution. This is described in more detail in the appendix of reference 1 for the two constant energy relation

$$E_K = K_1 \sin^2\theta + K_2 \sin^4\theta \qquad \ldots(6.5)$$

It was concluded therefore that, in the case of highly anisotropic materials in fields such that α will be significant the derivation of the anisotropy constants is by no means a straightforward process and a reappraisal of existing methods was undertaken.

The methods of torque curves analysis are based on four main methods:

1) Extrapolation to infinite field ($B^{-1} = 0$)

2) Torque curve correction

3) Torque maxima

4) Behaviour of the torque curve near the easy direction.

6.2 Extrapolation to infinite field

This relies on the fact that at infinite field, the angle between M_s (the magnetisation) and B (the applied field) becomes vanishingly small and that the torque will reach a limiting value. The most widely used method is to plot the torque values against B^{-1} to obtain a torque at infinite field. However some manipulation of equation (6.2) and equation (6.4) above shows that even in this case with only one anisotropy constant and the use of the approximation $\sin \alpha = \alpha$

$$\frac{L}{K_1} = (1 - \frac{1}{2} K^2) \sin 2\varphi - K \sin 4\varphi + \frac{3}{2} K^2 \sin 6\varphi \quad \ldots(6.6)$$

where $K = \frac{B_A}{2B}$ and B_A the anisotropy field = $2 K_1/M_s$.

On examination of equation (6.6) it is clear that the extrapolation does not, in general, have a B^{-1} dependence. The inclusion of higher order constants in the energy expansion will modify this conclusion slightly but it appears that the justification for this method is largely historical as discussed in reference 1.

6.3. Correction of torque curves

For each value of the torque curve $L(\varphi)$ it is possible to calculate a value of α from equation (6.4) and subsequently to produce, by simple θ-axis correction, a curve as a function of θ. In principle, curves measured at different field strengths so corrected will then become superposed. In practice, some field dependence is often observed (reference 2) and extrapolation to infinite field is then employed on the apparent anisotropy constants which are derived from the corrected

torque curves by Fourier analysis.

That all spurious effects will disappear at infinite field, or that, if they do, they obey a B^{-1} dependence, is questionable. However this method has been justified in some cases. Aubert (reference 3) found that his measurements on nickel could not be superimposed unless a value for the saturation magnetisation of nickel different from that accepted at the time was employed. Subsequent measurements (4) vindicated this conclusion.

If however the field value is such that the sample energetically favours a two-domain state, then the torque dependence on field becomes more complex. It has been shown (1) from equations given in (19) that the critical field B_K below which the two-domain region exists for a disc shaped sample is

$$B_K = \frac{B_A + N M_s}{\left\{ \left[\frac{B_A^2}{N^2 M_s^2} + \frac{2B_A}{N M_s} \right] \cos^2\varphi + 1 \right\}^{\frac{1}{2}}} \qquad \ldots(6.7)$$

where N is the demagnetising factor in the plane of the disc.

The torque expression is then also a function of N and M_s for fields below B_K (6) and it is clear that the correction $\alpha = \sin^{-1} L/M_s B$ is no longer valid. This precludes the use of this method to derive a complete torque curve in those cases where a two domain region exists over part of the range of field rotation.

6.4. Torque maxima

This method relies on the observation that, theoretically, as the field is decreased, the torque curve, although sheared by α, still retains its maximum value. This will only be true up to $\theta_{max} + \alpha \leq 90^{\circ}$, where θ_{max} is the angle corresponding to the maximum torque. In the single constant case $\theta_{max} = 45^{\circ}$ then the applied field $B \geq B_A/\sqrt{2}$. For fields less than this value, the peak of the torque curve corresponds to points below the correct value of maximum torque projected to the hard axis; this is illustrated in fig. (6.1) after reference (1). Obviously, in this case, if any field dependence of the maximum is observed it becomes impossible to determine to what portion of fig. (6.1) the values correspond and any extrapolation procedure would be erroneous.

6.5. The intial slope

If the applied field is such that B/B_A is small, the magnetisation will be in any easy direction and θ will be small. It may then be shown that, for φ small, in the single constant case:

$$(2K_1 + M_s B)\alpha = 2K_1\varphi \qquad \ldots(6.8)$$

and so the torque expression becomes

$$L = M_s B\alpha = \frac{2K_1 M_s B}{2K_1 + M_s B}\varphi \qquad \ldots(6.9)$$

Hence

$$\left[\frac{dL}{d\varphi}\right]^{-1}_{\varphi=0} = \frac{1}{M_s B} + \frac{1}{2K_1} \qquad \ldots(6.10)$$

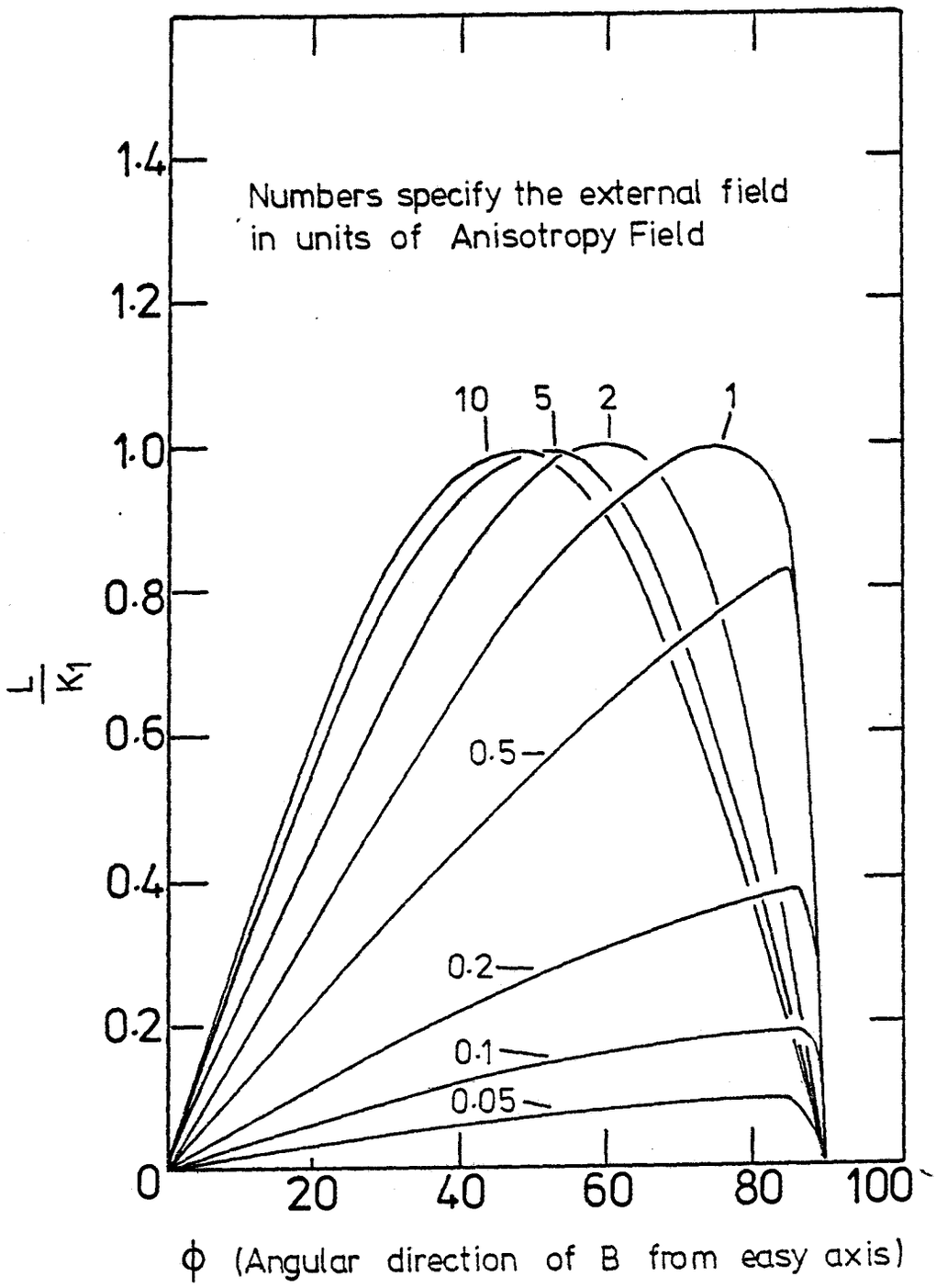

Fig. 6.1 Shearing of Torque Curves

Thus if the reciprocal of the slope of the torque curve at the easy axis is plotted against reciprocal field the intercept at $B^{-1} = 0$ should be equal to $1/2K_1$. This relation holds for a (100) easy direction for cubic symmetry, even when more than one constant is involved in the energy expression. Similar initial slope equations may be derived for other easy symmetry directions but they will normally contain more than one constant (see section 6.8).

These relations will hold true as long as the sample remains single domain which, near the easy direction where $\cos\varphi \to 1$, means that, with reference to equation (6.7), the applied field $B > NM_s$, a condition which is satisfied even when the external field is less than B_A. This method must therefore be the best to use in such circumstances.

6.6. Torque measurements on a single crystal of cobalt

The discussion in the preceding sections is mainly based on some theoretical predictions of Huq (5) using synthesised torque curves. These predictions were tested experimentally by performing measurements on a single crystal of cobalt, obtained from Metals Research Ltd., and nominally 99.99% pure.

The disc shaped sample 6mm in diameter and 0.65mm thick was aligned with the c-axis in the plane of the disc. Laue back reflection X-ray photographs showed clear well-defined spots indicating a homogeneous strain-free crystal. All measurements were made at room temperature using the torque magnetometer described in Ch.5.2. High field measurements at up to 2.0T were made, taking readings for angular positions of the magnet at 5° intervals, field values being chosen so

as to give equal spaced points on a reciprocal scale. The measurements were designed to give complete torque curves which could be used to derive 'true' anisotropy constants for the crystal in the manner of section (6.2).

Further measurements below 0.75T (approximately B_A for Co) were made for points $\pm 25^\circ$ from the easy c-axis in anticipation of initial slope extrapolations.

The recognised expansion for the anisotropy energy of cobalt in a plane containing the c-axis contains the two constants K_1 and K_2:

$$E_K = K_1 \sin^2\theta + K_2 \sin^4\theta \qquad \ldots(6.11)$$

Differentiating to obtain the torque expression:

$$L(\theta) = -(K_1 + K_2) \sin 2\theta + \frac{K_2}{2} \sin 4\theta \qquad \ldots(6.12)$$

As mentioned previously (section 6.3), the torque relation $L(\theta)$ equation (6.12) is a function of θ which is the angle between the field and magnetisation directions. So, after correction for the finite rotation of the sample, the angular position φ was corrected graphically using $\alpha = \sin^{-1} L/M_s B$ and $\theta = \varphi - \alpha$. A value of 1.432×10^6 A m^{-1} was used for the saturation magnetisation of cobalt at room temperature (Barnier et al, reference 6). The uncorrected curves for 0.9T and 2.0T are shown in figure (6.2). After correction, the curves for the high field measurements were found to almost superimpose and Fourier analysis yielded consistent values of $(K_1 + K_2)$ and $\left(\frac{K_2}{2}\right)$ for the first components (see equation 6.12). These results are shown in figure (6.3). Absolute values of $(5.2 \pm 0.2) \times 10^5$ Jm^{-3}

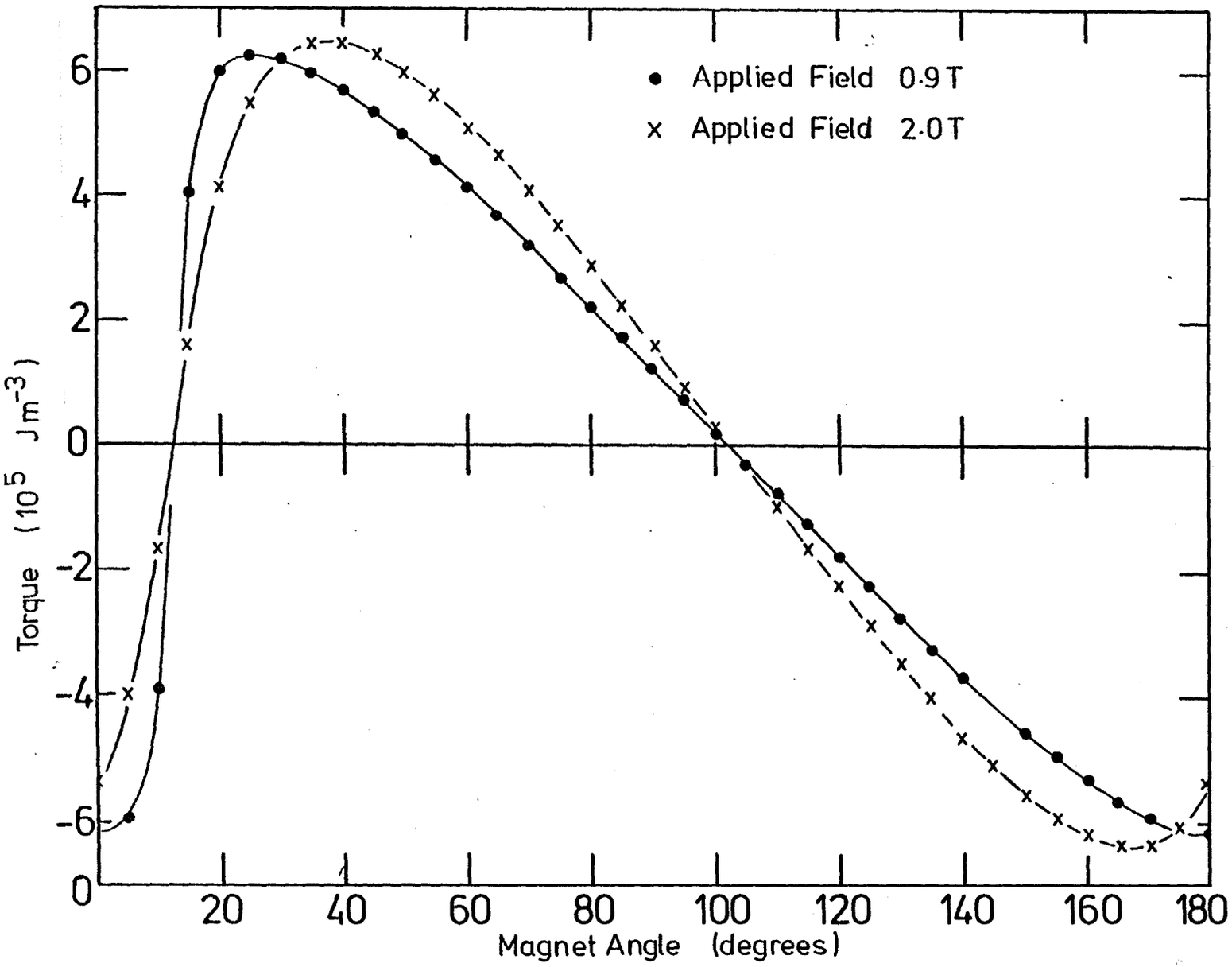

Fig. 6·2 Uncorrected Torque Curves for Co Single Crystal

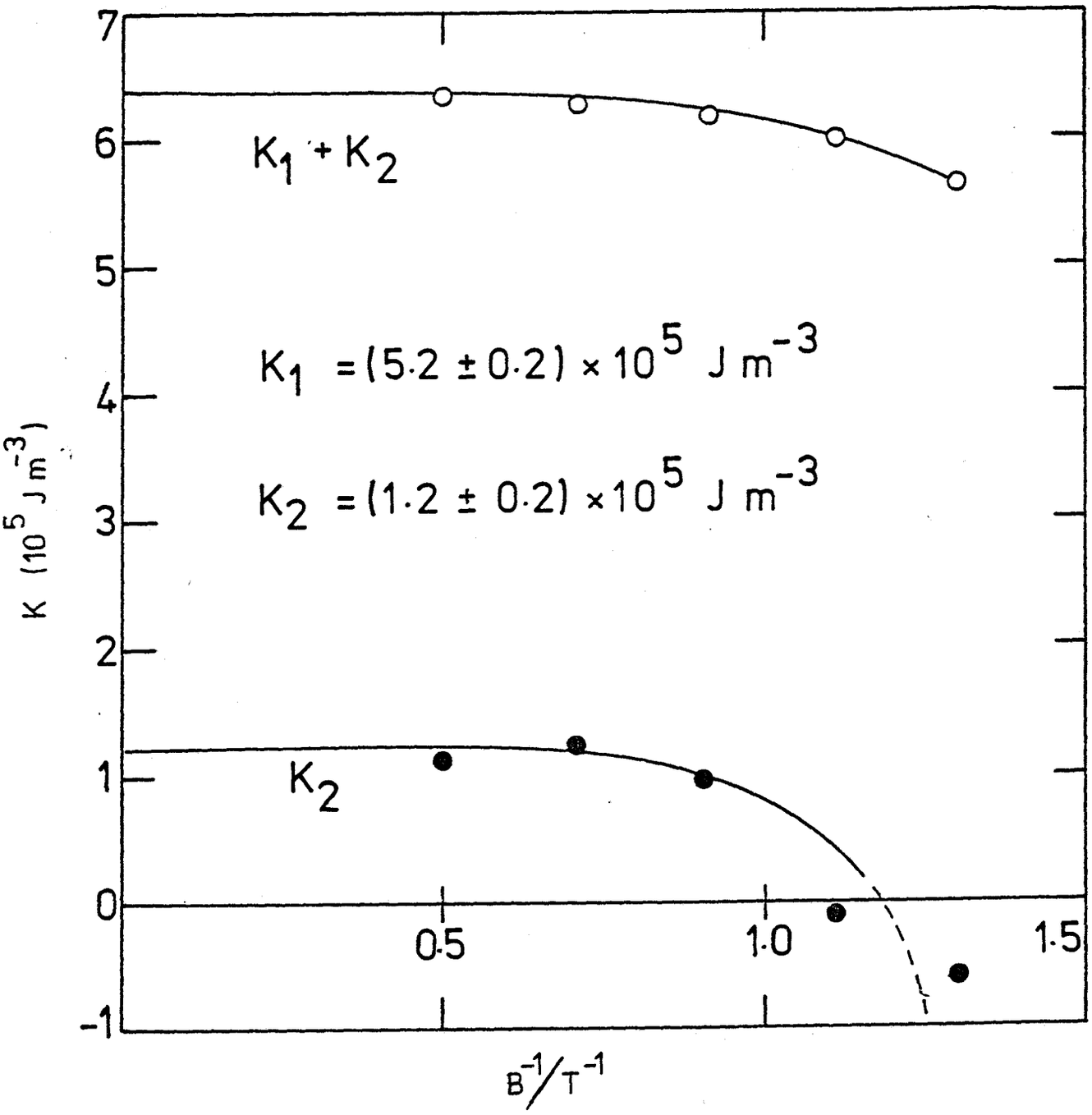

Fig. 6·3 Apparent Anisotropy Constants of Cobalt at Room Temperature

and $(1.2 \pm 0.2) \times 10^5$ Jm^{-3} were obtained for K_1 and K_2 respectively.

As expected, Fourier analysis of the uncorrected curves led to a strong field dependence of K_1 and K_2. Extrapolation to $B^{-1} = 0$ although within experimental error, giving a linear regression for the 2θ component, produced a value differing by some 10% from that obtained from the corrected curves. The 4θ component did not have a linear dependence on B^{-1} and could not be extrapolated to determine a reliable value for K_2.

Initial slopes were also determined down to fields as low as 0.1T; the extrapolation to $B^{-1} = 0$ for $\left(\frac{dL}{d\varphi}\right)^{-1}$ is shown in figures 6.4(a) and (b). Even at low field values the linearity is still quite good. However for the cobalt sample used, B_K is approximately 0.02T and thus there is some departure from the theoretical predictions. This is undoubtedly due to the differences between the 'ideal' and the real crystal used in the experiment. At fields greater than the theoretical B_K local impurities or inclusions may pin domain walls, hence sustaining the multi-domain region and effectively reducing the value of the anisotropy torque.

A review of the values for the anisotropy constants of cobalt, determined by various workers is given by Rayner (7). The results obtained from the measurements reported above are in good agreement with the historical trend which shows values increasing as sample purity and crystallinity have been improved. A summary of these results is shown in table 6.1.

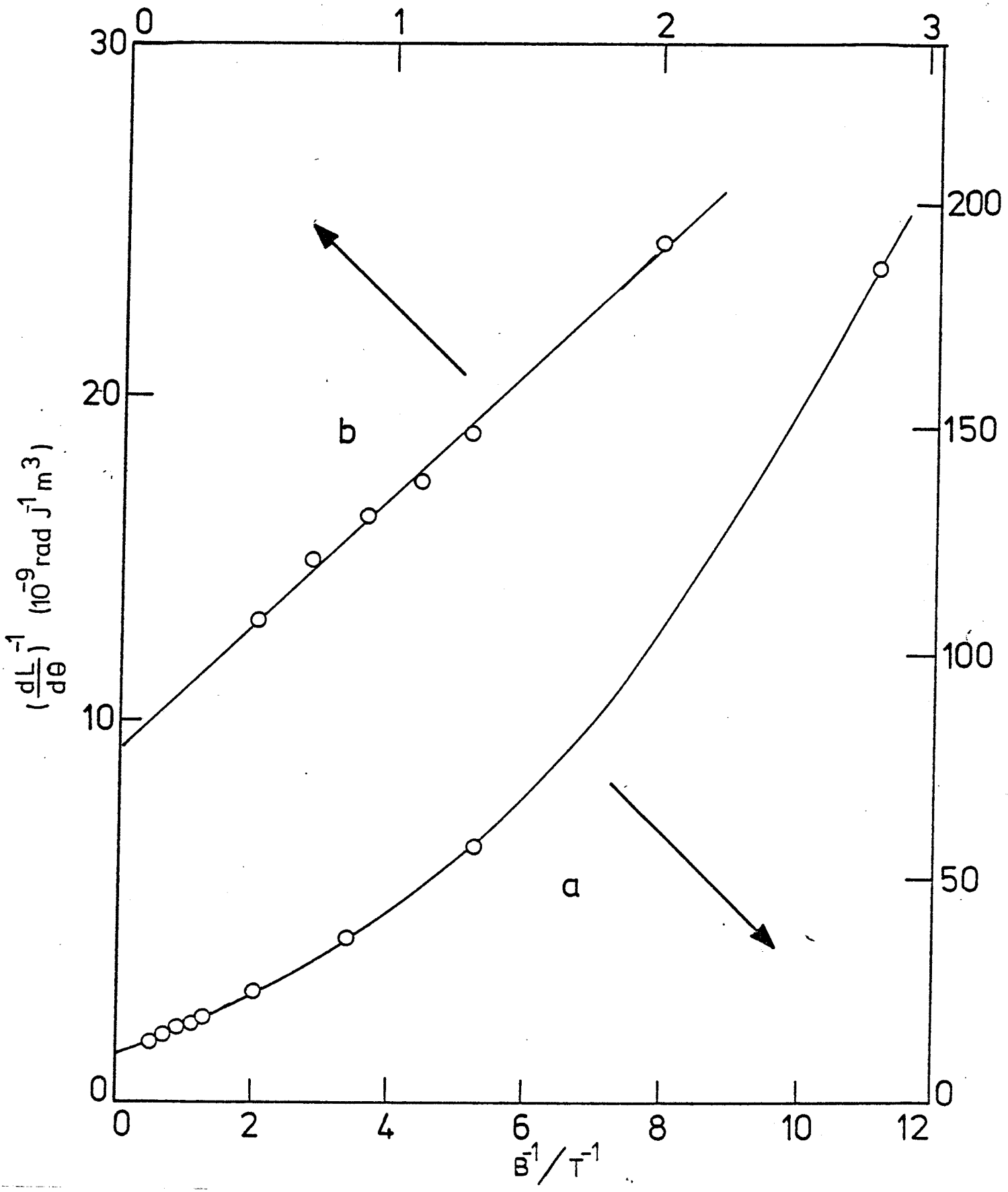

Fig. 6·4 Initial Slope Extrapolation of Cobalt Torque Curves

TABLE 6.1

Some published results for the anisotropy of cobalt.

Reference	Temp (K)	$K_1/10^5 Jm^{-3}$	$K_2/10^5 Jm^{-3}$
W. Sucksmith and J.E. Thompson, Proc. Roy. Soc. A225, 362 (1954)	97 209 293	7.90 6.44 5.28	1.04 0.97 0.95
W. Sucksmith and J.E. Thompson, Proc. Roy. Soc. A225, 362 (1954)	97 209 293	6.80 5.80 4.20	2.40 2.20 1.90
Y. Barnier, R.Pauthenet and G. Rimet, Cobalt 15, 14 (1962)	0 200 300	6.80 6.00 4.32	1.70 1.65 1.50
R.M. Bozorth, Phys. Rev. 96, 2 (1954)	293	4.30	1.20
K. Tajima and S. Chikazumi, Japan J. Appl. Phys. 6, 897 (1967)	293	4.60	-

6.7. Torque curves of $GdAl_2$

Torque curves were measured for the single-crystal (110) disc of $GdAl_2$, produced as described in Ch.5.1. In this case the correction procedures as outlined in sections 6.1 to 6.3 (above) were unnecessary as the torque measured was so small. In fact a second transducer was constructed of increased sensitivity (approximately 20X) in order to achieve detectable deflections on the optical scale.

Measurements were made for up to five different fields values at seven temperatures between 4.2K and the Curie temperature (approximately 170K). Complete torque curves were taken and for each case points were measured as the field was rotated through 360° at intervals of 5°.

A (110) plane in a cubic crystal contains all three symmetry directions 100, 110 and 111 and the torque may be expressed by:

$$L = \frac{dE_K}{d\theta} = -\left[\frac{K_1}{4} + \frac{K_2}{64}\right]\sin 2\theta - \left[\frac{3K_1}{8} + \frac{K_2}{16}\right]\sin 4\theta + \frac{3K_2}{64}\sin 6\theta \quad \ldots(6.13)$$

As explained above, the magnitudes of the corrections for rotation of the sample and for non-alignment of the magnetisation and field were extremely small, a worst-case calculation at 4.2K and 0.9T giving a value of α less than 2×10^{-3} radian and a rotation correction of the same order of magnitude.

A Fourier analysis computer program was developed which took an arbitrary number of equally spaced points for the 2π rotation of

the field and derived a series of the form:

$$F(\theta) = \frac{A_o}{2} + \sum_n A_n \cos n\theta + \sum_n B_n \sin n\theta \qquad \ldots(6.14)$$

The sum was truncated for $n > 12$; the constant term was usually non-zero and gave an indication of the zero torque position on the optical scale. Both the sine and cosine coefficients were employed so that it was not necessary to arrange the zero angular displacement with the (100) direction of the crystal. If the (100) direction is displaced through an angle ε from the scale zero then the torque curve becomes, considering only even terms:

$$L(\theta) = \sum_n Q_{2n} \sin 2n(\theta + \varepsilon) \qquad \ldots(6.15)$$

which, when expanded, becomes

$$L(\theta) = \sum_n Q_{2n} \cos 2n\varepsilon \sin 2n\theta + Q_{2n} \sin 2n\varepsilon \cos 2n\theta \qquad \ldots(6.16)$$

Comparing this to equation (6.14) we obtain

$$Q_{2n} = (A_{2n}^2 + B_{2n}^2)^{\frac{1}{2}} \qquad \ldots(6.17a)$$

$$\varepsilon = \frac{1}{2n} \tan^{-1} \frac{A_{2n}}{B_{2n}} \qquad \ldots(6.17b)$$

Although the signs of the Q_{2n} are lost in (6.17a) they may be determined by inspection of the ε's (6.17b).

In practice the analysis gave small values of the odd coefficients and the even coefficients for n > 8 were of the same order of magnitude. However, the sin θ coefficient was large and very field-dependent. This was attributed to the axis of the magnet not bisecting the pole gap exactly (i.e. one pole piece was slightly nearer the sample). It was also found that the ε values for the coefficients were consistent except for that of the first (sin 2 θ) component. The magnitude of this component was also inconsistent with the anisotropy constants derived from the 4θ and 6θ components.

This effect was attributed to a spurious 2θ component which added to the true value and was probably due to the axes of rotation of magnet and magnetometer not being exactly co-incident. Unfortunately this meant that by comparing equations (6.13) and (6.15) it was not possible to check consistency with three independent equations for K_1 , K_2. However, as K_2 was small it was possible to determine K_1 with some accuracy.

The consistency of the ε values for the higher 2 n θ components at all fields and temperatures (31.7 ± 0.4 degrees) was sufficient to justify the use of the 4θ and 6θ components to determine K_1 (figure 6.5).

In practice, some field dependence of the value of K_1 was found; extrapolation vs B^{-1} was extremely linear and the variation of K_1 with temperature at $B^{-1} = 0$ is shown in figure (6.6). This leads to an extrapolated value for K_1 of $GdAl_2$ at 0 K of $-(2.8 \pm 0.1) \times 10^3$ J m^{-3} . Unfortunately the errors in the determination of K_2 are such that extrapolation to $B^{-1} = 0$ is not possible, but it may be deduced that K_2 has a value in the range $-(1.4 \pm 0.2) \times 10^3$ J m^{-3} at 0 K.

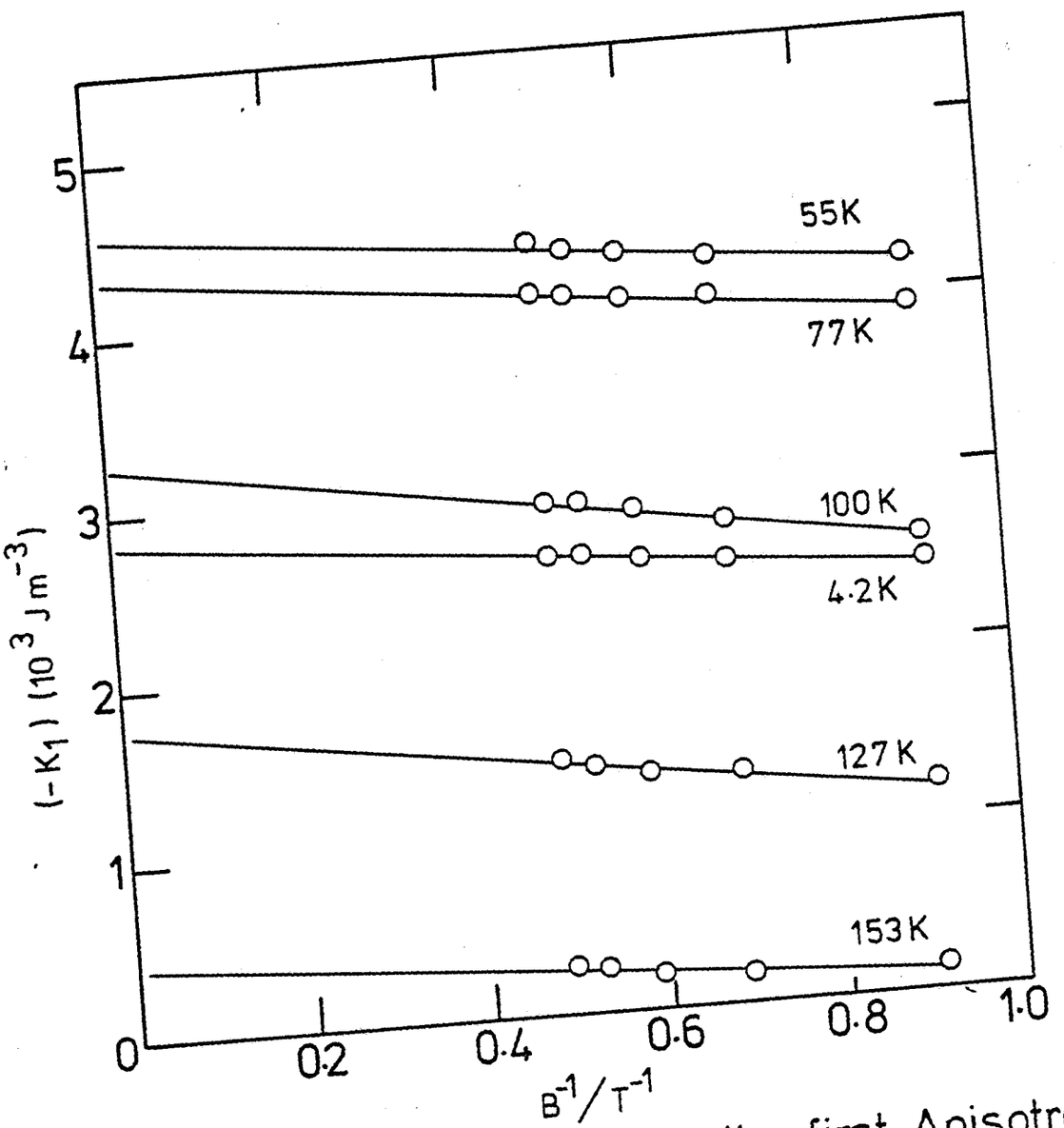

Fig. 6.5 Extrapolation of the first Anisotropy Constant to $B^{-1} = 0$ for $GdAl_2$

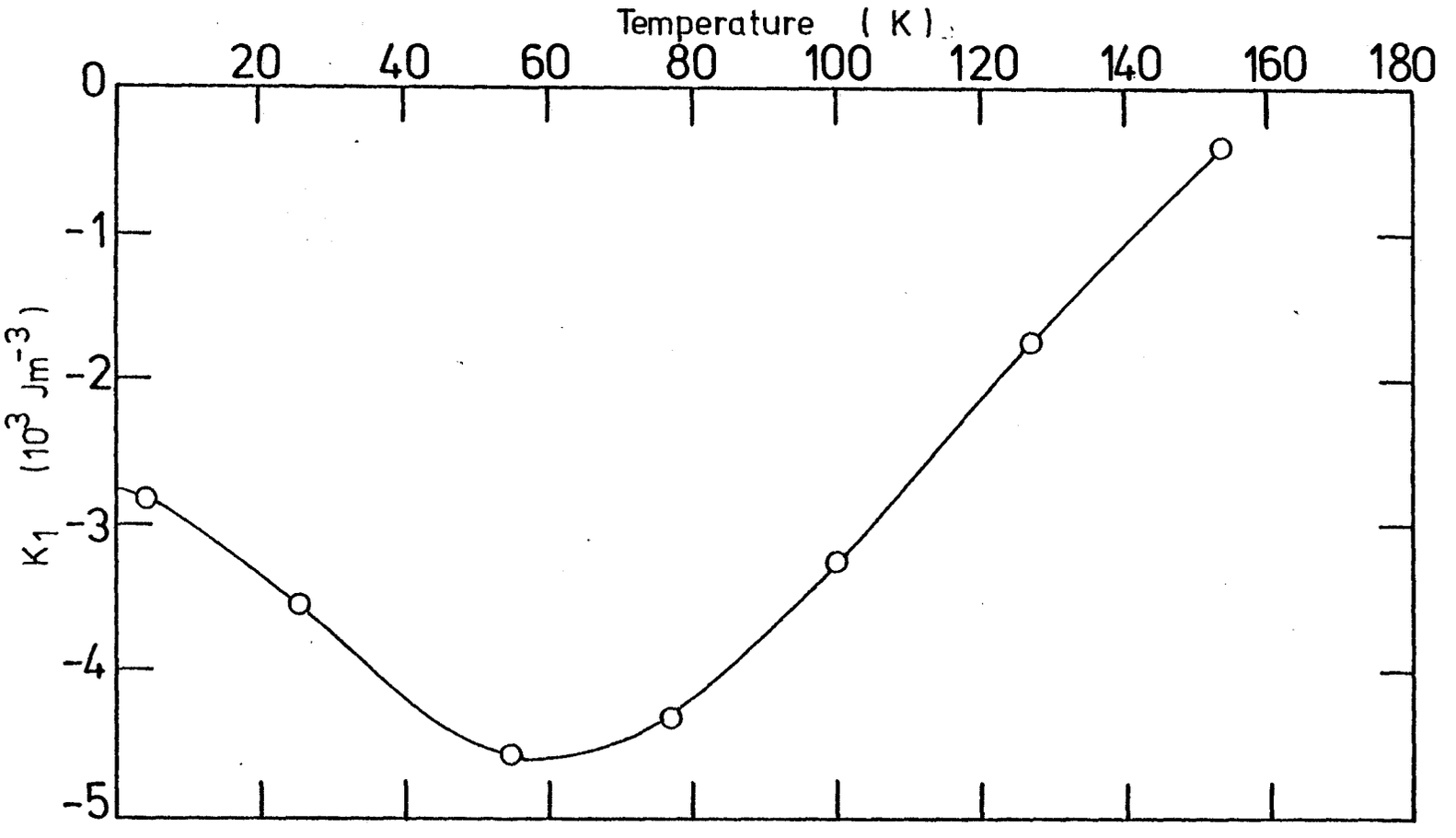

Fig. 6.6 Temperature Dependence of the first Anisotropy Constant of $GdAl_2$

The behaviour of K_1 at low temperatures indicates that the magnitude of K_1 is decreasing in a similar way to that of Gd metal at low temperatures (reference 8). Calculation of the change in K_1 due to magnetoelastic effects (9) yields a value much too small (approximately 3%) to account for this behaviour, even though the magnitude of the second magnetostriction constant h_2 is considerably greater than h_1 (see Ch. 7).

The derived constants, together with the angle ε were used to extract the spurious torque from the 2θ component. Although it was expected to be some geometrical function of the apparatus it proved difficult to quantify the effect. But, qualitatively, the spurious component may be said to increase both its magnitude and phase angle with increasing field and decreasing temperature. It was also found to change drastically in character each time the apparatus was dismantled and reassembled. This is strong evidence in favour of a position and magnetisation dependent effect. It must be stressed, however, that this, and the previously mentioned spurious $\sin\theta$ component (resolved out by Fourier analysis), were at the limit of resolution of the apparatus (an equivalent volume torque of approximately 10^2 J m^{-3}) and only became non-negligible when measurements were made on the almost isotropic $GdAl_2$ compound.

6.8. Effective anisotropy constants of dilute alloys of Tb in $GdAl_2$

As shown above, the compound $GdAl_2$ was found to be almost isotropic ($K_1(GdAl_2) < 10^{-2}K_1(Gd)$) and in the light of the discussion of field criteria for determination of anisotropy constants from torque curves, it was used as an isotropic host for the very anisotropic $TbAl_2$

compound. $TbAl_2$ has an anisotropy field B_A > 10T at 4.2K.

Torque measurements were then performed on single-crystals grown from material of nominal composition $Gd_{0.95}\ Tb_{0.05}\ Al_2$ and $Gd_{0.98}\ Tb_{0.02}\ Al_2$. It is expected that the Tb will be substitued on the rare earth lattice. The crystals were oriented and two discs containing (110) planes were cut.

Measurements were made for each temperature for five different field intensities chosen to give equal spaced points on a reciprocal scale. Temperatures were held constant at 4.2, 25, 55, 77 100, 120 and 140 Kelvin. The less sensitive transducer (1.08×10^{-4} Nm/mm deflection) was used for most torque curves measured. However, for the 120K and 140K measurements on the 2% sample, the more sensitive transducer (8.40×10^{-6} Nm/mm deflection) was used. Results were also duplicated for the 2% samples at 77K and 100K using both transducers. Derived values of the anisotropy constants at these two temperatures agreed, within experimental error, for the two transducers.

It was found necessary to make an angular correction as described in section 6.2, for the torque curves below 77K for the 5% sample. The curves α-corrected where necessary, were Fourier decomposed and the results are shown in figure 6.7. The two-constant relation for torque was identical to equation 6.13 which was used for $GdAl_2$.

In these measurements, as with those on cobalt, no significant spurious torques were detected, the signal-to-noise ratio being considerably greater than for the measurements on $GdAl_2$.

Initial slope values were obtained from the torque curves

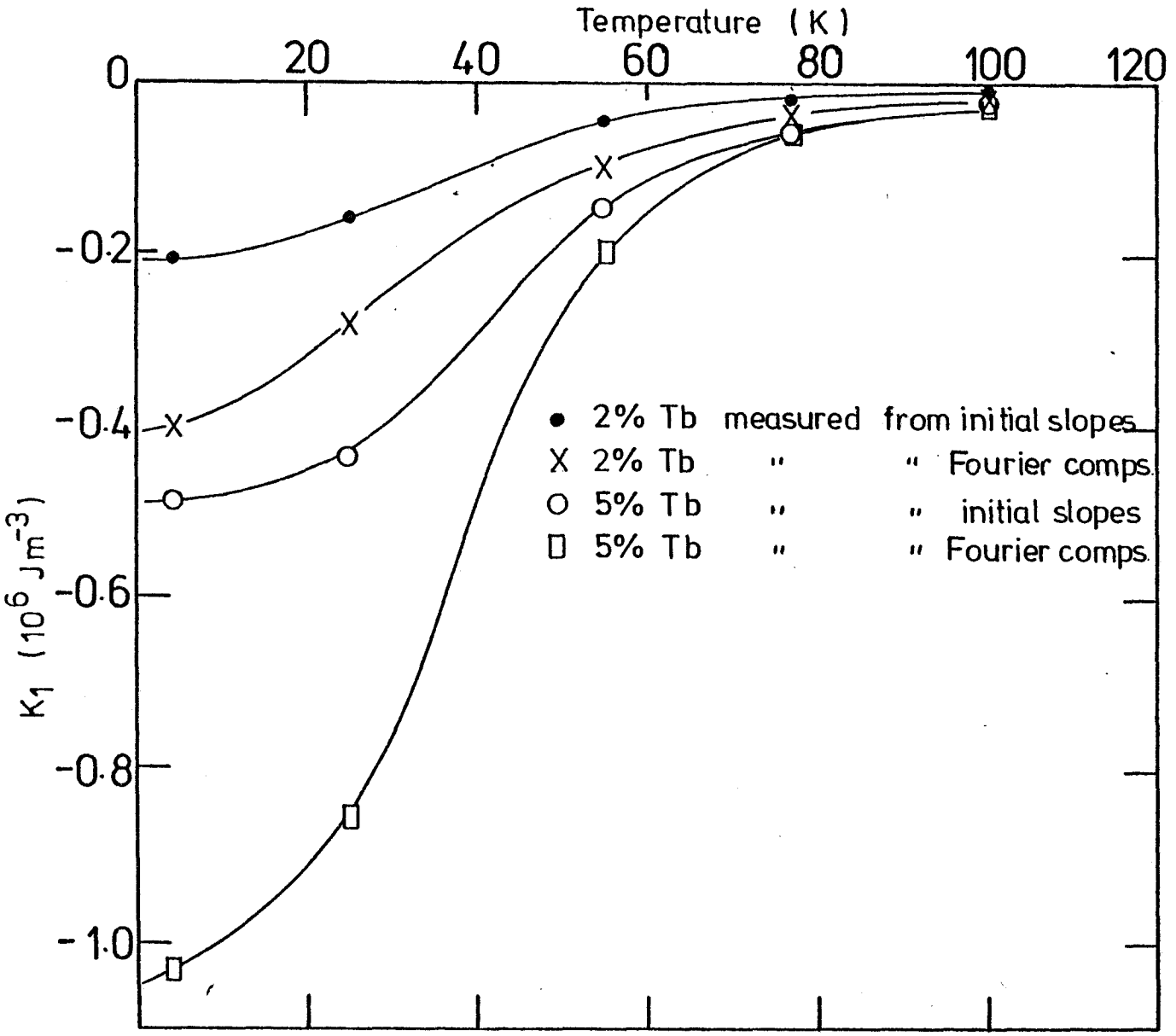

Fig. 6.7 Temperature Dependence of Apparent Anisotropy Constants of Dilute Alloys of Tb in $GdAl_2$

for all three symmetry directions where $L(\varphi) = 0$ in the (110) plane (i.e. 100, 110 & 111 type directions).

These initial slopes however, are only related in the manner of section 6.5 to the first anisotropy constant K_1 when the [100] direction is easy. In this case it is hard, and therefore the field dependence of $\left(\frac{dL}{d\varphi}\right)^{-1}$ is strong and, in any case, the value of α in this direction is not necessarily small. Also it is possible that the value of the critical field B_K (section 6.3, equation 6.7) is such that, at this angle, the two-domain state will be energetically favourable and then the analysis of section 6.3 breaks down, but relations for the initial slope values in the two other symmetry directions (most importantly (111) which is easy in these compounds (reference 10)) were derived (see Appendix B) and values were obtained for K_1 and K_2 from:

For (111) symmetry $$\left(\frac{dL}{d\varphi}\right)^{-1}_{\alpha=0} = \frac{1}{-\frac{4}{3}K_1 - \frac{4}{9}K_2} + \frac{1}{M_s B} \qquad \ldots(6\ 18a)$$

and for (110) symmetry $$\left(\frac{dL}{d\varphi}\right)^{-1}_{\alpha=0} = \frac{1}{K_1 - \frac{K_2}{2}} + \frac{1}{M_s B} \qquad \ldots(6\ 18b)$$

using extrapolation to $B^{-1} = 0$.

The values at the intercept were then solved simultaneously to obtain the valuesfor K_1 and K_2. Figure 6.7 shows the values for K_1 which were obtained. Unfortunately, the errors in K_2 are such that a reliable temperature dependence could not be extracted from the data but values of $-(2.1 \pm 0.2) \times 10^5$ J m^{-3} and $-(4.9 \pm 0.2) \times 10^5$ J m^{-3} were obtained for K_1 at 0 K for the 2% and 5% samples respectively.

6.9. Determination of the anisotropy constant K_1 for $TbAl_2$

There is considerable difficulty in determining the means by which the anisotropic Tb ion contributes to the total anisotropy of the dilute alloy single-crystals.

A simple theory, which assumes that the Tb ions are strongly exchange coupled to the Gd lattice such that the directions of Gd and Tb spins are the same at all orientations of the applied magnetic field leads to the conclusion that, since the contribution to the total magnetocrystalline anisotropy of the Gd ions is negligible (see section 6.7), the effect of the $GdAl_2$ is simply to dilute the magnitude of the anisotropy torque due to the $TbAl_2$. Hence, a scaling factor proportional to concentration was employed to yield the results shown in figure 6.8 for the first anisotropy constant K_1 of $TbAl_2$. The value determined from the initial slopes at 0 K is -10^7 J m^{-3} which is in fair agreement with the value of -7×10^6 J m^{-3} reported by Barbara et al (11) obtained from magnetisation measurements in fields up to 15T. K_1 obtained from the corrected torque curves is somewhat larger having a value of -2×10^7 J m^{-3} at 0 K.

The discrepancy between the two methods of determination of K_1 must be explained in terms of the model used because the scaling factors of 50 and 20 for the 2% and 5% samples give consistent values of K_1 for each method. The explanation must lie in the assumption that for the torque measurements, the Tb and Gd spins are at all times parallel. An examination of the relative magnitudes of the single-ion anisotropy energy and the nearest-neighbour exchange energy leads to the explanation used in the following section.

6.10 Discussion

The exchange parameter variation for nearest-neighbour exchange in the rare earth dialuminide series has been derived by Kaplan et al (10) in terms of an exchange field, H_{ex}, which scales across the rare earth series. An absolute value in terms of an exchange field for $TbAl_2$ is given by Purwins et al (12). An explanation of the variation of Curie temperature for the rare earth diosmiumides (Bozorth 13) also derives a value for the first exchange constant in the Laves phase. A consensus value is 0.91 meV for J_{sf} in the expression:

$$E_{ex} = J_{sf} (g_J - 1) J \cdot (g_{J'} - 1) J' \qquad \ldots(6.19)$$

where J and J' are the total angular momentum quantum numbers for the two rare earth nearest-neighbours.

This leads to an exchange energy of the form:

$$E_{ex} = \Gamma \cos \gamma \qquad \ldots(6.20)$$

where γ is the angle between the spins.

The value of Γ is 1.44×10^{-3} a J per ion pair for Gd-Tb exchange interaction and 1.31×10^{-3} a J per ion pair for Gd-Gd exchange.

When this is compared to a value for the anisotropy energy per ion of 0.265×10^{-6} a J for Gd (K_1 from this work) then the assumption of section 6.9 is correct for the $GdAl_2$ as would be expected. However K_1 for $TbAl_2$ (from reference 11) leads to a value of 425×10^{-6} a J per ion which is not a small perturbation on Γ, so that the Tb impurity spins will not always be exactly parallel to the Gd spins in the torque measurements.

However, in the case of the initial slope measurements, in an easy direction all the spins will be very nearly parallel provided that the anisotropies of the Gd and Tb ions are of the same sign; which is the case ((111) is easy in both $GdAl_2$ and $TbAl_2$) and thus the assumption of section 6.9 may be justified.

Hence, in the first analysis, the acceptance of the initial slope values for the first anisotropy constant of $TbAl_2$ was thought to be correct. Subsequently a computer program was developed for the numerical determination of the distribution of spin directions as one moves away from the impurity site through the host lattice. The method was in some respects similar to that used by Miwa and others (references 14-17) who used spin-wave notation to interpret the results of Chikazumi et al (18) on dilute alloys of rare earths in gadolinium metal. The strategy used in this work was to minimise the sum of anisotropic energies in the crystal, when a field was applied at an angle φ to the easy axis, with respect to the angular positions of a series of spins. Preliminary results showed a perturbation of the spin directions of the host material by the anisotropic impurity spin, see diagram 6.8.

Further work should be able to determine theoretical torque curves for the assembly of spins which may be analysed in a similar fashion to the experimental results above. Some difficulty is to be expected in reducing the number of adjustable parameters in the energy expression to obtain unique solutions.

An outline of the method used and some results are presented in chapter 8.

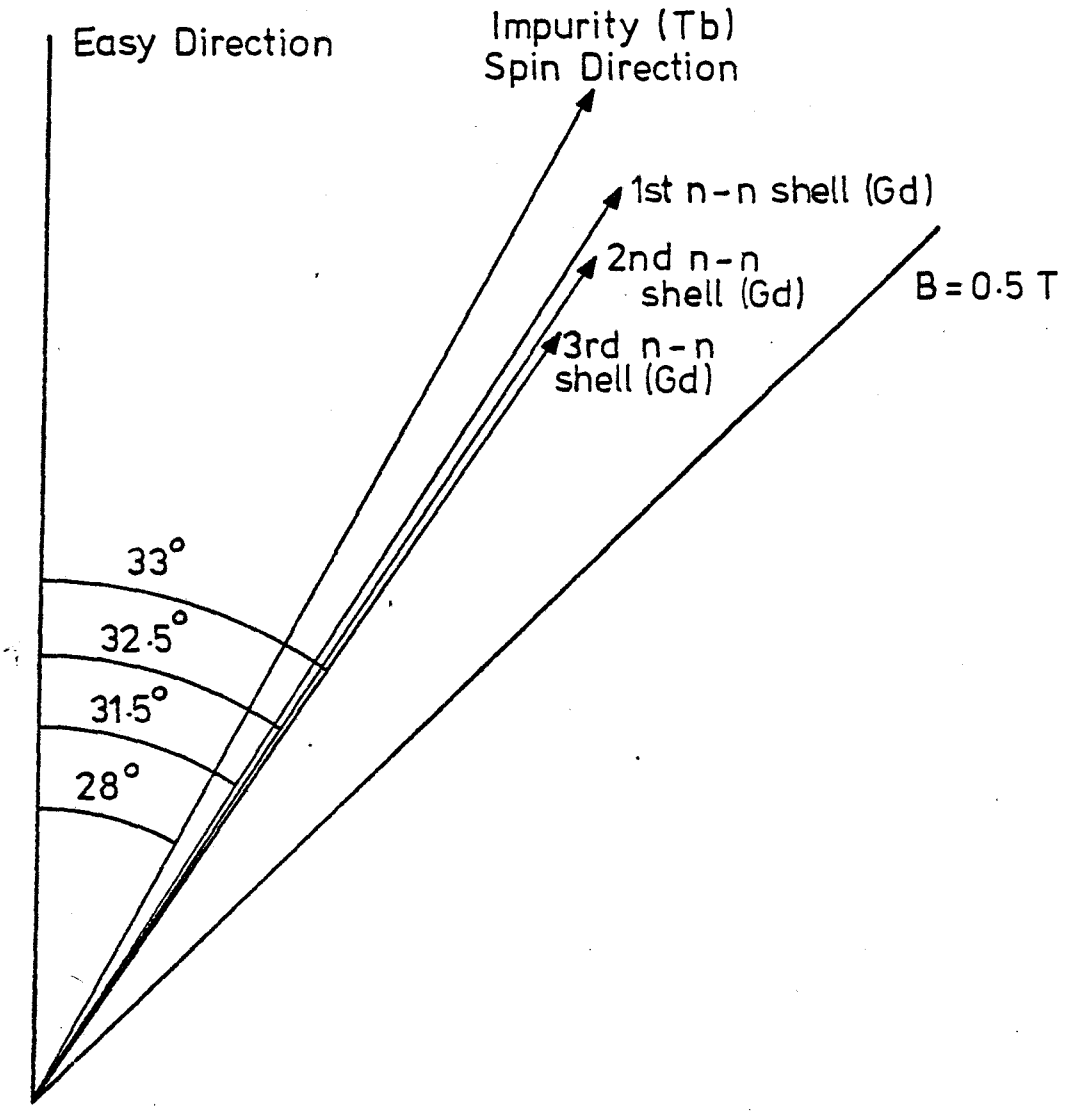

The spin deviation for shells of nearest neighbours from a 'hard' impurity site with a field of 0·5 T applied at an angle of 45° to the easy axis.
(Theoretical Model : see Ch 8)

Fig. 6·8

CHAPTER 7

7. MEASUREMENT OF THE MAGNETOSTRICTION CONSTANTS OF $GdAl_2$ $Gd_{0.98}Tb_{0.02}Al_2$ and $Gd_{0.95}Tb_{0.05}Al_2$

7.1. Introduction

As shown in section 4.2 the semi-empirical relation involving the first two constants for the magnetostriction of a crystal with cubic symmetry is given by:-

$$\frac{d\ell}{\ell} = h_o + h_1(\alpha_1^2\beta_1^2 + \alpha_2^2\beta_2^2 + \alpha_3^2\beta_3^2 - \tfrac{1}{3}) + 2h_2(\alpha_1\alpha_2\beta_1\beta_2 + \alpha_2\alpha_3\beta_2\beta_3 + \alpha_3\alpha_1\beta_3\beta_1) \quad \cdots(7.1)$$

where the α's and β's are the direction cosines for the directions of the applied field and measurement respectively, and $d\ell/\ell$ is related to the 'ideal' demagnetised state. Suitable choice of field direction and measurement directions makes it possible to determine the constants h_1 and h_2 independently.

7.2. Measurements on $GdAl_2$

For these measurements the disc with a (100) plane was used. According to Asgar (1) this particular plane is convenient if only the first two constants are to be evaluated as this plane introduces the minimum error due to misalignments of gauge and misorientation of the plane. Also as the gauges were cemented on in symmetry directions, (110) and (100), no correction for the anisotropy was needed.

7.2.1 Determination of h_1

In this case the strain gauge was cemented to the disc using alignment marks under a microscope, in the (100) direction, previously determined from X-ray back reflection photographs. From equation 7.1 the strain observed when the field is applied at an angle θ in the plane is given by

$$\frac{d\ell}{\ell}(\theta) = h_1 (\cos^2\theta - \tfrac{1}{3}) \qquad \ldots(7.2)$$

The strain value was then measured with the field both perpendicular and parallel to the gauge, (i.e. $\theta = 0$ and $\theta = 90^{\circ}$). The difference in these two values gave the value of h_1. Because this measurement involved two saturation magnetisation directions the initial demagnetised state did not have to be considered. These measurements were performed at a series of temperatures between 4.2K and approximately 250K for an applied field of 1.94 Tesla. Further measurements, at 77K, were made for the maximum and minimum strain values as a function of field up to the maximum field available of 2.5T. The results obtained are plotted in figures 7.1 and 7.2a. The value of h_1 extrapolated to 0 K is $(0.9 \pm 0.1) \times 10^{-6}$.

7.2.2 Determination of h_2

The method used was similar to that used to obtain h_1, in this case the strain gauge was cemented, to the opposite face of the disc from the (100) gauge, in a (110) direction by the same method. If the appropriate values of the direction cosines are substituted into equation 7.1 for the field at an angle θ to the (100) direction

in a (100) plane we obtain in this case:

$$\frac{d\ell}{\ell}(\theta) = \frac{2}{3} h_1 + h_2 (\cos\theta \sin\theta) \qquad \ldots(7.3)$$

For the field perpendicular and parallel to the gauge ($\theta = 45^\circ$ and $\theta = 135^\circ$) the difference between these minimum and maximum values gave the value of h_2. As for the measurements of h_1 these were repeated for the temperature range 4.2K to 250K for a constant applied field; and at 77K for the perpendicular and parallel directions with increasing field up to the maximum field available of 2.5T. The results obtained are plotted in figure 7.1 and 7.2b. The value of h_2 extrapolated to 0 K is $(-26.1 \pm 0.2) \times 10^{-6}$.

7.2.3. Discussion

The temperature dependence of h_1 and h_2 (figure 7.1) will contain contributions from the form effect. These contributions were calculated in the uniform strain approximation using the equations 21. 19 - 21 given by Carr (2). The values of $h_1(f.e) = 0.73 \times 10^{-6}$ and $h_2(f.e) = 0.76 \times 10^{-6}$ at 4.2K were then subtracted from the measured values. However a more important contribution was found to be from the dipole-dipole interaction. Since the form effect strains had been subtracted, the dipolar contribution corresponding to an infinite crystal was calculated using the formulae of Akulov (3) and the dipole-sums of McKeehan (4) for the diamond lattice on which the Gd ions are situated. These formulae are; where S_1 and S_2 are related to the dipole sums of McKeehan.

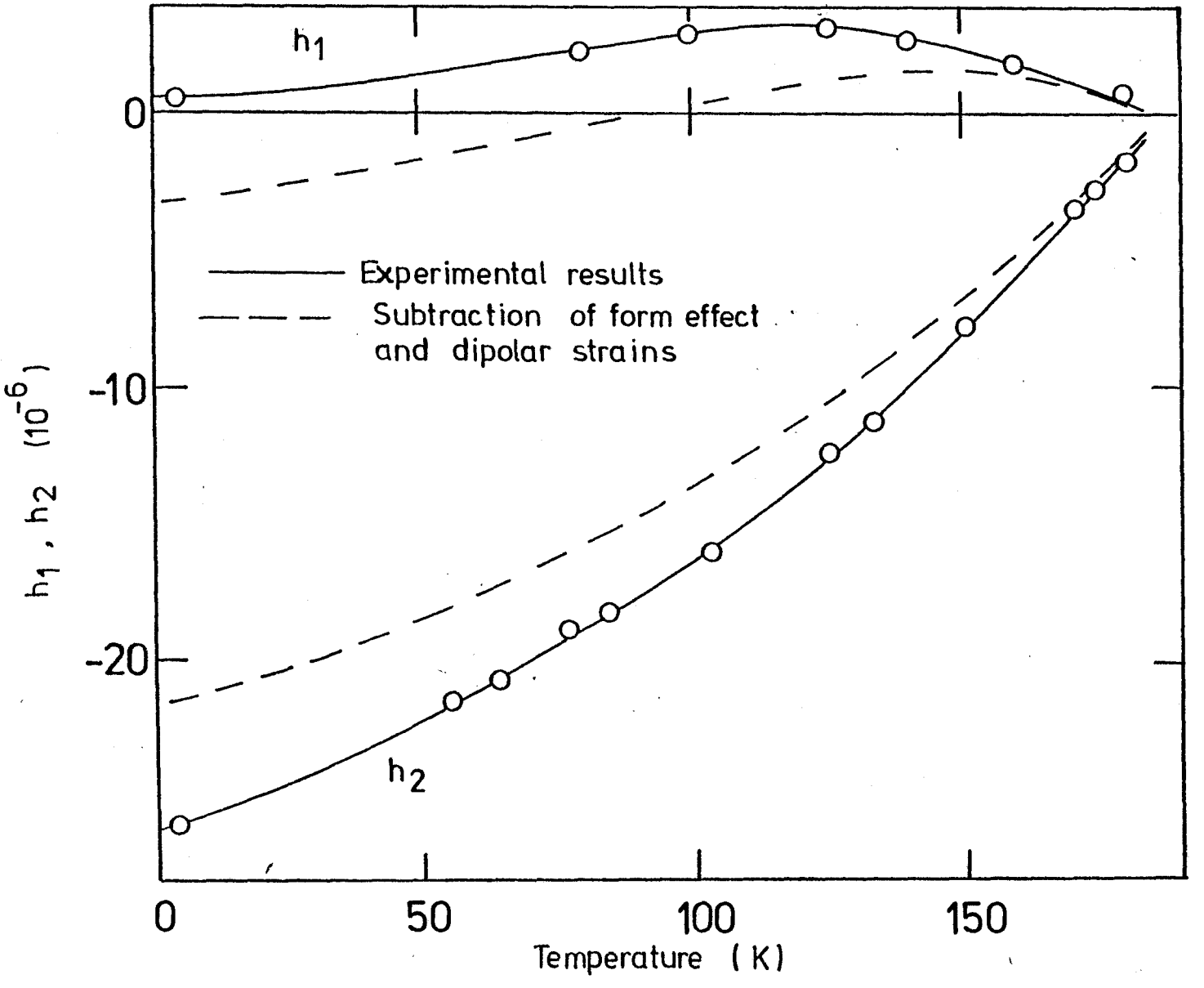

Fig. 7.1 h_1 and h_2 for $GdAl_2$

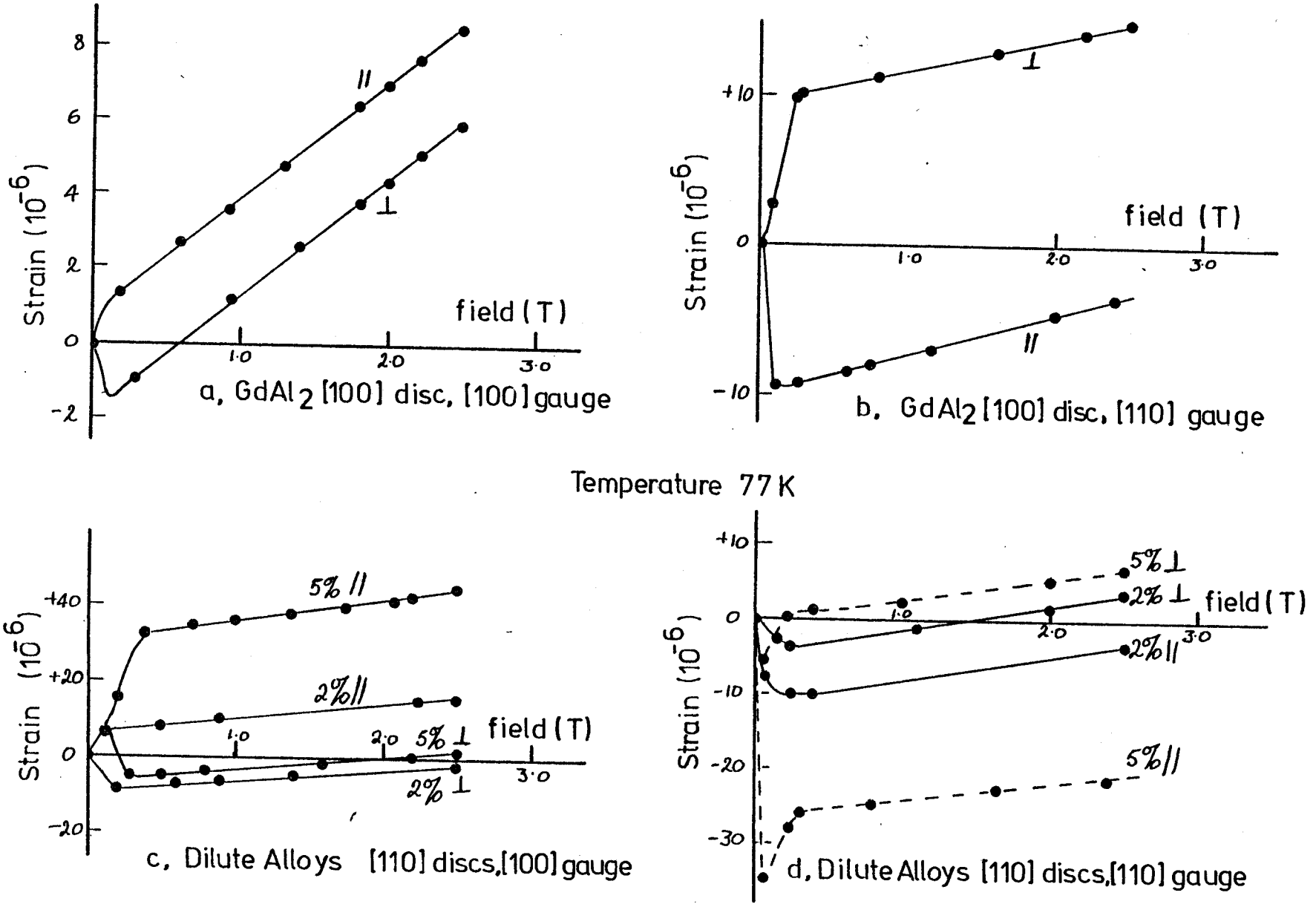

Fig. 7·2 Forced Magnetostriction with Field Applied Perpendicular (⊥) and Parallel (||) to the Strain Gauges

$$h_1\,(\text{dip}) = -\frac{1}{16}\,\frac{M^2 S_1}{C_{11} - C_{12}} \qquad \ldots(7.4a)$$

$$h_2\,(\text{dip}) = -\frac{\frac{1}{32}\,M^2 S_2}{C_{44}} \qquad \ldots(7.4b)$$

Values of the elastic constants C_{11}, C_{12} and C_{44} were taken from the data of Schiltz and Smith (5), and the values of the magnetisation from the sources given for figure 2.2. At 4.2K the dipolar contributions were calculated to be $h_1\,(\text{dip}) = 3.0 \times 10^{-6}$ and $h_2\,(\text{dip}) = -5.3 \times 10^{-6}$. The values of h_1 and h_2 with these contributions subtracted are also shown in figure (7.1).

Therefore it can be seen that along with the anisotropy, the magnetostriction of $GdAl_2$, although small, exhibits some unusual features. These are the unusual temperature dependence of K_1 and the small (almost negligible) value of h_1 together with a comparatively large h_2. The conclusion is, therefore, that there are two contributions to both the anisotropy and magnetostriction of $GdAl_2$ which are of the same sign for h_2 but of opposite signs for K_1 and h_1. The temperature dependence may then be accounted for in terms of different temperature dependences of the contributions.

In this compound the mechanisms involved in producing these effects must necessarily be of second order or higher because of the s-state of the gadolinium ion. Kaplan et al (6) have concluded that there is an anisotropic s-f exchange in $GdAl_2$ and this is supported by the temperature dependences of K_1 and h_2 (figures 6.6 and 7.1 and also

reference (7)),which are expected to scale as the square of the reduced magnetisation or less. The agreement is quite good but the conclusion by no means certain.

Further contributions could arise from excited states of the Gd ion, but these states are so far above the groundstate in energy that the admixture of even the 1% of excited states necessary to account for the results seems unlikely. It seems more probable that the measured effects arise from some non-s-state character of the conduction bands.

7.3. Measurements on the dilute alloys $Gd_{0.98}Tb_{0.02}Al_2$ and $Gd_{0.95}Tb_{0.05}Al_2$

In this case, because only limited amounts of crystal were available the measurements were performed on the (110) discs of the alloys used in the torque measurements (chapter 6). As explained previously this plane is particularly useful as it contains all three main cubic symmetry directions. In this case also gauges were cemented on in symmetry directions and hence no corrections to the magnetostriction for the anisotropy causing non-alignment of magnetization and field vectors was needed. For the two dilute alloys the procedures used to determine h_1 and h_2 were identical, for each crystal.

7.3.1. Determination of h_1

As with $GdAl_2$, the gauges were cemented to the crystals in (100) directions. Reference again to equation (7.1) gives the strain

observed in this direction when the field is applied at an angle θ in the (110) plane:

$$\frac{d\ell}{\ell}(\theta) = h_1 (\cos^2\theta - \tfrac{1}{3}) \qquad \ldots(7.5)$$

this is identical to equation (7.2). The strain was then measured with the applied field parallel and perpendicular to the gauge, (i.e. $\theta = 0$ and $\theta = 90$). The difference in the two saturated directions gave h_1 (as in section 7.2.1). Measurements were performed at several temperatures between 4.2K and 200K for an applied field of 2.27T. Further measurements of 77K were also made for increasing field up to 2.5T of the strain with the (100) gauge both parallel and perpendicular to the field direction.

The results obtained, for both crystals, are given in figures 7.3 and 7.2c .

7.3.2. Determination of h_2

In this case second gauges were cemented to the opposite faces (to the (100)gauges) of the (110) crystals in a <110> direction. Substituting the appropriate values of α's and β's into equation (7.1) leads to the relation

$$\frac{d\ell}{\ell}(\theta) = h_1 (\tfrac{1}{2}\sin^2\theta - \tfrac{1}{3}) + h_2 (\tfrac{1}{2}\sin^2\theta) \qquad \ldots(7.6)$$

where the field is applied at θ to the 100 direction. If the field is then rotated from parallel to perpendicular to the gauge (i.e. $\theta = 90^\circ$ and $\theta = 0^\circ$ respectively) then the strain difference is equal to

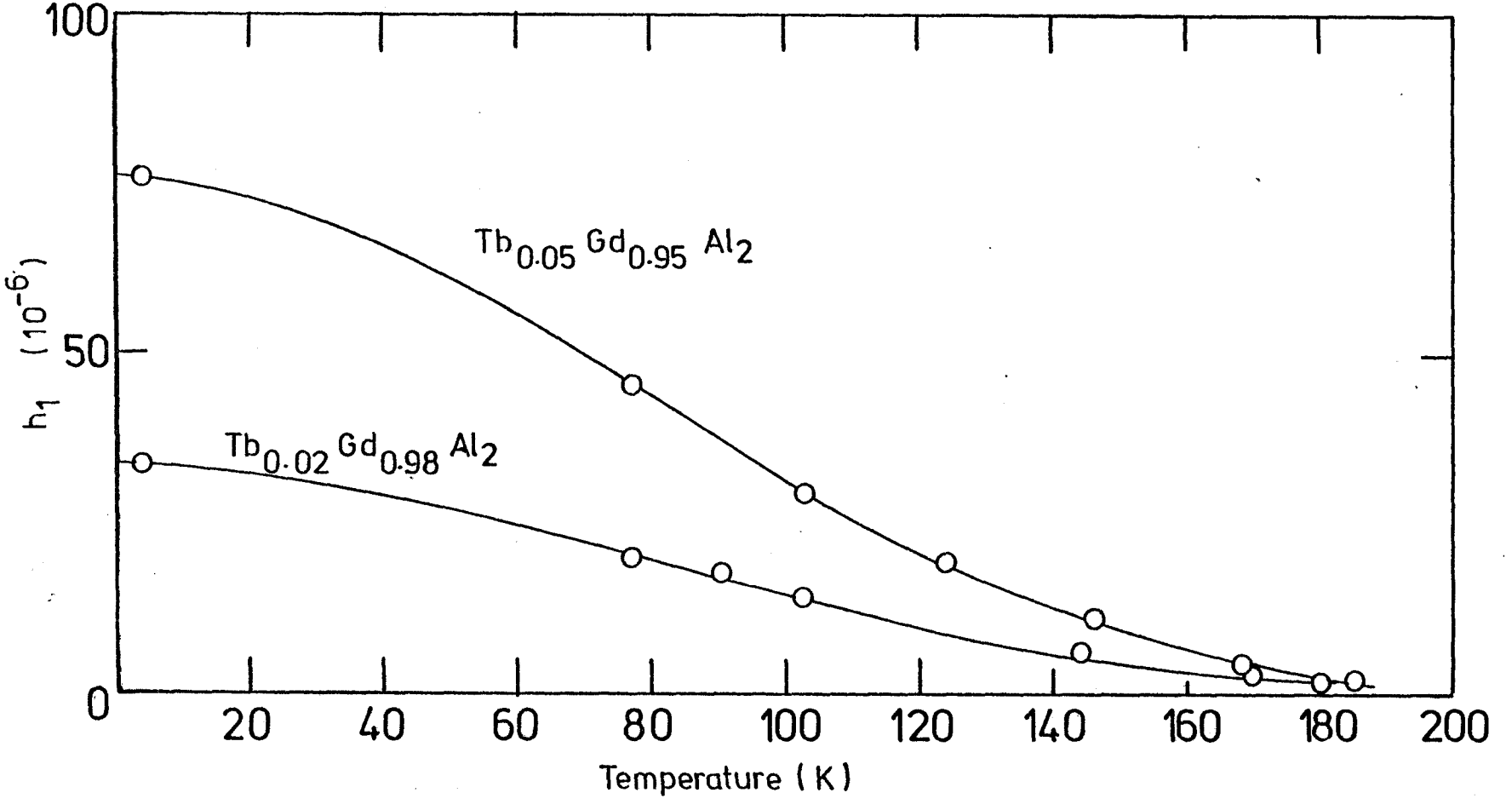

Fig. 7.3 h_1 for $Tb_{0.05}Gd_{0.95}Al_2$ and $Tb_{0.02}Gd_{0.98}Al_2$

$\frac{1}{2}(h_1 + h_2)$. Measurements were performed for constant applied field (2.27T) at several temperatures between 4.2K and 200K. The forced measurements at 77K were also repeated. The results obtains, for both crystals, are given in figures 7.4 and 7.2d.

The values of the observed components of the strain and the derived effective values of h_1 and h_2 for the dilute alloys is shown in table 7.1.

7.4. Measurements of the thermal expansion of $GdAl_2$, $Gd_{0.98}Tb_{0.02}Al_2$ and $Gd_{0.95}Tb_{0.05}Al_2$

Because of the cryostat and sample holder design it was found difficult to ensure small rates of temperature increase or decrease so that these measurements of thermal expansion described here and for the dilute alloys (section 7.3) are not expected to be accurate (see sample errors on figure 7.5). But during the course of determining the magnetostriction constants it was found possible to also measure the linear expansion of $GdAl_2$ and the dilute alloys, between 77K and room temperture by means of the strain gauges attached to them. The curves of $d\ell/\ell$ vs T were all found to be of a similar appearance exhibiting an invar-type anomaly below the ordering temperature. The curve for $GdAl_2$ is shown in figure 7.5.

If we consider the definition of the linear thermal expansion coefficient α at a temperature T:-

$$\alpha_T = \frac{1}{\ell_T}\left[\frac{d\ell_T}{dT}\right]_T \qquad \ldots(7.7)$$

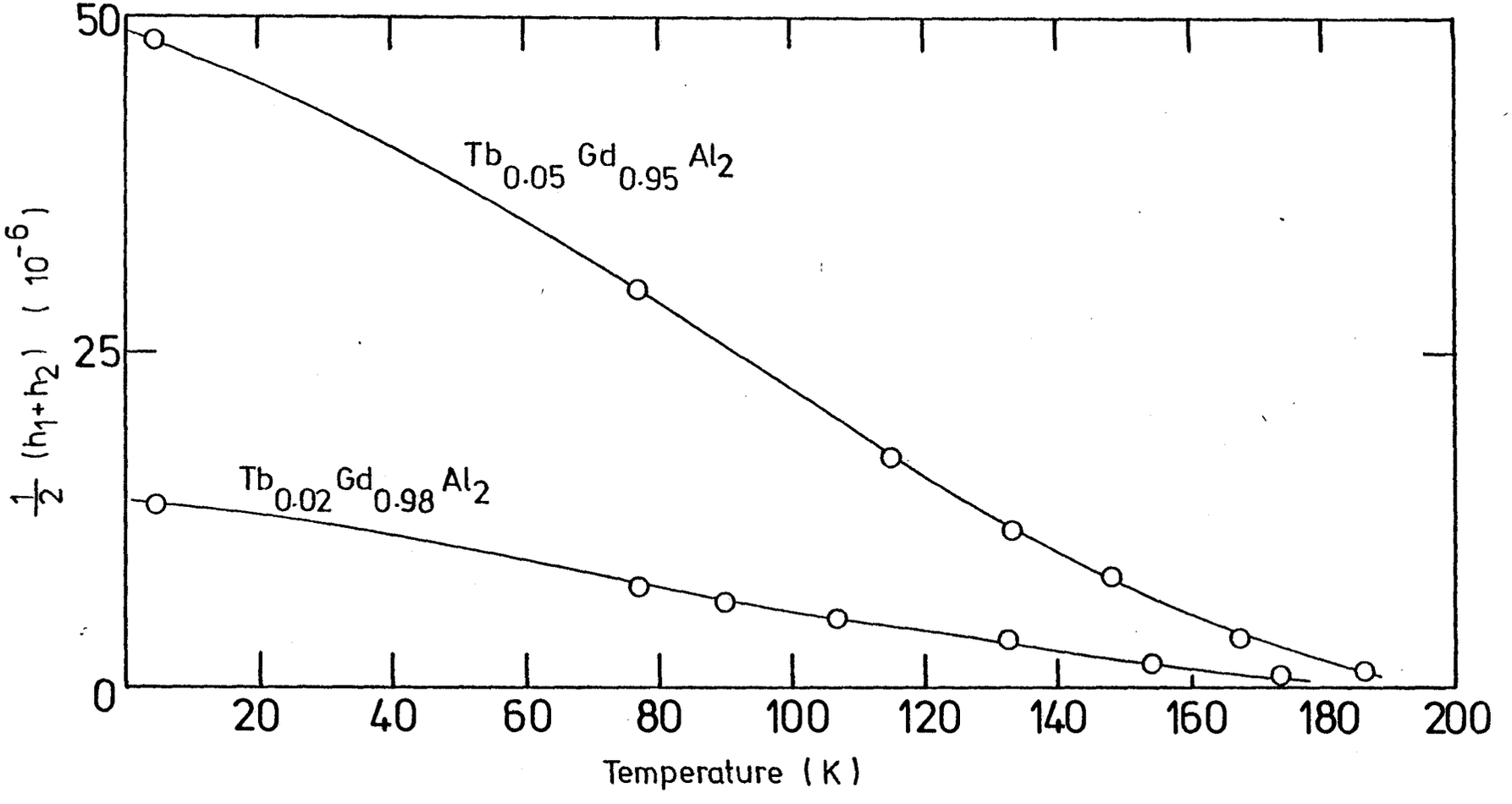

Fig. 7.4 $\frac{1}{2}(h_1+h_2)$ for $Tb_{0.05}Gd_{0.95}Al_2$ and $Tb_{0.02}Gd_{0.98}Al_2$

TABLE 7.1

Magnetostriction constants at 4.2K for $GdA\ell_2$ and the dilute alloys containing 2% and 5% Tb.

Sample	h_1 (meas) $\times 10^{-6}$	h_2 (meas) $\times 10^{-6}$	$\frac{1}{2}(h_1 + h_2)$ meas $\times 10^{-6}$	h_1 (derived) $\times 10^{-6}$	h_2 (derived) $\times 10^{-6}$
$Gd\ A\ell_2$	0.9	-25.9	-	6.0	-25.1
$Gd_{0.98}\ Tb_{0.02}\ A\ell_2$	33.9	-	13.6	-	-
$Gd_{0.95}\ Tb_{0.05}\ A\ell_2$	75.8	-	48.4	-	-
$Tb\ A\ell_2$	-	-	-	1400.0	920.0

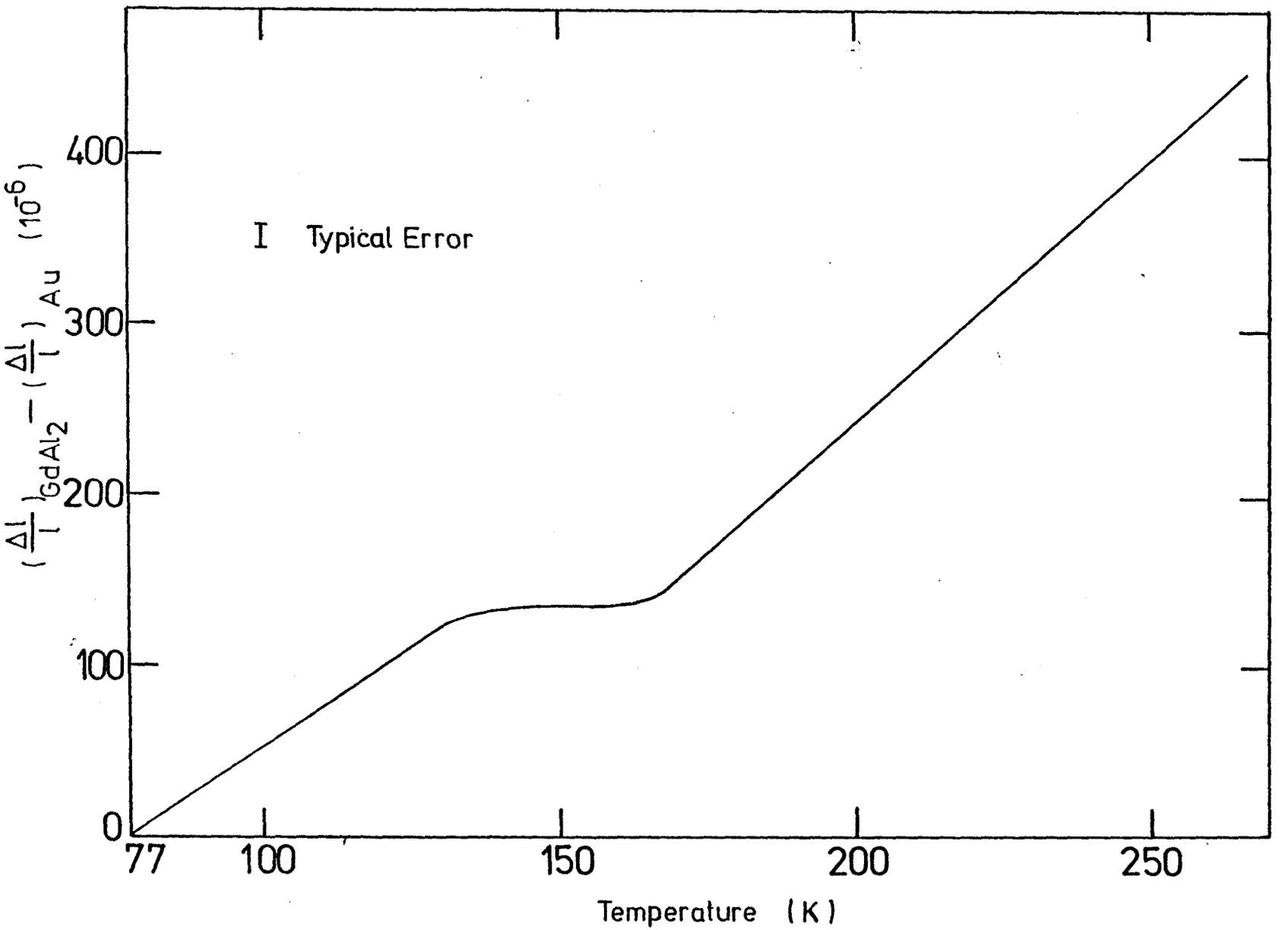

Fig. 7.5 Thermal Expansion of $GdAl_2$ (with Au compensating gauge)

and compare this to the definition of the slope of the $d\ell/\ell$ vs.T. curves i.e :-

$$\text{slope} = \underset{T_1 \to T_2}{\text{Lt}} \frac{\left(\frac{\Delta\ell}{\ell}\right)_{T_1} - \left(\frac{\Delta\ell}{\ell}\right)_{T_2}}{\delta T} \qquad \ldots(7.8)$$

If the value of $\frac{\Delta\ell}{\ell}$ is referred to a length at a reference temperature T_o , ℓ_o we know that :

$$\ell_T = \ell_0 \ (1 + \alpha T) \qquad \ldots(7.9)$$

and that:

$$\left(\frac{\Delta\ell}{\ell}\right)_{T_1} - \left(\frac{\Delta\ell}{\ell}\right)_{T_2} = \frac{\ell_o^2}{\ell_T} \ \delta\ell \qquad \ldots(7.10)$$

where $\delta\ell = \ell_{T_1} - \ell_{T_2}$

Hence the slope S becomes:

$$S = \frac{\ell_o}{\ell_T^2} \left[\frac{\delta\ell}{\delta T}\right]_{\text{Lt } \delta T \to 0} \simeq \frac{\ell_o}{\ell_T} \ (\alpha_T) \qquad \ldots(7.11)$$

From (7.9) and (7.11) :

$$S = \frac{\alpha}{1 + \alpha T} \qquad \ldots(7.12)$$

As the value of α is approximately 10^{-6} the slope of the $d\ell/\ell$ versus T curve may be taken as the thermal expansion coefficient α . The values of α for all three samples (5 gauge directions in total) are within

(the large) experimental error of each other so a composite curve of α, showing the anomaly below the ordering temperature was obtained and is given as figure 7.6. It must be taken into account that, as the strain measuring system consisted of two gauges the active on $GdAl_2$ being compensated by a similar gauge cemented onto a gold dummy sample in close proximity to it, the value of α obtained from these measurements is, in fact, α ($GdAl_2$) - α (Au) over the temperature range. The thermal expansion of gold is well documented (8) but due to the large errors involved this measurement can only be regarded as a qualitative one.

7.5. Determination of the magnetostriction constants of $TbAl_2$ from the dilute alloy measurements

For the dilute alloys it is possible, assuming a linear dependence of the magnetostriction on terbium concentration to use the results on the two alloys to obtain values of h_1 and h_2 for both $TbAl_2$ and $GdAl_2$. Because $GdAl_2$ has a small magnetostriction (section 7.2) the measurements on the dilute alloys will give the magnetostriction constants for $TbAl_2$ wheras measurements on 100% single crystal $TbAl_2$ would not be of any use because the large anisotropy (Chapter 6) would prevent the rotation of the magnetisation vector into the 'hard' (100) direction with the low fields available for this work.

The magnetostriction arising from the $TbAl_2$ has been calculated therefore from the magnetostrictions of the two dilute alloys using:-

$$h_M\,(Gd_{0.95}\,Tb_{0.05}\,Al_2) = 0.05 \times h_T + 0.95 \times h_G \qquad \ldots(7.13a)$$

$$h_M\,(Gd_{0.98}\,Tb_{0.02}\,Al_2) = 0.02 \times h_T + 0.98 \times h_G \qquad \ldots(7.13b)$$

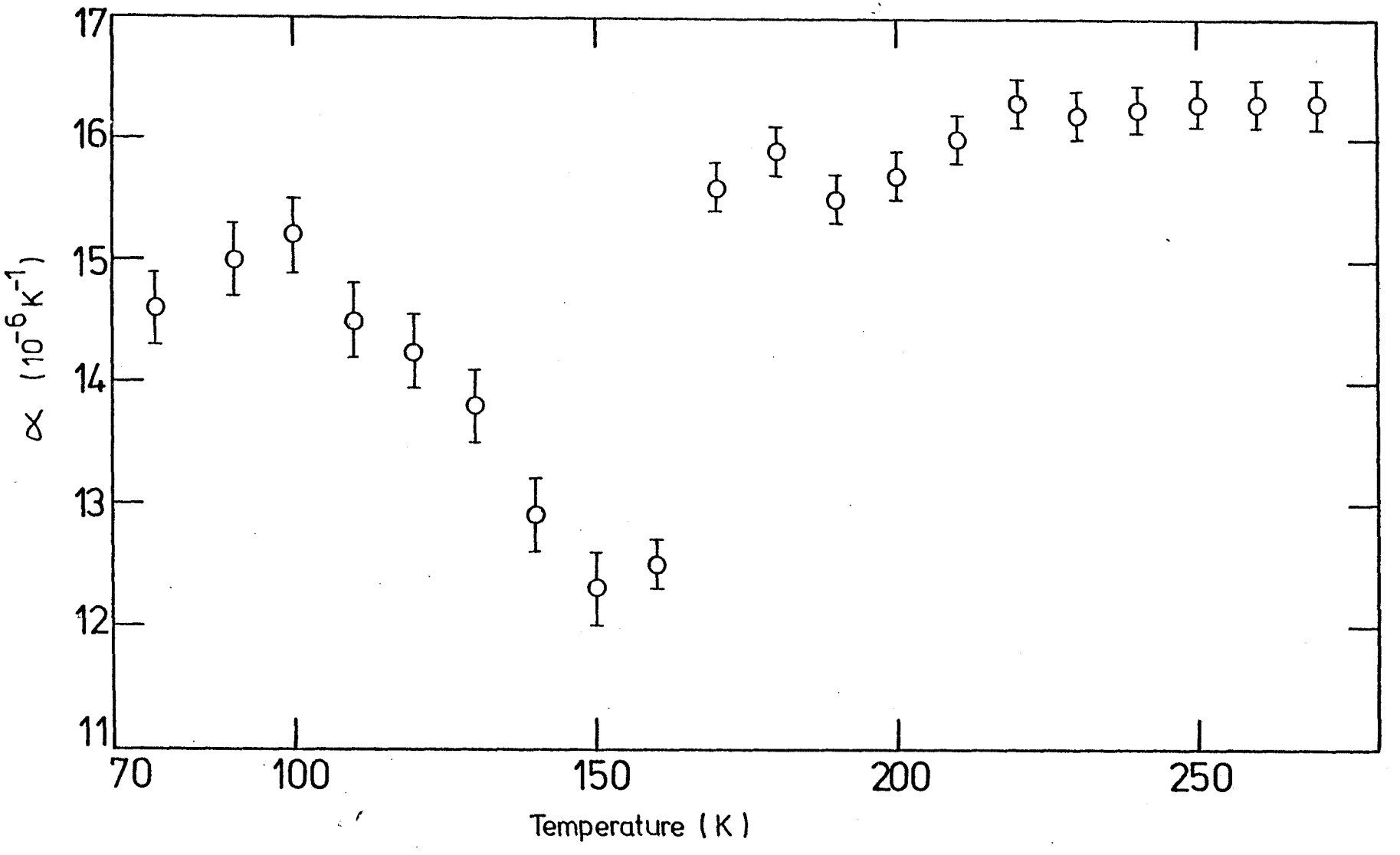

Fig. 7·6 Thermal Expansion Coefficient of $GdAl_2$ ($\alpha_{meas} + \alpha_{Au}$)

Where h_M , h_T and h_G are the particular magnetostriction constants (h_1 or h_2) of the measured sample, $TbAl_2$ and $GdAl_2$ respectively. The two equations were then solved simultaneously, using the experimental results to obtain h_1 and h_2 for both $GdAl_2$ and $TbAl_2$. The derived values for $GdAl_2$ are compared with those obtained by direct measurement (section 7.2) in figure (7.7). The values of h_1 and h_2 for $TbAl_2$ are shown in figure (7.8).

The values derived from the simultaneous solution for the dilute alloys are (at 4.2K) for $TbAl_2$: $h_1 = 1400 \times 10^{-6}$, $h_2 = 920 \times 10^{-6}$ and for $GdAl_2$: $h_1 = 6.0 \times 10^{-6}$, $h_2 = -25.1 \times 10^{-6}$. The larger derived value for h_1 of $GdAl_2$ compared with the direct measurement at lower temperatures is attributed to anisotropy effects which allow the angle between the (100) direction and the magnetisation, α, to become finite in the dilute alloy case. This is illustrated in section 6.10 when discussing the torque measurements and occurs because even 5% substitution of Tb means that in the fields available the angle α becomes significant at the lower end of the temperature range. In this case the effective measured h_1 is reduced for the 5% sample and this has the effect of increasing h_1 ($GdAl_2$) when solved simultaneously with the 2% measurements, (figure 7.7). Obviously for $GdAl_2$ the direct measurements are more reliable, but for the case of $TbAl_2$ when only relatively small fields are available, the derivation of the magnetostriction constants from dilute alloy measurements is a valuable exercise.

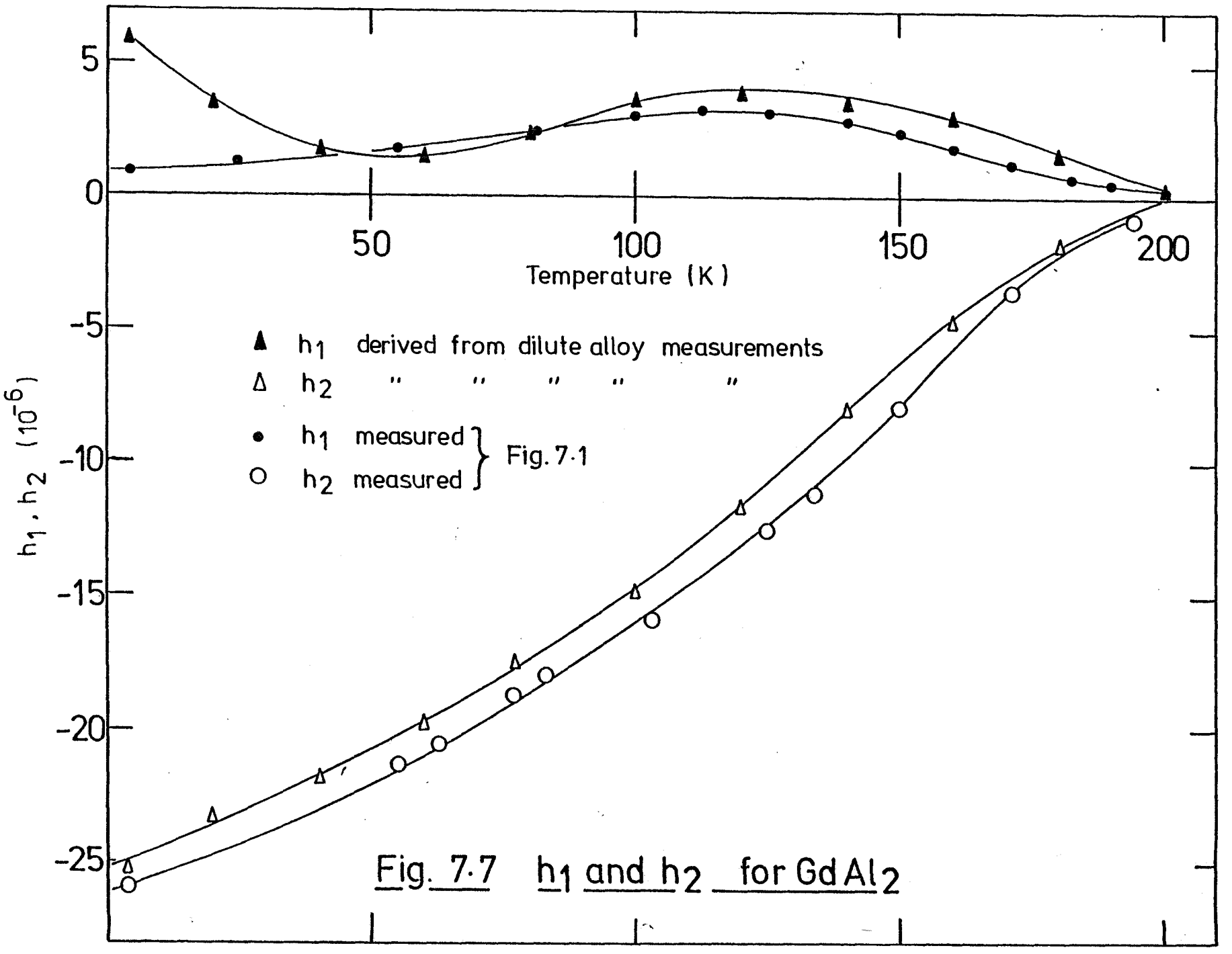

Fig. 7·7 h_1 and h_2 for $GdAl_2$

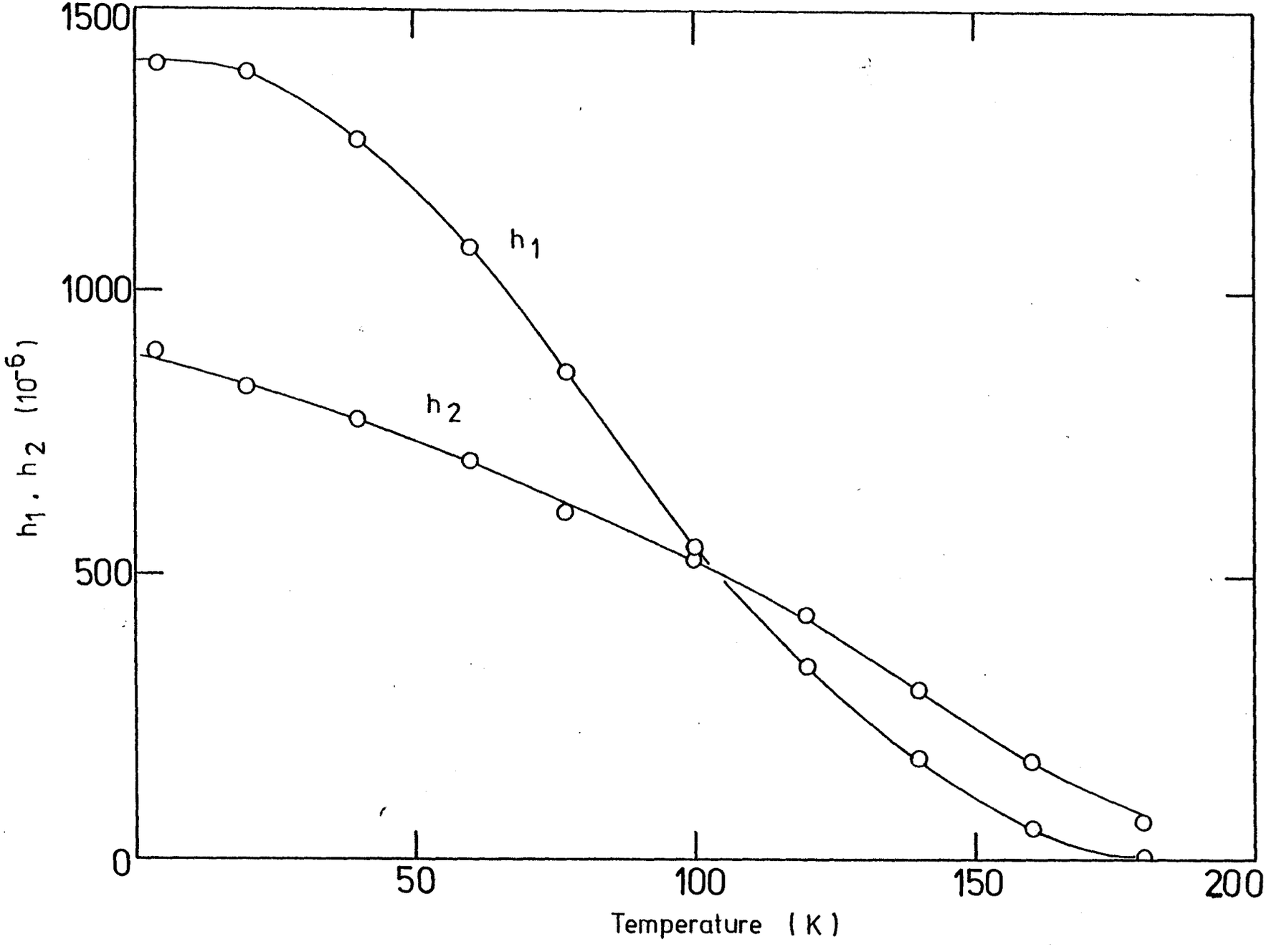

Fig.7.8 h_1 and h_2 for $TbAl_2$ (derived from dilute alloy measurements)

CHAPTER 8

8. A THEORETICAL CALCULATION FOR DILUTE ALLOY SYSTEMS

8.1. Introduction

To obtain insight into the behaviour of an alloy system containing two magnetic species, a computer program was developed to solve numerically for the equilibrium orientations of an array of spins. Numerical values used for the parameters defining the problem were those for the system Tb in $GdAl_2$ on which experimental measurements had been made (Chapter 6).

The model used was a semi-classical one in which the spins interact with each other by a nearest-neighbour only isotropic exchange. The anisotropies of the spins were described by the single-ion anisotropy constants obtained from bulk measurements on single species materials.

An initial approach which considered an equilibrium sum of torques within the crystal was discarded in favour of an energy sum which was minimised with respect to the spin orientations for each applied field direction, φ. Because the torque is then just the slope of this energy function ($-dE/d\varphi$) it was then a simple matter to derive torque curves.

The results show that it is often possible to analyse torque measurements on a dilute alloy system in terms of single bulk anisotropy constants which will have a connection to those of the two magnetic species. Furthermore, in this case, where the $GdAl_2$ contribution to the total torque is negligible, it is also possible to derive bulk anisotropy constants for the impurity material ($TbAl_2$).

Similar systems, using dilute rare earths in gadolinium metal, have been investigated in some detail theoretically by Miwa and others (1,2,3) to interpret the experimental results of Chikazumi (4).

Chikazumi himself used a simple model involving only two spins whose properties were scaled in proportion to their concentrations. The extended calculations of Miwa use a spin-wave approach to the problem, but the calculations are extremely involved and it is difficult to see the effect on the final result of approximations introduced during the calculation. In any case the spin-wave effect is necessarily a transverse one and it may not be applicable to a longitudinal perturbation of the spin directions. However the configuration used in these calculations stems from the idea of a spin direction deviation within the host material in the neighbourhood of the impurity, which was introduced by Asada and Miwa in reference (2) (figure 1), and is reproduced in figure (8.1).

8.2. Physical Principles

a) Geometric: In the cubic Laves phase structure of the RAl_2 compounds the magnetic rare earth ions lie on a diamond lattice with the tetrahedral axis in the (111) cube direction. The aluminium sites are not considered in a magnetic analysis. Therefore the central ion of the system was taken to be Tb (impurity) which has four Gd (host) ions as nearest-neighbours. The next nearest-neighbours consist of three more Gd ions associated with the first four and in turn, these each have three more associated with them. Thus the calculation simply considered each shell of ions as having the same spin orientation and to be exchange coupled only to nearest-neighbours. The R-R nearest-neighbour separation for the cubic C15 Laves structure is the same for each successive shell and equal to $\sqrt{3}\ a\ /\ 4$ where a is the lattice parameter.

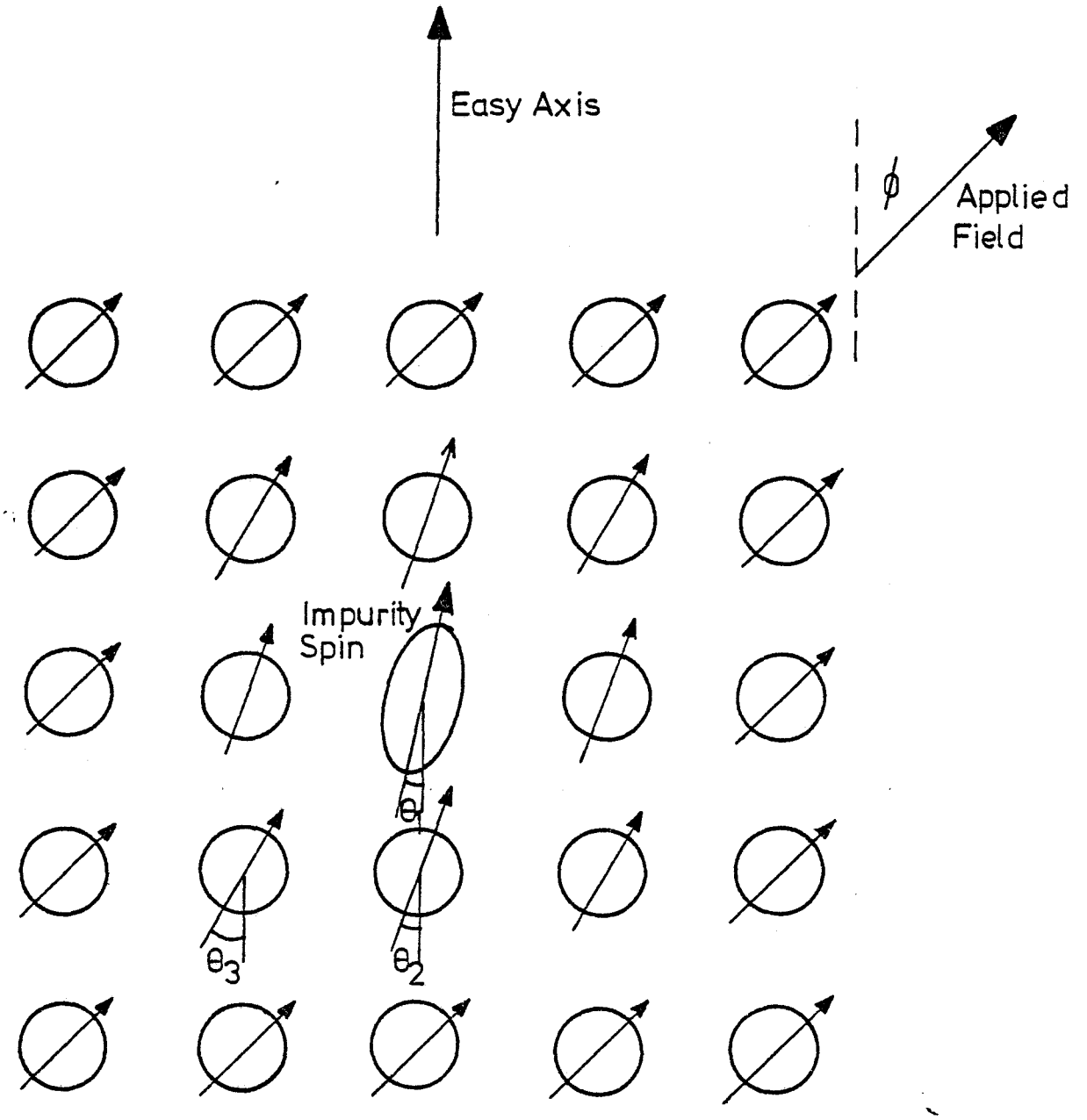

Schematic representation of spin direction deviations of a host material with a strongly anisotropic impurity spin at the centre and a field applied away from the easy axis

Fig. 8·1

b) Anisotropy: The variables in the energy expression were chosen to be the angular positions θ_i of the successive shells of spins with respect to the easy axis defined by the anisotropy constants K_i. For the Tb-$GdAl_2$ case both $TbAl_2$ and $GdAl_2$ have <111> easy (which implies K_1, $K_2 < 0$) but for the numerical calculation K_1(Tb) and K_1(Gd) were taken to be positive and K_2(Tb) and K_2(Gd) equal to zero.

Thus the energy due to the anisotropy, E_A, was written:-

$$E_A = K_a \sin^2\theta_1 + 4K_b (\sin^2\theta_2 + 3 \sin^2\theta_3 + 3^2\sin^2\theta_4 + \ldots\ldots) \quad \ldots(8.1)$$

Where K_a is K_1 for Tb and K_b, K_1 for Gd. The energy is thus the total energy of the array.

c) Exchange: The ions are considered to interact only by nearest-neighbour exchange where the form of the exchange energy for a single ion pair will be

$$E_{ij} = \mathcal{J}_{sf}\, S_i \cdot S_j \quad \ldots(8.2)$$

Where $\mathcal{J}_{sf}$ is the single-ion exchange constant and S_i , S_j are the two spins. Hence the interaction energy will have a cosine dependence on the angular variables θ_i:-

$$E_{ex} = 4\Gamma_a \cos(\theta_1 - \theta_2) + 12\Gamma_b (\cos(\theta_2 - \theta_3) + 3\cos(\theta_3 - \theta_4) + \ldots) \quad \ldots(8.3)$$

where Γ_a and Γ_b are the exchange energies associated with (Tb-Gd) and (Gd-Gd) exchange.

d) Magnetic Field: When a magnetic field is applied in a direction φ then the spins will try to align themselves with the field. They will rotate until the anisotropy torque is equal and opposite to that produced by the field. For a single-ion the field energy is:

$$E = - m \cdot B \qquad \ldots (8.4)$$

which may be written as:

$$E = - g_J \mu_B J B \cos (\theta_i - \varphi) \qquad \ldots (8.5)$$

where θ_i is the orientation of the spin J in field B applied at an angle φ, both with respect to the same axis.

8.3. The Numerical method

This method employed N.A.G. library standard subroutine E04CCF which is designed to minimise any arbitrary function with respect to any number of variables. It uses an iterative method which sets up a simplex of n + 1 points in n dimensional space (where n is the number of variables), thus for two variables the simplex will be a triangle. The first vertex is entered as the first set of variables and the remainder of the system is generated by the subroutine. The procedure then eliminates points which are largest and subsequently reduces the sides of the simplex to converge on the minimum point. This method, due to Nelder and Mead (5) is slower than other methods but is robust and particularly suited for minimising complex functions.

The function was supplied in the form of the sum of terms for anisotropy, exchange and field energies above and the output of the equilibrium values of the θ_i was obtained for magnetic field orientations at 5° intervals for a 90° rotation. A flow chart for the operation of the program is given in figure (8.2).

8.4. Input parameters

The energy function was calculated and minimised in terms of energy per ion. The units used were 10^{-24} Joules (ppJ). The single-ion anisotropy constant was taken to be a^3/n times the bulk anisotropy constants where a is the lattice parameter and n the number of atoms in the unit cell (in this case, n=8). This gave anisotropy energies, per ion, ignoring K_2, of 425 ppJ for the terbium ion in $TbAl_2$ (6) and 0.265 ppJ for the gadolinium ion in $GdAl_2$ (this work). The energy contribution due to the magnetic field is calculated from the magnetic moment per ion (in Bohr magnetons). Values used were 7.0 μ_B/Gd (7) and 9.2 μ_B/Tb (8). Hence the energies in $ppJT^{-1}$ per ion are 64.9 and 85.3 respectively.

Finally values for the exchange interactions (Γ_a and Γ_b equation (8.3)) were determined using the known value of the exchange field for $TbAl_2$ (9) and the scaling factor for the rare earth series given in figure 5 of reference (10) to determine Γ_b. The assumption that, for Tb-Gd exchange, the exchange constant was the arithmetic mean of that for Gd and Tb was made in order to derive Γ_a. The calculation finally gave values of 1510 ppJ and 1370 ppJ per ion pair for Gd-Tb and Gd-Gd exchange respectively.

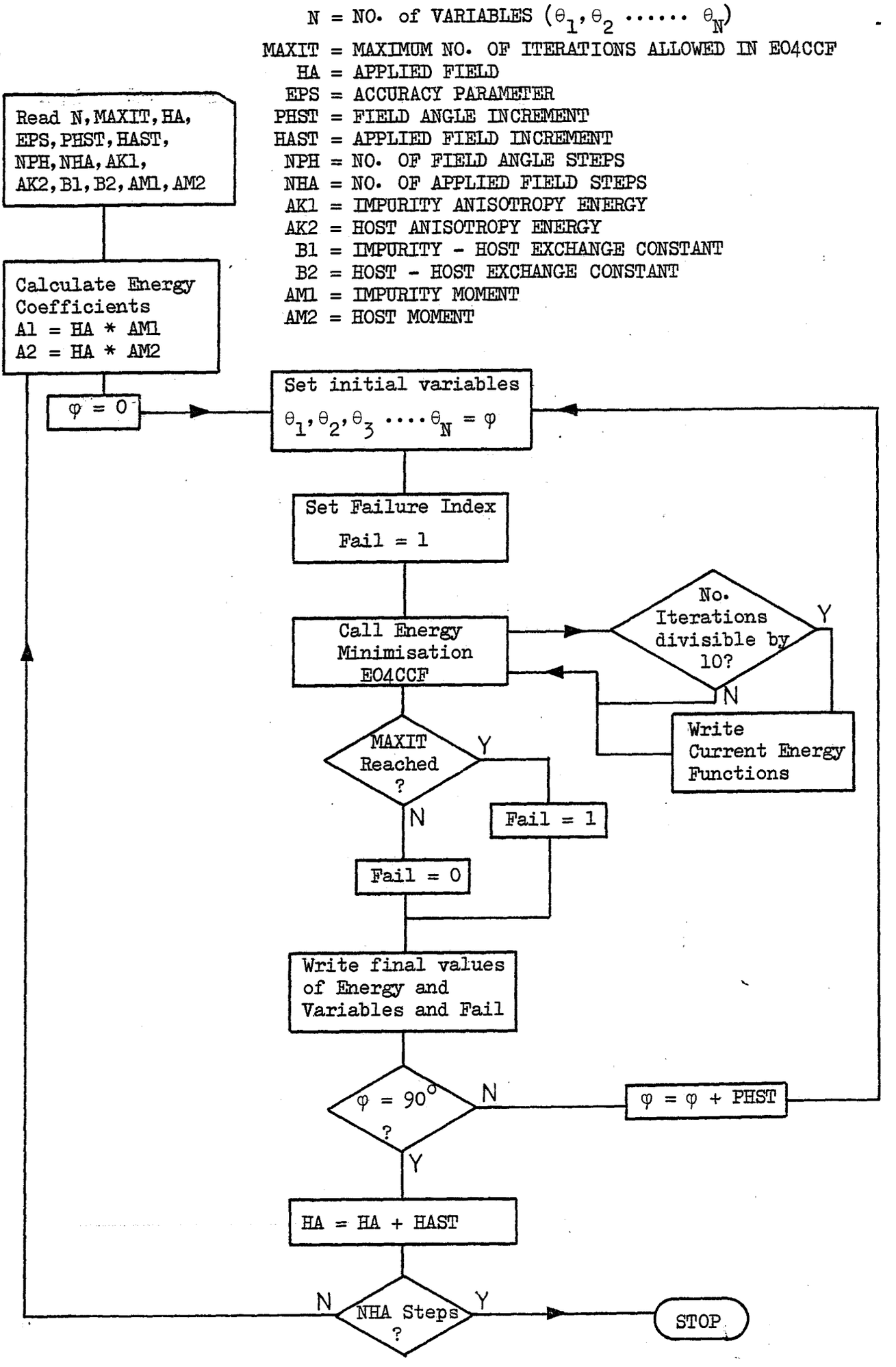

Fig. 8.2 Flowchart for computer calculation

The numerical minimisation was performed for field values from 0.5T to 3.0T in 0.5T steps. At each field value the function was minimised for field directions at 5° intervals between 0 and 90° .

The energy function itself consisted of a sum of terms like equations (8.1), (8.3) and (8.5) in a number of variables. The most convenient case used was for four variables (i.e. terms up to θ_4). This corresponded to one terbium per 53 gadolinium ions, which is approximately 2% atomic, and therefore a similar case to the first dilute alloy sample, (Chapter 6). A further calculation with the central Tb replaced by Gd was undertaken to ascertain the orientation of the bulk material without impurity spin. An alternative approach, also employed, was to minimise with respect to ten variables (i.e. terms up to θ_{10}) to determine how far from the impurity spin its influence on the host became negligible. The ten variable case corresponds to a concentration of Tb ions of 1 : 39 365.

8.5. Results and further analysis

The primary result of the calculations was that the spin disturbance, which may be interpreted as a local variation of the magnetisation was extremely long range, for the system considered and significant at 5 or 6 nearest-neighbour distances (equivalent to ($\sqrt{3}a/4$) from the impurity at low fields. Even at high field values the ten shell calculation showed that the disturbance to the spin directions was significant (approximately 0.1°) for the fourth shell of Gd ions surrounding the anisotropic Tb impurity ion. This corresponds to one Tb for each 160 Gd ions, a concentration of less than 0.7%.

It must be stressed that the system considered is rather extreme, but the same sort of effects must be expected for other dilute alloy systems.

Once the extent of the spin disturbance had been derived it was thought necessary, in the light of the experimental results (Chapter 6), to extend the calculation to determine torque curves for the theoretical system. In this case the four spin calculation was employed because it corresponded approximately to the 2% alloy. The energy function was now known and could be tabulated as a function of the field direction φ. The slope of this curve ($-dE/d\varphi$) was then the value of the torque and torque curves could be plotted (figure 8.3). These theoretical curves were then analysed as if they were single species crystals using the method of peak height, Fourier analysis of corrected curves and initial slope. (An explanation of these methods is given in chapter 6).

Then using the derived value of K_1 for the crystal and assuming the contribution of the gadolinium to be negligible the results were scaled up to obtain a derived anisotropy for the terbium. Obviously this will be expected to be the input value used for the program (7×10^6 J m^{-3} or 425 ppJ/ion).

The results are rather surprising: both the peak height and Fourier transform methods give, within the rounding inaccuracies in the arithmetic, the value of $7 \times 10^6 \pm 1\%$ J m^{-3} for the first anisotropy constant of $TbAl_2$; but the initial slope method is subject to extremely large (> 10%) inaccuracies, giving a consistently low value for the first anisotropy constant. It is also observed that the corrected torque curves which should be pure (sin 2θ), do not have a maximum at 45° but contain approximately 10% (sin 4θ) and 1% (sin 6θ) components, (Table 8.1).

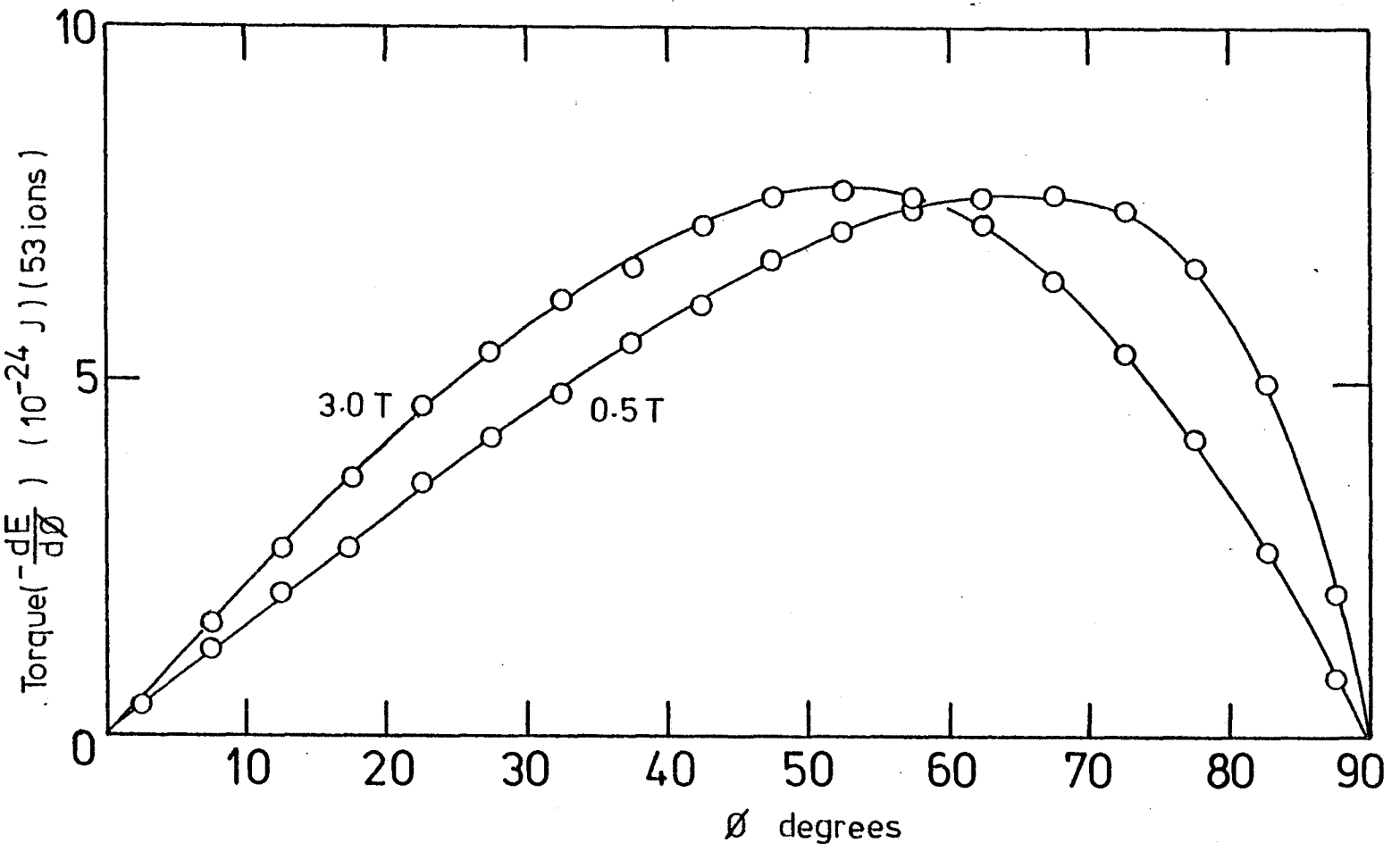

Fig. 8·3 Torque Curves from Energy Minimisation Programme for the 53-spin System

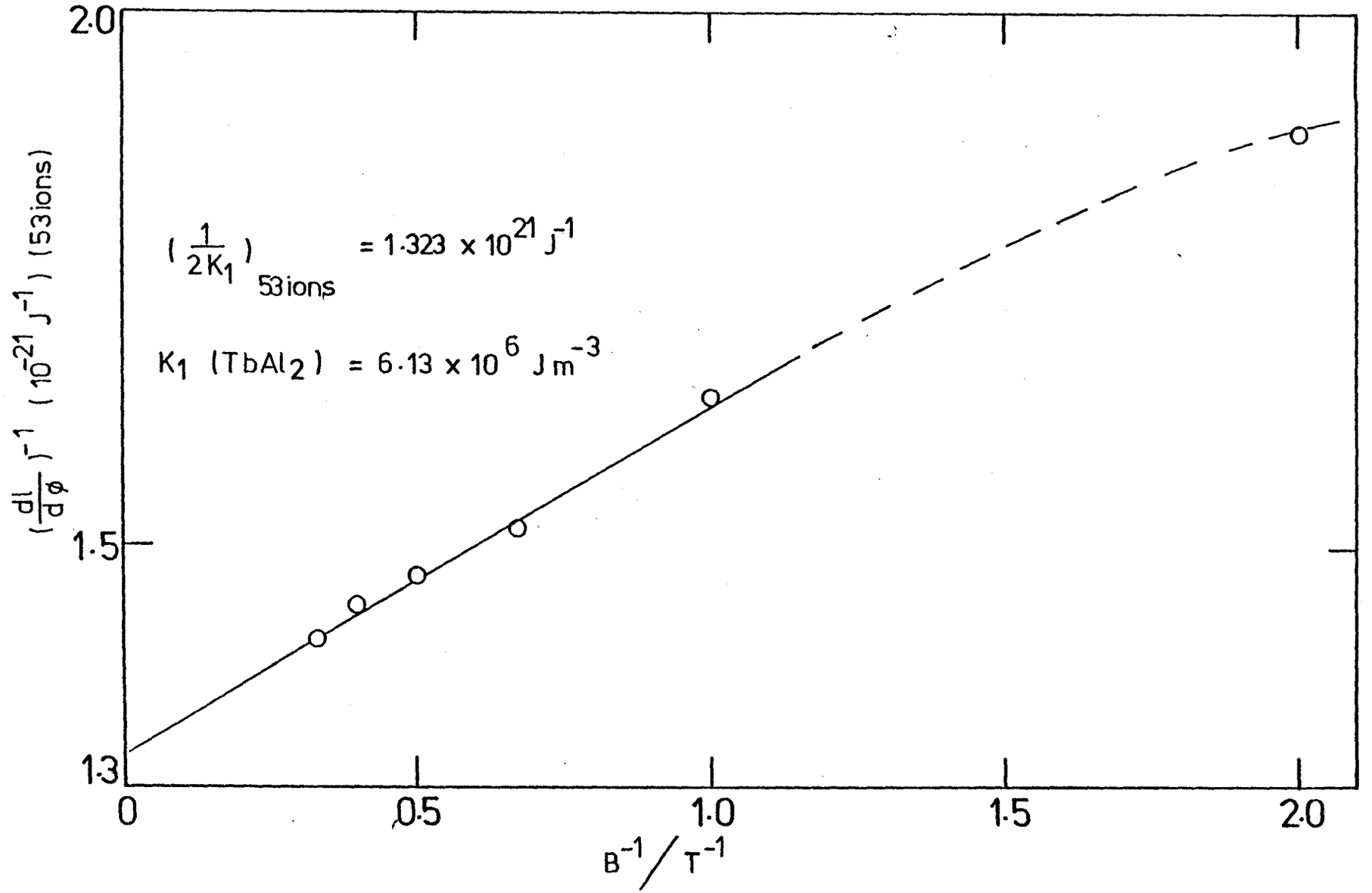

Fig. 8·4 Initial Slope Extrapolation for Theoretical Torque Curves

TABLE 8.1

Fourier components of the corrected torque curves:

$L(\theta) = A_2 \sin 2\theta + A_4 \sin 4\theta + A_6 \sin 6\theta$

Component	Magnitude	
	10^{-24} J.deg^{-1} (53 ions)	10^{6} Jm^{-3} (normalised to 100% $TbA\ell_2$)
A_2	7.616	7.07
A_4	0.672	0.624
A_6	0.069	0.064

8.6 Discussion

Some explanation of the discrepancies observed between the results in Chapter 6, for the dilute alloys of Tb-$GdAl_2$, may now be offered as well as an indication of the best method to be used for the analysis. As expected, if it can be shown that the anisotropic impurity may be rotated over the full range of θ_1, (angle between the anisotropic spin and the crystal axis) then the method of correcting the torque curves and Fourier analysis is extremely useful. However, contrary to the case of the single-species crystal, determination of anisotropy constants from torque curves by means of an initial slope extrapolation is not at all accurate. The explanation of this is not clear, but along with the additional component in the corrected torque curves these errors must be associated with the spin direction variation through the crystal.

The anisotropy constants of highly anisotropic materials may be obtained by torque measurements in laboratory fields if a suitable magnetically isotropic host can be found to supply a 'handle' which, via exchange coupling, may be used to rotate the anisotropic ions.

These calculations have shown that the method of initial slope breaks down for the non-homogeneous magnetisation introduced by the impurity and therefore cannot be used with confidence for the dilute alloy case.

APPENDIX A

A theoretical analysis of the torque transducer system

The overall construction of the transducer systems used in the experiments may be seen in figure 5.2.2 of Chapter 5.

The assembly considered in this analysis is shown in figure A1. It consists of two parallel rigid plates connected by three spring strips of constant width x, thickness y and length z. The strips are rigidly fixed perpendicular to the plates with their x dimension in a radial direction from the axis of the transducer and with their long axes (z) intersecting the plates on the circumference of a circle, radius r at 120° to each other.

If one disc is rotated with respect to the other, about the central axis by an angle θ, then the strips will be bent as shown in figure A2. The restoring forces R will act on the disc and a total couple $3 \cdot R \cdot r$ will be produced (figure A3).

Considering figure A2 it can be seen, by symmetry, that when the strips are bent they adopt the configuration of two cantilevers deflected by $\frac{1}{2}\, r\, \theta$ at their ends.

Bending beam theory gives, for a virtual load H at the end of a beam length $z/2$ rigidly fixed at its other end, the expression:

$$\frac{1}{2}\, r\, \theta = \frac{1}{3}\, H \cdot \left(\frac{z}{2}\right)^{3} \cdot \frac{1}{E \cdot I} \qquad \ldots\ A\ (1)$$

Where E is the Young's Modulus of the beam and I its Second Moment of Inertia.

For a beam of width x and thickness y, the second moment of inertia I is given by:

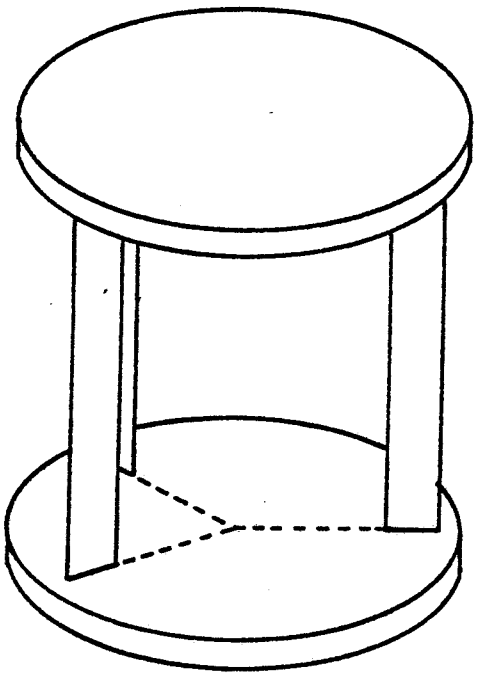

Fig. A1

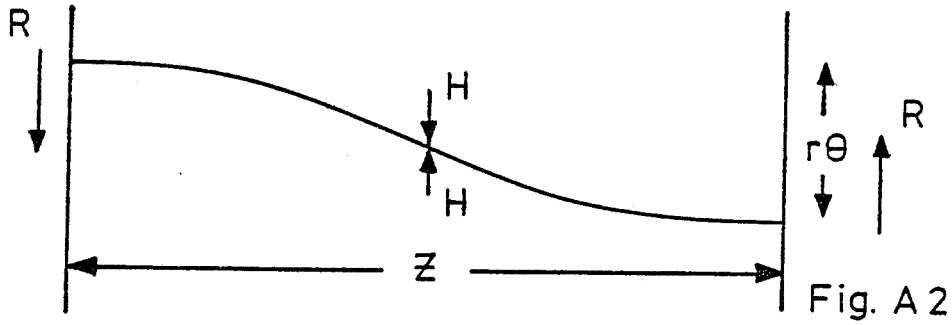

Fig. A 2

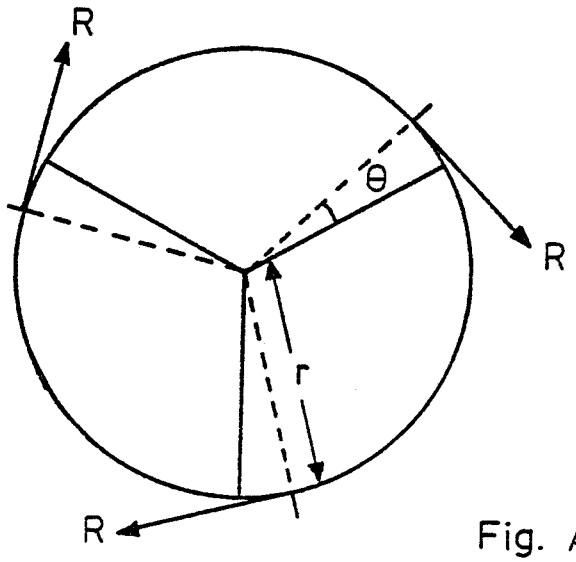

Fig. A3

$$I = \int_{\frac{-y}{2}}^{\frac{+y}{2}} q^2 \, dA \quad , \quad \text{where } dA = x \cdot dq \qquad \ldots\ldots A\ (2)$$

When evaluated this gives:

$$I = \frac{x\,y^3}{12} \qquad \ldots\ldots A\ (3)$$

Re-arranging A(1) and substituting for I, the reaction on the support R is:

$$R = H = \frac{r\,\theta\,E\,x\,y^3}{z^3} \qquad \ldots\ldots A\ (4)$$

Therefore the torque T produced by the transducer per unit angular deflection is given by:

$$T = \frac{3 \cdot R \cdot r \cdot}{\theta} = \frac{Er^2\,x\,y^3}{z^3} \qquad \ldots\ldots A\ (5)$$

This equation was used to predict the effect of spring dimension changes on transducer sensitivity. However only limited success was achieved because of variations of the Young's Modulus, E, of the spring material used (phosphor-bronze). Therefore it is necessary to use the same batch of material, or that of constant quality unless a separate determination of the Young's Modulus of the springs is made, before employing equation A(5).

APPENDIX B

Derivation of initial slope expression for the symmetry directions of a [110] plane in a cubic crystal

The initial slope of a torque curve at a symmetry direction (where the torque is zero) may be related to the anisotropy constants and a term in reciprocal field ($^1/B$) where B is the applied field. Thus an extrapolation of values obtained for the initial slopes against B^{-1} to $B^{-1} = 0$ will give the value of the anisotropy constant(s) involved.

The expression for the torque of a crystal which has the [110] plane as the plane of rotation is given by: (chapter 6, equation 6.13)

$$L = -\left[\frac{K_1}{4} + \frac{K_2}{64}\right]\sin 2\theta - \left[\frac{3K_1}{8} + \frac{K_2}{16}\right]\sin 4\theta + \frac{3K_2}{64}\sin 6\theta \qquad \cdots B(1)$$

Where the K_1 and K_2 are the anisotropy constants and θ is the angle between the magnetisation and the [100] direction.

However, as discussed in section 6.1, a finite angle will exist between the applied field and the magnetisation directions. The torque curve is then measured as a function of $(\theta + \alpha)$ where α is given by the relation:

$$\alpha = \sin^{-1}\frac{L}{M.B} \qquad \cdots B(2)$$

from equation 6.4.

Thus we need to derive the values of $\frac{\partial L(\varphi)}{\partial \varphi}$ for each of the symmetry directions [100], [110] and [111] where φ is the angle between the applied field and the < 100 > axis of the crystal i.e. $L(\varphi)$ is the measured data.

From equation B(1)

$$\frac{\partial L}{\partial \varphi} = -2\left[\frac{K_1}{4} + \frac{K_2}{64}\right] \cos 2(\varphi - \alpha).(1 - \frac{\partial \alpha}{\partial \varphi}) - 4\left[\frac{3K_1}{8} + \frac{K_2}{16}\right] x \ldots.$$

$$\cos 4(\varphi - \alpha).(1 - \frac{\partial \alpha}{\partial \varphi}) + \frac{6.3K_2}{64} \sin 6(\varphi - \alpha).(1 - \frac{\partial \alpha}{\partial \varphi}) \quad \ldots B(3)$$

From equation B(2), taking sin $\alpha = \alpha$ if α small:-

$$\frac{\partial \alpha}{\partial \varphi} = \frac{\partial L}{\partial \varphi} \cdot \frac{1}{MB} \quad \ldots B(4)$$

For a symmetry direction L = 0, i.e. $\alpha = 0$ from equation B(2).

$$\left[\frac{\partial L}{\partial \phi}\right]_{L=0} = \left[-2\left(\frac{K_1}{4} + \frac{K_2}{64}\right) \cos 2\theta - 4\left(\frac{3K_1}{8} + \frac{K_2}{16}\right)\cos 4\theta + \frac{6.3}{8} K_2 \cos 6\theta\right]\left(1 - \frac{\partial \alpha}{\partial \phi}\right) \quad \ldots B(5)$$

If we let the terms within the square brackets on the right hand side of equation B(5) be Q then suitable manipulation of equations B(4) and B(5) leads to:

$$\left(\frac{\partial L}{\partial \varphi}\right)^{-1}_{L=0} = \frac{1}{Q} + \frac{1}{M.B} \quad \ldots B(6)$$

This equation may then be evaluated by substituting the values of θ of each symmetry direction into Q. Each of the directions has an exact fractional result and these are given in equations B(7), B(8) and B(9) below.

For the < 100 > direction, $\cos 2\theta = \cos 4\theta = \cos 6\theta = 1$

$$\left(\frac{\partial L}{\partial \theta}\right)^{-1}_{100} = \frac{1}{2K_1} + \frac{1}{MB} \qquad \ldots B(7)$$

For the < 110 > direction, $\cos 2\theta = -\cos 4\theta = \cos 6\theta = -1$

$$\left(\frac{\partial L}{\partial \theta}\right)^{-1}_{110} = \frac{1}{K_1 - \frac{K_2}{2}} + \frac{1}{MB} \qquad \ldots B(8)$$

For the < 111 > direction, $\cos 2\theta = -\frac{1}{3}$; $\cos 4\theta = -\frac{7}{9}$; $\cos 6\theta = \frac{23}{27}$

$$\left(\frac{\partial L}{\partial \theta}\right)^{-1}_{111} = \frac{1}{-\frac{4}{3}K_1 - \frac{4}{9}K_2} + \frac{1}{MB} \qquad \ldots B(9)$$

REFERENCES

CHAPTER 2

1) J.H. Wernick and S. Geller , Trans. metall. Soc. AIME 218, 866 (1960)

2) J.B. Friauf, J. Am. Chem. Soc. 49, 3107 (1927)

3) K.H.J. Buschow and J.H.N. van Vucht, Phillips Res. Repts., 22, 239 (1967)

4) H.J. Williams, J.G. Wernick, E.A. Nesbitt and R.C. Sherwood
J. Phys. Soc. Jap., 17, B1, 91 (1962)

5) H.G. Purwins, Z. Phys. 233, 27 (1970)

6) M. Godet, E. Walker and H.G. Purwins, J. Less Comm. Metals 30, 301 (1973)

7) B. Barbara, M.F. Rossignol, H.G. Purwins and E. Walker, Phys. Stat. Sol. (a)
22, 553 (1974)

8) H.G. Purwins, E. Walker, B. Barbara, M.F. Rossignol and P. Bak,
J. Phys. C, 7, 3572 (1974)

9) P. Bak, J. Phys. C, 7, 4097 (1974)

10) B. Barbara, M.F. Rossignol, H.G. Purwins and E. Walker, Colloques
Int. CNRS, 242, 51 (1974)

11) I.R. Harris, R.C. Mansey and G.V. Raynor, J. Less Comm. Metals, 9, 270 (1965)

12) W.M. Swift and W.E. Wallace, J. Phys. Chem. Sol., 29, 2053 (1968)

13) H. Oesterreicher and W.E. Wallace, J. Less Comm. Metals, 13, 91 (1967)

14) H. Oesterreicher, Inorg. Chem., 13, 2807 (1974)

15) V. Jaccarino, B.T. Matthias, M. Peter, H. Suhl and J.H. Wernick,
Phys. Rev. Lett. 5, 251 (1960)

16) K.H.J. Buschow, J.F. Fast, A.M. van Diepen and H.W. de Wijn,
Phys. Stat. Sol. 24, 715 (1967)

17) H. Hacker, R. Gupta and M.L. Shepard, Phys. Stat. Sol. (a) 9, 601 (1972)

18) U. Herbst, J. Schraub, E. Dormann and K.H.J. Buschow, Phys. Stat. Sol. (b)
61, K101 (1967)

19) N. Kaplan, E. Dormann, K.H.J. Buschow and D. Lebenbaum, Phys. Rev. B,
7, 40 (1973)

20) M.A.Rudermann and C.Kittel, Phys. Rev. 96, 99 (1954)
T. Kasuya, Prog. Theor. Phys. (Kyoto) 16, 45 (1956)
K. Yosida, Phys. Rev. 106, 893 (1957)

21) A. H. Millhouse, H-G. Purwins and E. Walker, Solid State Commun. 11, 707 (1972)

22) W. Bührer, M. Godet, H-G. Purwins and E. Walker, Sol State Commum. 13, 881 (1973)

23) H-G. Purwins, J.G. Houmann, P. Bak and E. Walker, Phys. Rev. Lett 31 1585 (1973)

24) H.J. vanDaal and K.H.J. Buschow, Solid State Commun. 7, 217 (1969)

25) R.J. Schiltz and J.F.Smith, J.App.Phys. 45, 4681 (1974)

26) M. Godet, Helv. Phys. Acta. 46, 770 (1974)

CHAPTER 3

1) M. I. Darby and E. D. Isaac, IEEE Trans. Magn. MA10, 259 (1974)

2) R. R. Birss, Symmetry and Magnetism, Ch. 5 (North Holland, 1964)

3) H. Zijlstra, Experimental Methods in Magnetism (North Holland, 1967)

4) R. M. Bozorth, Ferromagnetism (Van Nostrand, N.Y. 1951)

5) E. A. Turov and A. J. Mitsek, Zh. E. T. F. 37, 1127 (1959)

6) C. Zener, Phys. Rev. 96, 1335 (1954)

7) R. R. Birss and G. J. Keeler, Phys. Stat. Sol (b) 64, 357 (1974)

8) J. Kanamori, Magnetism Vol. I, Ed: G. T. Rado and H. Suhl (Acad. Press, N. Y. 1963)

9) W. P. Wolf, Phys. Rev. 108, 1152 (1957)

10) J. H. Van Vleck, Phys. Rev. 52, 1178 (1937)

11) P. W. Anderson, Solid State Physics, Ed: F. Seitz and D. Turnbull Vol. 14 (Acad. Press N.Y. 1963)

12) T. Moriya, Magnetism Vol. 1. Ed: G. T. Rado and H. Suhl (Acad. Press N.Y. 1963)

13) N. Akulov, Z. Phys. 100, 197 (1936)

14) F. Keffer, Phys. Rev. 100, 1692 (1955)

15) F. Keffer and T. Oguchi, Phys. Rev. 117, 718 (1960)

16) J. H. Van Vleck, J. Phys. Radium (Paris) 20, 114 (1959)

17) H. B. Callen and E. Callen, J. Phys. Chem. Solids, 27, 1271 (1966)

18) R. R. Birss, Symmetry and Magnetism p. 167 (North Holland, 1964)

19) W. Sucksmith and J. E. Thomspon, Proc. Roy. Soc. (London) A225, 362 (1954)

20) W. J. Carr Jr. Phys. Rev. 109, 1971 (1958)

21) J. J. Rhyne and A. E. Clark, J. Appl. Phys. 38, 1379 (1967)

22) R. Z. Levitin and B. K. Ponomarev, Soviet Phys. J. E. T. P., 26, 1121 (1968)

23) W. D. Corner, W. C. Roe and K. N. R. Taylor, Proc. Phys. Soc. 80, 927 (1962)

24) C. D. Graham Jr., J. Appl. Phys. 34, 1341 (1963)

25) K. Tohyama and S. Chikazumi, J. Phys. Soc. Japan, 35, 47 (1973)

26) M. S. S. Brooks and D. A. Goodings, J. Phys. C. 1, 1279 (1968)

27) W. J. Carr Jr., Encyclopedia of Physics, p. 292 (Springer-Berlin, 1966)

28) W. P. Mason, Phys. Rev. 96, 302 (1954)

29) S. Chikazumi, Physics of Magnetism (John Wiley and Sons, 1964)

30) B. D. Cullity, Introduction to Magnetic Materials (Addison Wesley, 1972)

CHAPTER 4

1) W. J. Carr Jr., Encyclopedia of Physics (Springer-Berlin, 1966)

2) A. E. H. Love, A Treatise on the Mathematical Theory of Elasticity, 4th Ed. (C. U. P., 1944)

3) R. R. Birss, Symmetry and Magnetism, p. 192, (North-Holland, 1966)

4) R. R. Birss and E. D. Isaac, Magnetic Oxides Ch. 6 (John Wiley and Sons, 1975)

5) R. Becker and W. Döring, Ferromagnetismus (Springer-Verlag Berlin, 1939)

6) W. Döring and G. Simon, Ann. Phys. 5, 373 (1960)

7) P. K. Baltzer, Phys. Rev. 108, 580 (1954)

8) J. Alstad and S. Legvold, J. App. Phys. 35, 1752 (1964)

9) R. M. Bozorth and T. Wakiyama, J. Phys. Soc. Japan, 18, 97 (1963)

10) M. A. Asgar, Ph. D. Thesis, University of Southampton (1970)

11) J. C. Slonczewski, J. App. Phys. 32, 253S (1961)

12) W. I. Dobrov, Phys. Rev. 134, A734 (1964)

13) R. Alben and E. R. Callen, Phys. Rev. 186, 522 (1969)

14) J. Kanamori, Magnetism, Vol. I, Ed: G. T. Rado and H Suhl, (Acad. Press N. Y. 1963)

15) W. P. Wolf, J. de Phys. 32, C1 - 26 (1971)

16) R. Becker, Z. Phys. 62, 253 (1930)

17) F. C. Powell, Proc. Camb. Phil. Soc. 27, 561 (1931)

18) L. W. McKeehan, Phys. Rev. 43, 1022 (1933)

19) N. Tsuya, Sci. Res. Inst. Tohoku Univ., B8, 161 (1957)

20) H. Kornfeld, Z. Phys. 22, 27 (1924)

21) A. E. Clark, B. F. de Savage, N. Tsuya and S. Kawakami, J. App. Phys. 37, 1324 (1966)

22) E. R. Callen and H. B. Callen, Phys. Rev. 129, 578 (1963)

23) E. R. Callen and H. B. Callen, Phys. Rev. 139, A455 (1965)

24) R. C. Hall, J. App. Phys. 28, 707 (1957)

25) J. A. J. Lourens and L. Alberts, Solid State Commun. 2, 141 (1964)

26) W. E. Coleman and A. S. Pavolvic, Phys. Rev. 135, A426 (1964)

27) S. Chikazumi, Physics of Magnetism (John Wiley and Sons, 1964)

28) R. Gersdorf, Physica, 26 553, 1028 (1960)

29) W. F. Brown Jr., Rev. Mod. Phys. 25, 131 (1953)

30) R. Gersdorf, J. H. M. Stoelinga and G. W. Rathenau, Physica 27, 381 (1961)

CHAPTER 5

1) H.G.Purwins, Z.Phys. 233, 27 (1970)

2) M.Godet, E.Walker and H.G.Purwins, J.Less-Comm. Metals 30, 301 (1973)

3) J.H.Wernick and S.Geller, Trans. AIME,218, 866 (1960)

4) K.H.J. Buschow and J.H.N.Van Vucht,Phillips Res.Repts.22, 233 (1967)

5) J.C.Brice, The Growth of Crystals from the Melt (North-Holland, 1965)

6) Metals Research Ltd., Publication No.7221

7) D.H.Dennison, M.J.Tschetter and K.A.Geschneidner Jr., J.Less-Comm. Metals, 11, 423 (1966)

8) British Oxygen Company Manual "Inert Gas Purifier Type AGP Ar/He

8a) W.Bardsley, Phys.Bull. 25,340 (1974)

9) I.R.Harris, R.C.Mansey and G.V.Raynor, J.Less-Comm. Metals 9, 270 (1965)

10) L.V.Auroff and M.J.Buerger, The Powder Method (McGraw Hill 1958)

11) J.S. Abell, Private Communication

12) B.Barbara, M.F.Rossignol, H.G.Purwins and E.Walker, Phys.Stat.Sol.(a) 22, 553 (1974)

13) G.Asti and S.Rinaldi, Phys.Rev.Lett. 28, 1584 (1972)

14) M.Huq, Ph.D. Thesis, University of Southampton (1975)

15) A.A.Aldenkamp, C.P.Marks and H.Zijlstra, Rev.Sci.Instrum. 31, 544 (1960)

16) P.Weiss, J.Phys.(Paris) 4, 469 (1905)

17) W.L.Webster, Proc.Roy.Soc. 107, 496 (1925)

18) R.F.Penoyer, Rev.Sci.Instrum. 30, 711 (1959)

19) G.T.Croft, F.J.Donohoe and W.F.Love, Rev.Sci.Instrum. 26, 360 (1955)

20) A.P.King, G.Robinson, J.A.Cundall and M.J.Hight, J.Sci.Instrum 41, 766 (1964)

21) M.A.Asgar, Ph.D.Thesis, University of Southampton (1970)

22) F.Pourarian, Ph.D Thesis, University of Southampton (1974)

23) D.L.Rayner, Ph.D. Thesis, University of Southampton (1976)

24) K.M.Al-Rawi, M.Phil Thesis, University of Southampton (1977)

25) Micro-Measurements Ltd., Strain Gauge Application Notes.

CHAPTER 6

1) J. F. Burd, M. Huq and E. W. Lee, J. Magn. magn. Mat. 5, 000 (1977)

2) W. D. Corner, W. Roe and K. N. R. Taylor, Proc. Phys. Soc. 80, 927 (1962)

3) G. Aubert, J. App. Phys. 39, 504 (1968)

4) J. Crangle and G. M. Goodman, Proc. Roy. Soc. A321, 477 (1971)

5) M. Huq, private communication

6) Y. Barnier, R. Pauthenet and G. Rimet, Cobalt 15, 14 (1962)

7) D. L. Rayner, Ph. D. Thesis, University of Southampton (1976)

8) M. Huq, Ph. D. Thesis, University of Southampton (1975)

9) W. J. Carr Jr., Encyclopedia of Physics (Springer - Berlin, 1966)

10) N. Kaplan, E. Dormann, K. H. J. Buschow and D. Lebenbaum, Phys. Rev. B, 7, 40 (1973)

11) B. Barbara, M. F. Rossignol, H. G. Purwins and E. Walker, Phys. Stat. Sol. (a) 22, 553 (1974)

12) H. G. Purwins, E. Walker, B. Barbara, M. F. Rossignol and P. Bak, J. Phys. C, 7, 3573 (1974)

13) R. Bozorth, B. T. Matthias, H. Suhl, E. Corenzwit and D. D. Davis, Phys. Rev. 115, 1595 (1959)

14) T. Asada and H. Miwa, J. Phys. Soc. Japan, 33, 936 (1972)

15) H. Miwa, Suppl. Prog. Theor. Phys. 46, 138 (1970)

16) K. Tajima, J. Phys. Soc. Japan, 31, 441 (1971)

17) T. Asada, J. Phys. Soc. Japan, 35, 85 (1973)

18) S. Chikazumi, K. Tajima and K. Toyama, J. de Phys. Suppl. 32, C1-179 (1971)

19) C. Voigt and H. H. Pelster, Phys. Stat. Sol. (a) 17, K97 (1973)

CHAPTER 7

1) M.A.Asgar, Ph.D. Thesis, University of Southampton (1970)

2) W.J.Carr Jr., Encyclopedia of Physics (Springer-Berlin) p 272 (1966)

3) N.Akulov, Z.Phys. 52, 389 (1928)

4) L.W.McKeehan, Phys.Rev. 43, 1022 (1933)

5) R.J.Schiltz and J.F.Smith, J.App.Phys. 45, 4681 (1974)

6) N.Kaplan, E.Dormann, K.H.J. Buschow and D.Lebenbaum, Phys.Rev. B, 7, 40 (1973)

7) J.F.Burd and E.W.Lee (to be published J.Phys.C)

8) F.C.Nix and D.MacNair, Phys.Rev. 60, 597 (1941)

CHAPTER 8

1) K. Tajima, J. Phys. Soc. Japan, 31, 441 (1971)

2) T. Asada and H. Miwa, J. Phys. Soc. Japan, 33, 936 (1972)

3) T. Asada, J. Phys. Soc. Japan, 35, 85 (1973)

4) S. Chikazumi, K. Tajima and K. Toyama, J. de Phys. Suppl. 32, C1-179 (1971)

5) J. A. Nelder and R. Mead, Computer J. 7, 308 (1965)

6) B. Barbara, M. F. Rossignol, H. G. Purwins and E. Walker, Phys. Stat. Sol. (a) 22, 553 (1974)

7) H. Oesterreicher and W. E. Wallace, J. Less-Comm. Metals 13, 91 (1967)

8) A. H. Millhouse, H. G. Purwins and E. Walker, Solid State Commun. 11, 707 (1972)

9) H. G. Purwins, E. Walker, B. Barbara, M. F. Rossignol and P. Bak, J. Phys. C, 7, 3573 (1974)

10) N. Kaplan, E. Dormann, K. H. J. Buschow and D. Lebenbaum, Phys. Rev. B, 7, 40 (1973)